
UNIVERSITÀ DEGLI STUDI DI FIRENZE
DIPARTIMENTO DI FISICA
Facoltà di Scienze Matematiche, Fisiche e Naturali



PHD THESIS IN PHYSICS
XXI CYCLE - FIS/03

**Anderson localization
of a weakly interacting
Bose-Einstein condensate**

PRESENTED BY

Chiara D'Errico

SUPERVISOR PROF. GIOVANNI MODUGNO

COORDINATOR PROF. ALESSANDRO CUCCOLI

REFEREES PROF. THIERRY GIAMARCHI

PROF. ANNA VINATTIERI

Contents

Introduction	1
1 Anderson Localization	3
1.1 Localization in a one-dimensional system	5
2 Ultra-cold gases in disordered potentials	13
2.1 Control of interaction via Feshbach resonances	14
2.2 Optical dipole potentials	16
2.2.1 Dipole forces	17
2.2.2 Optical lattices	18
2.3 Periodic potentials	19
2.3.1 Bloch theorem	19
2.3.2 Dynamics of a Bloch wavepacket	22
2.3.3 Bloch oscillations	23
2.4 Disordered optical potentials	29
2.4.1 Laser speckles	29
2.4.2 Quasi periodic one-dimensional optical lattices	31
3 Anderson localization in incommensurate lattices	37
3.1 Theory of localization of non-interacting particles	38
4 Experimental realization of a weakly interacting Bose-Einstein condensate	49
4.1 Realization of BEC of ^{39}K with tunable interaction	50
4.1.1 Weakly interacting ^{39}K condensate	55
4.2 Interferometric determination of the zero crossing position	57
5 Experimental observation of Anderson localization with a	

non-interacting BEC	63
5.1 Observation of Anderson localization	63
5.1.1 Realization of the quasi-periodic lattice	64
5.1.2 Diffusion dynamics	64
5.1.3 Exponential distribution of the localized BEC	71
5.1.4 Analysis of the momentum distribution	74
5.1.5 Interference of multiple localized states	80
5.2 Interacting one dimensional disordered system	83
5.2.1 Experimental observation of effects of weak interaction	84
Conclusions	91
A Scattering theory	93
B Aubry-André Hamiltonian in momentum space	97
Bibliography	101

Introduction

Localization of particles and waves in disordered media is one of the most intriguing phenomena in modern physics. This phenomenon has been originally studied by P. W. Anderson, fifty years ago, in the paper "Absence of diffusion in some random lattices" [1], in the context of transport of electrons in crystals. For this study, in 1977 Anderson was awarded the Nobel Prize in physics.

Anderson studied the transport of non-interacting electrons in a crystal lattice, described by a single particle with random on-site energy. In his model he showed that when the amplitude of the disorder becomes higher than a critical value, the diffusion in the lattice of an initially localized wavepacket is suppressed. He predicted a transition between extended and localized states, that, due to the presence of electron-electron and electron-phonon interactions, has not been directly observed for electrons in a crystal. The interplay between disorder and interaction, in fact, is still an interesting open question in the modern condensed matter physics. First effect of weak nonlinearities have been recently shown for light waves in photonic lattices [2, 3].

The Anderson transition is a much more general phenomenon and has been studied in many other systems where interactions or non-linearities are almost absent. This term, in fact, can be generalized to electromagnetic waves, acoustic waves, quantum waves, etc. However Anderson transition was never observed for matter waves. Ultracold atoms offer a new possibility for the study of disorder-induced localization. The physics of disorder on this kind of systems has been accessible thanks to the introduction of laser speckles [4] and quasi-periodic optical lattices [5]. Preliminary investigations have been done in regimes where the observation of the localization was precluded either by the size of the disorder or by delocalizing effects of nonlinearity

[4, 6, 7, 8, 9]. Only recently the Anderson localization has been observed for matter-waves [10, 11], and this thesis describes one of such studies.

In particular, in this thesis we report on the study of the disorder induced localization of a Bose-Einstein condensate in a lattice system, following the original idea of Anderson [1]. The atom-atom interaction in the condensate can be tuned to zero independently of the other parameters [12]. We introduce disorder on the structure of the lattice by using a weaker incommensurate secondary lattice, which produces a quasi-periodic potential. This kind of system corresponds to an experimental realization of the so called Harper [13] or Aubry-André model [14], which displays a transition from extended to localized states analogous to the Anderson transition. The main advantage of using this kind of disorder is the fact that it offers the possibility to observe the transition already in one dimension [15], whereas in the case of pure random disorder, a system with more than two dimensions would be needed [16].

We clearly observed Anderson localization by investigating transport properties, spatial and momentum distributions. We studied, in fact, the diffusion of the BEC in the bichromatic lattice and we observed that disorder is able to stop the transport into the lattice, when its strength is high enough to localize the system. We studied also the spatial distribution and we found that while the condensate after the diffusion in the single lattice has a gaussian profile, when the disorder is strong enough to localize the system the distributions present an exponential behaviour, emblematic characteristic of Anderson localization. The other possibility we exploited to observe the Anderson localization is the investigation of the momentum distribution, whose width is inversely proportional to the width of the spatial wavefunction and gives important information on the eigenstates of the system.

Chapter 1

Anderson Localization

In the last decades a great interest in the study of disordered structures has grown. This is mainly due to the fact that disorder is everywhere, since in nature perfect ordered systems do not exist. Any system, in fact, is characterized by a disordered structure if it is observed in a sufficiently small scale (crystals with impurities, amorphous substances, fractales surfaces, etc). One of the main properties of disordered potentials is the fact that they are characterized by localized eigenstates, with a localization length $\ell \ll L$ smaller than the size of the system.

One of the most interesting phenomena in solid-state physics, related to the study of disordered potentials, is Anderson localization that describes the absence of diffusion induced by disorder for electrons in crystals. Anderson presented in 1958 a model [1] in which he supposed to have a periodic array of sites j , that he called "lattice", regularly or randomly distributed in three-dimensional space. He assumed to have generic "entities" occupying these sites, that could be electrons or any other kind of particles. The model simply assumes to have an energy E_j , which can randomly vary from site to site, for the particle that occupies site j and to have an interaction matrix element $V_{jk}(\mathbf{r}_{jk})$, which transfers the electrons from one site to the next. Anderson studied the behavior of the wave function of a single particle on site n at an initial time, as a function of the time. He found that there is no transport at all, in the sense that even increasing the time the amplitude of the wave function around the site n falls off rapidly with the distance. An Anderson localized state is characterized by an exponential decay of the amplitude of

the wave function, as the distance from the localization point increases, over a spatial extension larger than the mean distance between two fluctuations of the potential.

The presence of interactions between particles can strongly influence the possibility to observe the disorder induced localization. So the ideal system for this kind of physics is a non interacting sample. For this reason, the intriguing phenomenon of Anderson localization has never been observed in atomic crystals, where thermally excited phonons and electron-electron interactions represent deviations from the Anderson model [1]. After realizing that Anderson localization is a wave phenomenon relying on interference, the Anderson's idea was extended to optics [17, 18]. During the '80, the localization was initially observed for photons (naturally non-interacting) in non-absorbing scattering media. The first prediction [19] and observation of coherent backscattering [20, 21] (weak localization), have been followed by the observation of strong localization of light in highly scattering dielectric media [22, 23, 24, 25, 26, 27]. However in all these studies the potential was fully random without the periodic structure of the lattice that characterizes the original Anderson's model.

The first observation of Anderson localization in a perturbed periodic potential has been the transverse localization of light caused by random fluctuations on a two dimensional photonic lattice [2] (Fig.1.1). Measuring the transverse diffusion (in the plane perpendicular to the propagation direction), they demonstrated how ballistic transport becomes diffusive in the presence of disorder, and that crossover to Anderson localization occurs at a higher level of disorder. More recently in 1D disordered photonic lattices the transition from free ballistic wave packet expansion to exponential localization has been observed [3].

The first observation of Anderson localization in matter waves arrived only recently in two complementary experiments [10, 11], one of which is the subject of this thesis. Ultra-cold atoms are a perfect system for the study of disorder-induced localization, mainly for the possibility to control the interaction strength. In the first work [10] an exponential localization has been observed for a Bose-Einstein condensate released into a one-dimensional waveguide (where interactions are negligible as an effect of the low atomic

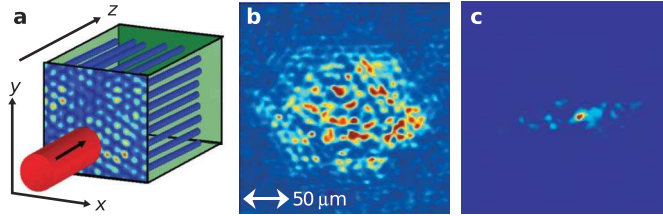


Figure 1.1: Transverse localization scheme [2]. (a) A probe beam entering a disordered lattice, which is periodic in two transverse dimensions but invariant in the propagation direction. (b,c) Experimentally observed diffraction pattern after propagation in the completely periodic lattice (b) and in one particular realization of disordered lattice (c).

density) in the presence of a controlled random disorder created by laser speckle (Subsection 2.4.1). Conversely, in our experiments [11] we observe Anderson localization in a one-dimensional quasi-periodic lattice of a BEC where interactions are nulled via a Feshbach resonance (Section 2.1). We demonstrated that for larger enough disorder this kind of system is characterized by the presence of exponentially localized states, analogous to the Anderson ones. We clearly observed the localization by investigating transport properties, spatial and momentum distributions.

1.1 Localization in a one-dimensional system

The quantum transport properties of a system are intimately related to the underlying symmetries of the Hamiltonian. In a perfectly periodic system all the eigenstates are extended Bloch waves [28]. For a random potential in a one-dimensional system, where there is no trace of translational symmetry, we instead expect to have an opposite behavior and the eigenfunctions must be spatially localized. This phenomenon can be produced from two different causes, depending on the degree of disorder of the system. In the description of a one-dimensional crystal, in fact, Lifshitz introduced for the first time the distinction between *strong* and *weak* disorder [29]. In his original definition it was considered weakly disordered a crystal with low concentration of impurities, where the mean distance between two consecutive impurities was of the order of many lattice constants. The other extreme of strong disorder was associated to an high concentration of impurities. A weakly disordered

system presents Lifshitz localization, where a single fluctuation of the potential is enough to induce localization. On the contrary, Anderson localization occurs in strongly disordered systems and it is produced really by the high concentration of the impurities distributed in the system.

Even if the phenomenon of localization is generally present with a one-dimensional random disorder, it has to be discussed and analyzed for each model. In some cases, in fact, localization is present only with particular parameters [30].

We can deduce the behavior of the Anderson localized wavefunctions in a simple model, as done by Mott [31]. With this simple problem of quantum mechanics, we can deduce the emblematic characteristic of Anderson localization: the exponential decreasing of the wave function from the localization point. Let us start considering a one-dimensional periodic potential of length L , characterized by a series of barriers equally spaced, with the same width b and the same high V_0 :

$$V(x) = \begin{cases} 0 & \text{if } x \in D_i \\ V_0 & \text{if } x \in E_i \end{cases} \quad (1.1)$$

where we defined the domains:

$$\begin{aligned} D_i &\equiv [ia, (i+1)a - b] \\ E_i &\equiv [ia - b, ia] \end{aligned} \quad (1.2)$$

in which $V(x)$ is respectively 0 and V_0 . The Schrödinger equation can be given separately for regions D_i and E_i :

$$\begin{aligned} \frac{\partial^2 \psi}{\partial x^2} + \frac{2m}{\hbar^2} E \psi &= 0 \quad x \in D_i \\ \frac{\partial^2 \psi}{\partial x^2} + \frac{2m}{\hbar^2} (E - V_0) \psi &= 0 \quad x \in E_i \end{aligned} \quad (1.3)$$

If we solve the system for $E < V_0$ we have:

$$\psi(x) = \begin{cases} A_i e^{i\alpha x} + A'_i e^{-i\alpha x + \varphi_i} & \text{if } x \in D_i \\ B_i e^{\beta x} + B'_i e^{-\beta x + \phi_i} & \text{if } x \in E_i \end{cases} \quad (1.4)$$

with $\alpha^2 = 2mE/\hbar^2$ and $\beta^2 = 2m(V_0 - E)/\hbar^2$. By considering the periodicity of the potential, the Bloch's theorem asserts that the wavefunction solution

1.1. Localization in a one-dimensional system

of the Schrödinger equation can be written as:

$$\psi(x) = e^{ikx}u(x) \quad (1.5)$$

where $u(x)$ is a periodic function with the same periodicity of the potential $V(x)$:

$$u(x+a) = u(x) \quad (1.6)$$

In order to obtain the right solution we need to impose the continuity and the differentiability of $\psi(x)$:

$$\begin{cases} \psi(a^+) = \psi(b^-) \\ \dot{\psi}(a^+) = \dot{\psi}(b^-) \end{cases} \quad (1.7)$$

and the conditions of periodicity of $u(x)$:

$$\begin{cases} u(-b) = u(a-b) \\ \dot{u}(-b) = \dot{u}(a-b) \end{cases} \quad (1.8)$$

These equations give the conditions on the possible values of k and E . The shape of the eigenfunctions is $\psi(x) = e^{ikx}u(x)$, which corresponds to a periodic function $u(x)$ modulated by the exponential e^{ikx} . The shape of $u(x)$ is sinusoidal in the regions where $V(x) = 0$; whereas in the region where $V(x) = V_0$ the contribution of the two exponential functions has to be able to join the function inside the barrier with the function outside. The periodic part $u(x)$ of the wavefunction is reported in Fig. 1.2. In the perfect periodic system we considered, the wavefunction is distributed in an homogeneous way over the different wells of the potential.

The situation is completely different, instead, if we introduce the disorder on the periodic potential above. One possibility is to consider the case in which the different potential barriers are distributed at random distances (Fig.1.3):

$$V_R(x) = \begin{cases} 0 & \text{if } x \in D_i \\ V_0 & \text{if } x \in E_i \end{cases} \quad (1.9)$$

where we defined the domains:

$$\begin{aligned} D_i &\equiv [x_i + b, x_{i+1}] \\ E_i &\equiv [x_i, x_i + b] \end{aligned} \quad (1.10)$$

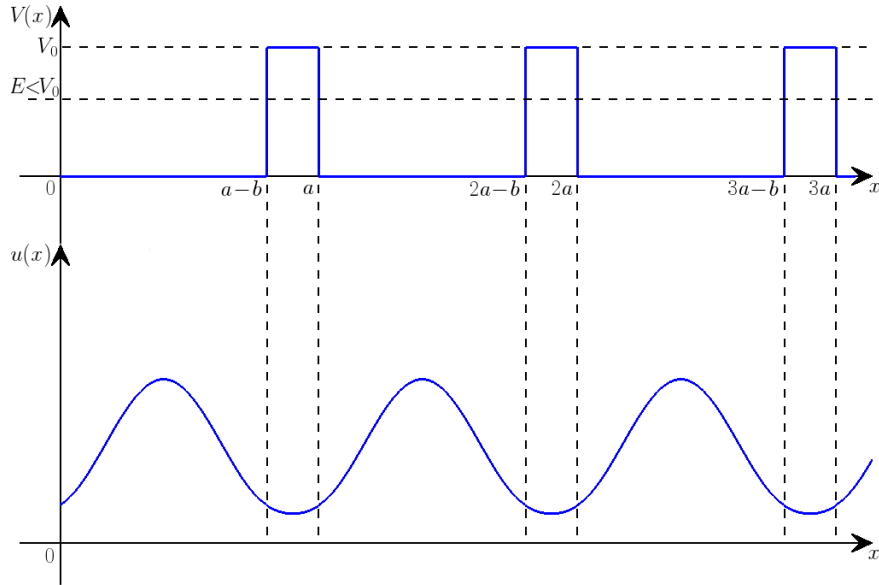


Figure 1.2: Qualitative representation of the ordered potential $V(x)$ introduced in eq. 1.1 and of the periodic part $u(x)$ of the wave function.

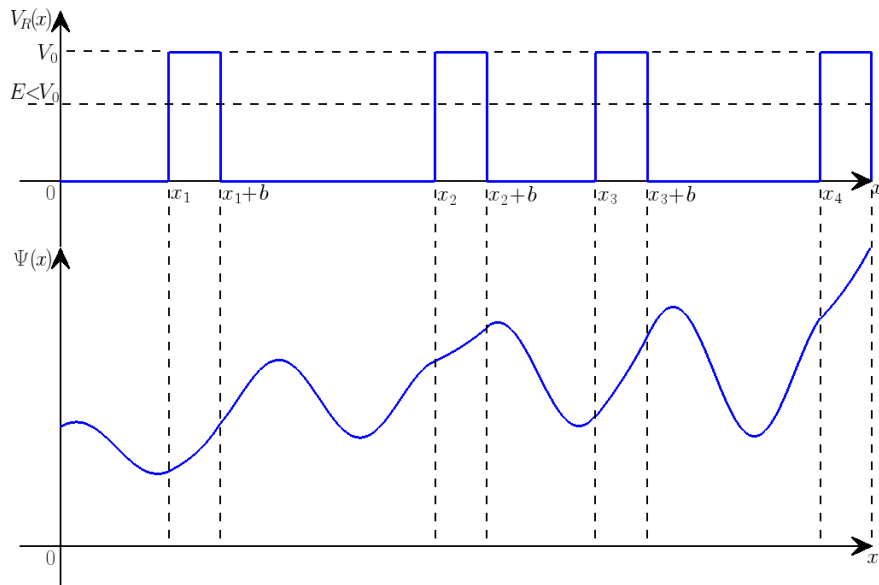


Figure 1.3: Qualitative representation of the disordered potential $V_R(x)$ introduced in eq. 1.9, and of the wave functions $\psi(x)$.

1.1. Localization in a one-dimensional system

in which $V_R(x)$ is respectively 0 and V_0 . As we already said, the position of each barrier x_i is a random variable, which has the following distribution

$$P(x_i) = \begin{cases} C \neq 0 & \text{if } b' < x_i - x_{i-1} < b'' \\ 0 & \text{otherwise} \end{cases} \quad (1.11)$$

where $b', b'' > b$. We chose b' and b'' small enough to be in the regime of strong disorder. The most important consequence of the introduction of the disorder, is that we lose the condition on the periodicity of the wavefunction. We can try to find the generic eigenstate $\psi(x)$ of the system, with energy $E < V_0$, whose expression remains of the same shape of eq. 1.4 and in the particular case of $A_i = A'_i$ can be considered as:

$$\psi(x) = \begin{cases} A_i \cos(\alpha x + \varphi_i) & \text{if } x \in D_i \\ B_i e^{\beta x} + B'_i e^{-\beta x + \phi_i} & \text{if } x \in E_i \end{cases} \quad (1.12)$$

By imposing the continuity and the differentiability of $\psi(x)$ in $x = x_i$ we obtain

$$\begin{cases} 2A_{i-1} \cos(\alpha x_i + \varphi_{i-1}) = B_i e^{\beta x_i} + B'_i e^{-\beta x_i + \phi_i} \\ 2\alpha A_{i-1} \sin(\alpha x_i + \varphi_{i-1}) = B_i \beta e^{\beta x_i} - B'_i \beta e^{-\beta x_i + \phi_i} \end{cases} \quad (1.13)$$

By imposing the continuity and the differentiability of $\psi(x)$ in $x = x_i + b$ we have:

$$\begin{cases} 2A_i \cos(\alpha(x_i + b) + \varphi_i) = B_i e^{\beta(x_i + b)} + B'_i e^{-\beta(x_i + b) + \phi_i} \\ 2\alpha A_i \sin(\alpha(x_i + b) + \varphi_i) = B_i \beta e^{\beta(x_i + b)} - B'_i \beta e^{-\beta(x_i + b) + \phi_i} \end{cases} \quad (1.14)$$

The eigenfunction has a sinusoidal shape outside from the barriers, with different phases φ_i , which can be considered random, as an effect of the random positions of the barriers. In the case of strong disorder we can suppose that the shape of the solutions for $x \in D_i$ doesn't contribute to the global shape of the wave function. Therefore, it is fundamental to find the behaviour of the wavefunction for $x \in E_i$. Under the barriers this is determined by the superposition of a growing and a decreasing exponential. Both of them are necessary in order to be able to satisfy the boundary conditions. If we suppose $B_i = 0$, in fact, the two conditions in $x = x_i$ become

$$\tan(\alpha x_i + \varphi_{i-1}) = \frac{\beta}{\alpha}. \quad (1.15)$$

We are considering the case of $E \ll V_0$, so $\alpha \ll \beta$ and it is possible to solve the equation only for particular values of the phase φ_{i-1} . It is necessary to consider both exponential (growing and decreasing) in the regions E_i , and the coefficients B_i and B'_i are both functions of φ_{i-1} and can be considered like random variables. Increasing x , the main contribution to $\psi(x)$ derives

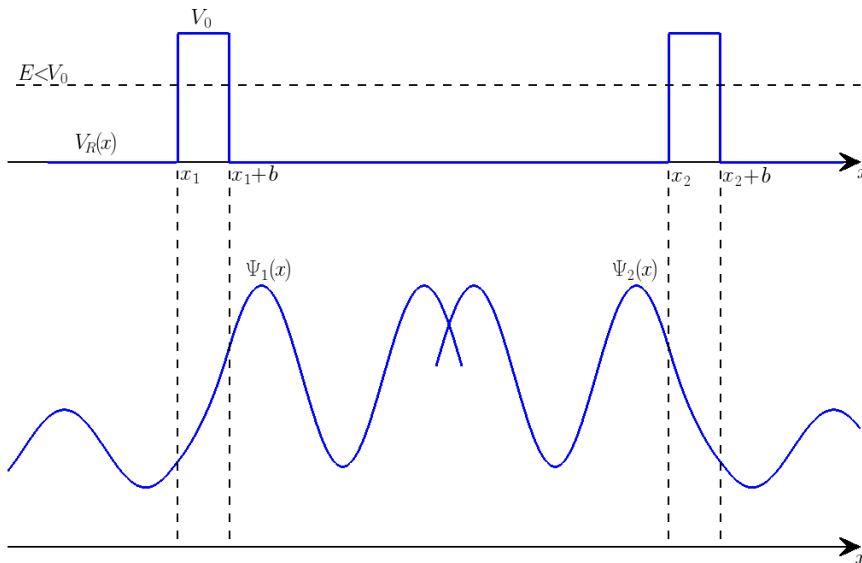


Figure 1.4: Wave functions for a forbidden value of the energy.

from the growing exponential. The eigenfunction is no more distributed over all the potential walls, like in the periodic case, but presents an exponential behaviour (Fig. 1.3).

We can repeat the same reasoning in a different reference system, by inverting the x axis ($x = 0$ becomes $x = L$ and vice versa). By imposing this time the conditions in $x = x_i + b$, we can deduce the same growing behaviour in the opposite direction. In general these solutions, that we found in the two different reference systems, will not fix in the middle, but we can choose values of the energy such that they do (Fig. 1.4) [31, 32].

We can introduce a *localization point*, where $\psi(x)$ assumes the maximum value. The wave function has the following property:

$$|\psi(x)|^2 \propto e^{-\frac{2|x-x_0|}{\ell}} + \vartheta(x) \quad (1.16)$$

1.1. Localization in a one-dimensional system

where ℓ is known like *localization length* and $\vartheta(x)$ is a function which takes into account that $\psi(x)$ is locally influenced by the shape of the potential. The wavefunction is characterized by an exponential decreasing from the localization point.

We mention that Gogolin demonstrated that a 1D correction to this exponential decreasing has to be taken into account [33, 34]. The rigorous mathematical demonstration of the existence of the Anderson transition has been successive [35].

1. ANDERSON LOCALIZATION

Chapter 2

Ultra-cold gases in disordered potentials

The system we used in order to study the phenomenon of Anderson localization is a weakly interacting Bose-Einstein condensate in a quasi periodic potential. Ultra-cold quantum gases are an incredibly interesting kind of system as the quantum behavior of the system becomes visible at very low temperature. In the last decades has been developed a great interest in this field of research, both from theoretical and experimental point of view, specially since 1995 with the achievement of Bose Einstein condensation [36, 37, 38]. Ultra-cold gases represent a formidable tool of experimental investigation because offer the possibility to easily control the parameters of the system: atom number, temperature, interaction, etc. An other important advantage is the versatility: they can be trapped in magnetic or optical potentials, or radio-frequencies; it is also possible to use periodic optical lattices in 1D, 2D and 3D. A quantum degenerate gas can also be easily revealed by absorption imaging system or fluorescence, which allow to observe the gas in real phase space or in momentum space. Different spectroscopic techniques (Bragg and Raman spectroscopy) have been also developed.

A Bose-Einstein condensate is usually characterized by the presence of a repulsive interaction between atoms. As we said in the last Chapter, to study Anderson localization we need to reduce as much as possible the amount of inter-atomic interaction. This is possible thanks to the presence of magnetic Feshbach resonances, which allow to tune the interaction from attractive to

repulsive or to bring it close to zero. We briefly show the basic principles of Feshbach resonances in Section 2.1.

The optical lattice is a fundamental component of the experiments described in this thesis. It offers the possibility to produce a perfectly periodic potential for the atoms. In Section 2.2 we present the basic concepts to describe how it is possible to generate an optical dipole trap and an optical lattice, using the intensity gradient of the light which interacts with the induced atomic dipole moment. In Section 2.3 we review the Bloch theory for non-interacting particles in a periodic potential. We analyse also the interferometric phenomenon of Bloch oscillations for atoms in a lattice, in presence of an external force. As we will see in Chapter 4, we used this kind of interferometer in order to check our capability to create a non interacting BEC. The phenomenon of Bloch oscillations, in fact, is strongly affected by the presence of inter-atomic interaction.

To study Anderson localization we need to introduce a disorder on the perfect periodic structure of the lattice potential. We have two experimental possibilities to create disorder (2.4). The first one is a random distribution of intensity created with laser speckles and the second one is the superposition of two lattices with incommensurate wavelengths. Both techniques has already been realized at LENS in order to study the physics of a Bose-Einstein condensate in random potentials [4, 7, 5].

2.1 Control of interaction via Feshbach resonances

As we derive in Appendix A, in a bosonic gas at low temperature and in a dilute regime, the dominant contact interaction between atoms can be described by a single parameter, the s -wave scattering length a . The sign of a determines the type of interaction: positive values of the scattering length correspond to repulsive interaction and negative values to attractive ones. The possibility to tune interaction in this kind of systems, or rather to tune the value of a , is offered by the presence of magnetic Feshbach resonances. Feshbach resonances phenomenon has been initially studied in nuclear physics [39, 40, 41] and has become successively important in atom physics [42, 43,

44], because it offers the great opportunity to control the inter-atomic interaction, in a resonant way.

A Feshbach resonance occurs in the process of scattering between two atoms when the collision energy is tuned in resonance with a molecular bound state by the application of an homogeneous magnetic field (Fig. 2.1). In this case

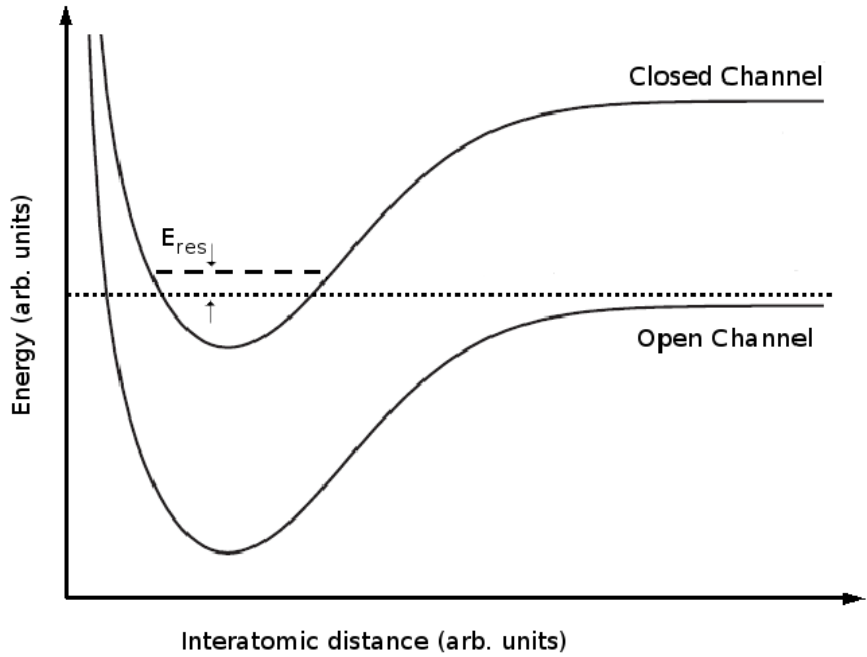


Figure 2.1: The energy detuning between a bound molecular level and the threshold of the two colliding atoms can be tuned by means of the external magnetic field.

the possibility to have a transition of the atoms pair to the molecular state produces an enhancement of the collision cross section. Near a Feshbach resonance, in fact, the scattering length a varies dispersively as a function of the magnetic field B :

$$a(B) = a_{bg} \left(1 - \frac{W}{B - B_0} \right) \quad (2.1)$$

where B_0 is the center and W is the width of the resonance, and it is possible by the application of an homogeneous magnetic field to control the atomic interaction from strongly attractive to strongly repulsive (Fig. 2.2). While these resonances are a general phenomenon, the specific parameters that determine the dependence of a on B rely on the particular atomic system under

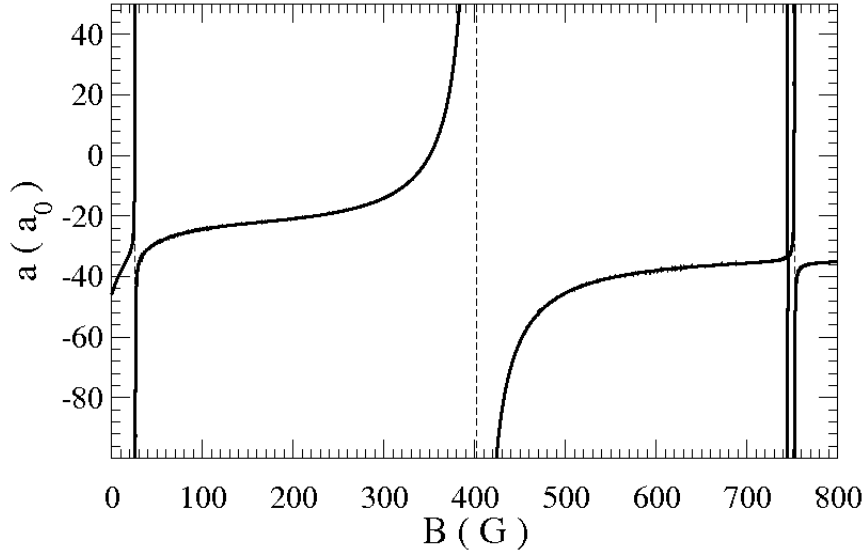


Figure 2.2: Magnetic field dependence of the effective scattering length for $|F = 1, m_f = 1\rangle + |F = 1, m_f = 1\rangle$ ^{39}K collisions. Dashed lines indicate the resonance positions. There is a broad resonance near 400 G which can be used to tune interaction with high accuracy.

study.

As we will see in the Chapter 5 the possibility to tune interaction is the fundamental component for the observation of Anderson localization. A repulsive interaction between particles, in fact, could induce delocalization, preventing the observation of the transition. In particular, in the case of ^{39}K that we explored in the experiment, the broad Feshbach resonance of Fig. 2.2 allows us to precisely tune a close enough to zero to create a weakly interacting BEC for localization studies.

2.2 Optical dipole potentials

The necessity to use magnetic Feshbach resonances imposes us to use optical potentials, instead of magnetic ones. In this section we will explain the basic properties of optical potentials in general, and of optical lattices.

2.2.1 Dipole forces

The **dipole force** is the conservative force that arises from the dispersive interaction between the intensity gradient of a light field and the induced atomic dipole moment. This mechanism can be used to create optical trapping potential to confine the atoms. The absorptive part of the dipole interaction in far-detuned light leads to residual photon scattering of the trapping light, which limits the performance of dipole trap. The rigorous quantum-mechanical treatment can be found in [45], but we will present a semiclassical approach [46], from which we can derive the main expressions for the dipolar force and the scattering rate. In this approach we consider the atom as a simple oscillator and the incident radiation beam as a classical radiation field:

$$\mathbf{E}(\mathbf{r}, t) = \hat{\mathbf{e}}\tilde{E}(\mathbf{r})e^{-i\omega t} + c.c. \quad (2.2)$$

which induces on the atom a dipole moment \mathbf{p} which oscillates at the same frequency ω of the driving field:

$$\mathbf{p}(\mathbf{r}, t) = \hat{\mathbf{e}}\tilde{p}(\mathbf{r})e^{-i\omega t} + c.c. \quad (2.3)$$

where $\hat{\mathbf{e}}$ is the unitary polarization vector. The amplitude \tilde{p} of the dipole moment is related to the field amplitude \tilde{E} by:

$$\tilde{p} = \alpha\tilde{E} \quad (2.4)$$

where the complex polarizability α depends on the driving frequency ω . The interaction potential of the induced dipole moment \mathbf{p} on the driving field \mathbf{E} is given by

$$U_{dip}(\mathbf{r}) = -\frac{1}{2}\langle\mathbf{p} \cdot \mathbf{E}\rangle = -\frac{1}{2\epsilon_0 c}\text{Re}(\alpha)I(\mathbf{r}) \quad (2.5)$$

where the brackets denote the time average over the rapid oscillating terms and $I(\mathbf{r})$ is the field intensity. From the gradient of the interaction potential, we can estimate the dipole force, which is proportional to the real part of the polarizability α and to the intensity gradient of the light. On the other hand, the imaginary part of the polarizability is related to the absorption of photons from the incident field by the atoms:

$$\Gamma_{sc}(\mathbf{r}) = \frac{P_{abs}}{\hbar\omega} = \frac{\langle\dot{\mathbf{p}} \cdot \mathbf{E}\rangle}{\hbar\omega} = \frac{1}{\hbar\epsilon_0 c}\text{Im}(\alpha)I(\mathbf{r}). \quad (2.6)$$

usually called *scattering rate*. Considering the atom as a two-level quantum system in a classical radiation field it is possible to calculate the analytical expression for the atomic polarizability $\alpha(\omega)$ [46]. In a far-off resonance regime (the detuning $\Delta = \omega - \omega_0$ between the incident radiation and the atomic resonance ω_0 is much larger than the radiative linewidth (Γ) the expression for the dipolar potential and the scattering rate are the following:

$$U_{dip}(\mathbf{r}) = \frac{3\pi c^2}{2\omega_0^3} \frac{\Gamma}{\Delta} I(\mathbf{r}) \quad (2.7)$$

$$\Gamma_{sc}(\mathbf{r}) = \frac{3\pi c^2}{2\hbar\omega_0^3} \left(\frac{\Gamma}{\Delta}\right)^2 I(\mathbf{r}) \quad (2.8)$$

Typically one sets $\Delta \gg \Gamma$ so the potential is conservative and Γ_{sc} can be neglected.

2.2.2 Optical lattices

The dipole potential above can be used to create a periodic potential for atoms. The simplest method is to create a standing wave that is the interference of two counter-propagating beams. This configuration is called *optical lattice*. We can derive the dipole potential felt by atoms, starting from the electric field expression for two counter-propagating plane waves:

$$\mathbf{E}_1(x, t) = \hat{\mathbf{e}} \tilde{E}_1 \cos(kx + \omega t + \delta) \quad (2.9)$$

$$\mathbf{E}_2(x, t) = \hat{\mathbf{e}} \tilde{E}_2 \cos(kx - \omega t - \delta) \quad (2.10)$$

where $k = \omega/c$ is the light wavevector. The intensity will be

$$I(x, t) = \epsilon_0 c |\mathbf{E}_1(x, t) + \mathbf{E}_2(x, t)|^2 \quad (2.11)$$

If we mediate over the rapid oscillating terms, we obtain

$$I(x) = \frac{1}{2} \epsilon_0 c \left[(\tilde{E}_1 - \tilde{E}_2)^2 + 4\tilde{E}_1 \tilde{E}_2 \cos^2(kx) \right] \quad (2.12)$$

In the particular case of $\tilde{E}_1 = \tilde{E}_2 = E_0$, remembering (2.7), the interaction potential exerted by the standing wave on the atoms is:

$$V_{dip}(x) = \frac{3\pi c^2}{2\omega_0^3} \frac{\Gamma}{\Delta} I_0 \cos^2(kx) = V_0 \cos^2(kx) \quad (2.13)$$

2.3. Periodic potentials

where $I_0 = 2\epsilon_0 c E_0^2$. This corresponds to a perfect sinusoidal whose spatial periodicity $\pi/k = \lambda/2$ depends from the wavelength of the laser light λ . Commonly the lattice depth is expressed in terms of energy recoil $E_r = \hbar^2 k^2 / 2m$:

$$s = V_0 / E_r. \quad (2.14)$$

2.3 Periodic potentials

2.3.1 Bloch theorem

Let us consider a gas of non interacting particles of mass m in a one dimensional periodic potential $V(x)$ [47]. We restrict to the one-dimensional case, because this corresponds to our experimental situation. If d is the spatial periodicity of the potential

$$V(x) = V(x + d) \quad (2.15)$$

and we are interested to solve the Schrödinger equation for a particle moving in this potential:

$$\hat{H}\psi(x) = \left[-\frac{\hbar^2}{2m} \frac{\partial^2}{\partial x^2} + V(x) \right] \psi(x) = E\psi(x), \quad (2.16)$$

Bloch Theorem asserts that solutions of (eq. 2.16) take the form of plane waves e^{iqx} modulated by functions $u_{n,q}(x)$ having the same periodicity of the potential:

$$\psi_{n,q}(x) = e^{iqx} u_{n,q}(x) \quad (2.17)$$

$$u_{n,q}(x) = u_{n,q}(x + d) \quad (2.18)$$

The eigenvalues $E_n(q)$ and the eigenstates $\psi_{n,q}(x)$ of the Hamiltonian \hat{H} are labelled with two quantum numbers: the *band index* n and the *quasi momentum* q .

In the motion of a particle in a periodic potential, the quasi momentum q plays the same role of the free particle vector p/\hbar without any external potential. However, since the potential $V(x)$ does not have a complete translational invariance, the Bloch states are not eigenstates of the momentum operator and $\hbar q$ is not the expectation value of the momentum. We can

better understand the analogy between q and the momentum p , if we study the dynamics of Bloch particles in the presence of an external applied force (subsection 2.3.3). The periodicity of \hat{H} implies that q is defined modulus $2\pi/d$, that is the period of the *reciprocal lattice*. The periodic structure in real space induces a periodicity also in momentum space, in which the elementary cells are the so called *Brillouin zones*. For a certain quasi momentum q there exist many different eigenvalues $E_n(q)$, identified with the band index n . The term *band* is due to the fact that the periodicity of the potential introduces in the energy spectrum allowed and forbidden zones (energy bands). Using a perturbative approach, the energy spectrum for a generic periodic potential $V(x)$ can be easily calculated in the limit of weak potential, where the wavefunction are not very different from plane waves, or for a very strong potential (*tight binding regime*), in which different wavefunctions have not overlap. In general, if we put (eq. 2.17) into (eq. 2.16), we have to solve:

$$\hat{H}_B u_{n,q} = E_n(q) u_{n,q}(x) \quad \text{with} \quad \hat{H}_B = \frac{1}{2m}(\hat{p} + q)^2 + V(x) \quad (2.19)$$

Since the functions $u_{n,q}(x)$ are periodic, they can be written as a discrete Fourier sum:

$$u_{n,q}(x) = \sum_l c_l^{(n,q)} e^{2ilkx} \quad (2.20)$$

with l integer and $k = 2\pi/d$. The potential can be written as:

$$V(x) = V_0 \cos^2(kx) = \frac{1}{4} V_0 (e^{2ikx} + e^{-2ikx} + 2) \quad (2.21)$$

Using these results, the eq. 2.19 can be written in matrix form as:

$$\sum_l H_{l,l'} c_l^{n,q} = E_{q,n} c_{l'}^{n,q} \quad \text{with} \quad H_{l,l'} = \begin{cases} (2l + q/\hbar k)^2 E_r & \text{if } l = l' \\ V_0/4 & \text{if } |l - l'| = 1 \\ 0 & \text{else} \end{cases}$$

The eigenvalues $E_n(q)$ and the eigenvectors $c_l^{n,q}$, which define the Bloch wave functions (eq. 2.17) and (eq. 2.20), can be easily calculated if the Hamiltonian is truncated for large positive and negative l . In fact, the coefficients $c^{(n,q)}$ become very small for large enough l , and a restriction to $-5 \leq l \leq 5$ is a good approximation if we consider only the lowest energy bands. In Fig. 2.3 there are some example of the band structure for different potential

2.3. Periodic potentials

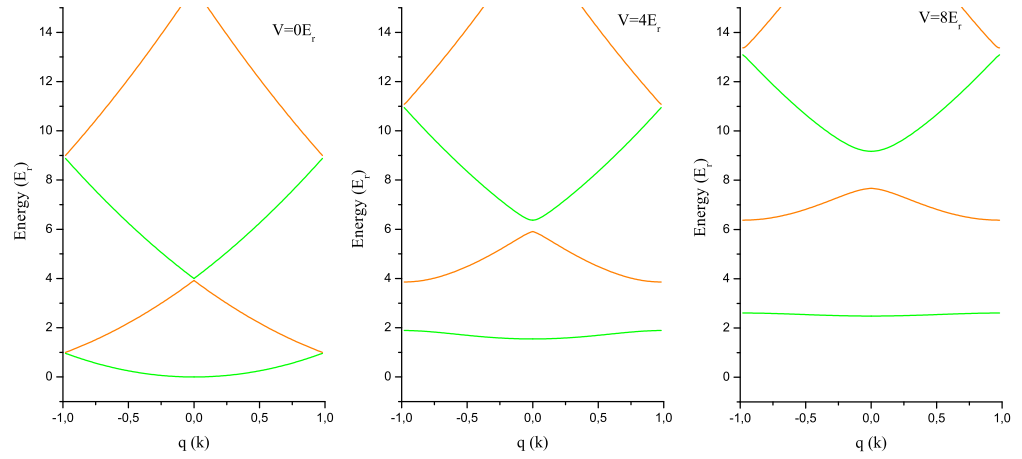


Figure 2.3: Energy of the Bloch state $E_n(q)$ versus quasi momentum q , for the first four energy bands, estimated expanding $u_{n,q}(x)$ as a discrete Fourier sum. The band structure is plotted for different lattice depths (0, 4 and 8 E_r). The energies are expressed in natural units ($E_r = \hbar^2 k^2 / 2m$).

depths of a one dimensional sinusoidal lattice. For vanishing lattice depths, the energy corresponds to the free particle parabola reduced to the first *Brillouin zone* and there are no energy gaps. Increasing the lattice depth, the band gaps increase and the width of the energy bands decrease. For deep lattices the lowest band becomes narrower and it is directly related to the tunneling matrix element J which describes the tunneling coupling between neighboring lattice sites [48]. The expressions of the energy of the first band and of J are respectively:

$$E_0(q) = E_0 - 2J \cos(qd) \quad (2.22)$$

and

$$J = (\max(E_0(q)) - \min(E_0(q)))/4. \quad (2.23)$$

Bloch states are totally delocalized eigenvalues of (eq. 2.16) for a given quasi momentum q and energy band n . These functions can also be written as the sum of an orthogonal and normalized set of wave functions maximally localized to individual lattice sites:

$$\psi_{q,n}(x) = \sum_{j=-\infty}^{\infty} e^{ijqd} w_n(x - jd) \quad (2.24)$$

where the $w_n(x)$ are the so called *Wannier functions* for a localized particle in the n^{th} energy band [49].

2.3.2 Dynamics of a Bloch wavepacket

Now we want to summarize the basic concepts describing the dynamics of a Bloch wavepacket in the presence of an external field. We can consider a superposition of Bloch states with a mean quasi momentum q and a spread δq much smaller than the width of the Brillouin zones. According to the Heisenberg's uncertainty principle, the corresponding wavefunction extends over many lattice sites, because the spatial extent $\delta x \sim 1/\delta q$ is much larger than the lattice spacing. It is possible to demonstrate that the group velocity of the wavepacket is

$$v_n(q) = \frac{1}{\hbar} \frac{\partial E_n(q)}{\partial q} \quad (2.25)$$

2.3. Periodic potentials

that is called *Bloch velocity* [47]. We observe that this velocity vanishes at the edge of the energy band, where $E_n(q)$ is flat.

The simplest model able to describe the dynamics of a Bloch wavepacket in the presence of external field is the *semiclassical model*, where the external field is treated classically and the periodic potential is treated quantum mechanically. The model makes the assumption that the external force F_{ext} doesn't change the energy spectrum of the system. The main approximation is the assumption that the external force F_{ext} is slowly varying on the periodic potential's scale and isn't strong enough to induce inter-band transitions. Within these assumptions, the temporal evolution of the position and of the quasi momentum are:

$$\dot{x} = v_n(q) = \frac{1}{\hbar} \frac{\partial E_n(q)}{\partial q} \quad (2.26)$$

$$\hbar \dot{q} = F_{ext} \quad (2.27)$$

it is interesting to emphasize that $\hbar q$ is not the momentum of the wave packet. In fact the evolution of the real momentum is determined by the total force. Instead, the evolution of the quasi momentum is only induced by the external force, and has no contribution from the force of the lattice.

We can calculate

$$\ddot{x} = \frac{d}{dt} \left[\frac{1}{\hbar} \frac{\partial E_n(q)}{\partial q} \right] = \frac{1}{\hbar} \frac{\partial^2 E_n(q)}{\partial q^2} \dot{q} = \frac{1}{\hbar^2} \frac{\partial^2 E_n(q)}{\partial q^2} F_{ext} \quad (2.28)$$

This relation can be interpreted as the second Newton's law for a particle subjected to the external force F_{ext} and with an *effective mass*

$$m_n^* = \hbar^2 \left[\frac{\partial^2 E_n(q)}{\partial q^2} \right]^{-1} \quad (2.29)$$

related to the band curvature.

2.3.3 Bloch oscillations

We discuss now the dynamics of a single particle in the one-dimensional periodic potential under the influence of a static force F . We have studied this phenomenon, known as Bloch oscillations, to check our capability to control

interaction around zero (Section 4.2), since it is particularly sensitive to the presence of inter-atomic interaction. We could use the semiclassical model, but we prefer to use an interferometric approach, because we are interested to emphasize the effect of the interaction on this kind of phenomenon.

A Bose-Einstein condensate is constituted by atoms which occupy the same quantum state and behave as the same particle, unlike the electron gas in a crystalline solid, composed by particles in different states. So Bose-Einstein condensates are the ideal tools for the investigation of fundamental issues of quantum mechanics and solid state physics linked to the dynamics of a single particle in a periodic potential. This kind of phenomena, in fact, are often not directly observable in other systems, where it is hard to isolate a single quantum particle and to trace its dynamics.

Let's us consider the case of a Bose-Einstein condensate in a periodic potential, created by means of a one-dimensional optical lattice. The BEC will be naturally described by a Bloch wavepacket. In a good approximation, the dynamics can be described by the one-dimensional Gross-Pitaevskii equation (GPE) [50]

$$i\hbar\partial_t\psi(x,t) = \left[-\frac{\hbar^2}{2m}\partial_x^2 + V(x) + g|\psi(x,t)|^2 \right] \psi(x,t) \quad (2.30)$$

where m is the atomic mass, g is the interaction strength, $V(x) = V(x+d)$ is the periodic lattice potential. The GPE (eq. 2.30) includes a nonlinear interaction term, whose presence complicates the single-particle Bloch picture, that is an excellent description for a non interacting system. Bloch waves (eq. 2.17) are still stationary solutions of (eq. 2.30) and, for a wide range of interaction strength, the main features found for the linear band structure are conserved.

The single particle energy spectrum instead is modified by the presence of a strong non-linearity. If we include in the system an external force F , the equation (eq. 2.30) becomes:

$$i\hbar\partial_t\psi(x,t) = \left[-\frac{\hbar^2}{2m}\partial_x^2 + V(x) + Fx + g|\psi(x,t)|^2 \right] \psi(x,t) \quad (2.31)$$

and the eigenstates of the linear system are the so called Wannier-Stark states $\Phi_{n,i}(x)$ [51], where n is the band index and i is the site index. We

2.3. Periodic potentials

will restrict to discuss the case in which F isn't strong enough to induce interband transitions, so we will omit the index n . Depending on the depth of the potential, Wannier-Stark functions extend over many periods of the lattice; they are related by a spatial translation $\Phi_i(x) = \Phi_0(x - di)$ and they are equally spaced in energy by $\Delta E = Fd$. The macroscopic wavefunction $\psi(x, t)$ of the condensate can be described as a coherent superposition of Wannier-Stark states $\Phi_i(x)$

$$\psi(x, t) = \sum_i \sqrt{\rho_i(t)} e^{j\varphi_i(t)} \Phi_i \quad (2.32)$$

with complex amplitudes of module $\sqrt{\rho_i}$ and phase φ_i . It is possible to demonstrate that the amplitudes ρ_i change only slowly in time compared to the phase φ_i and can be assumed to be constant [52]. The evolution of the phase can instead be approximated to:

$$\hbar\dot{\varphi}_i = -iFd - g\gamma_i\rho_i \quad (2.33)$$

where γ_i is a factor that depends from the parameters of the potentials and takes into account the site-to-site interaction. Let's we start from the non interacting case ($g = 0$). The phase of each state evolves according to the energy shift induced by the external potential, $\varphi_i(t) = -iFdt$. If we calculate the evolution of the wave function in momentum space, considering the translational properties of Wannier-Stark functions

$$\Phi_i(k) = e^{-jdik} \Phi_0(k) \quad (2.34)$$

we obtain:

$$\psi(k, t) = \Phi_0(k) \sum_i i\sqrt{\rho_i} e^{-jdi(k+ Ft)/\hbar} \quad (2.35)$$

The second part is the interference between different Wannier-Stark states, which results in equally spaced momentum peaks moving with constant velocity under the envelope of $\Phi_0(k)$ (Fig.2.4). The interference pattern is periodic in time with period $T_B = h/Fd$ and a measurement of the frequency of these oscillations, known as Bloch oscillations, allows a direct measurement of the external force.

In the interacting case in the phase evolution we have an additional term

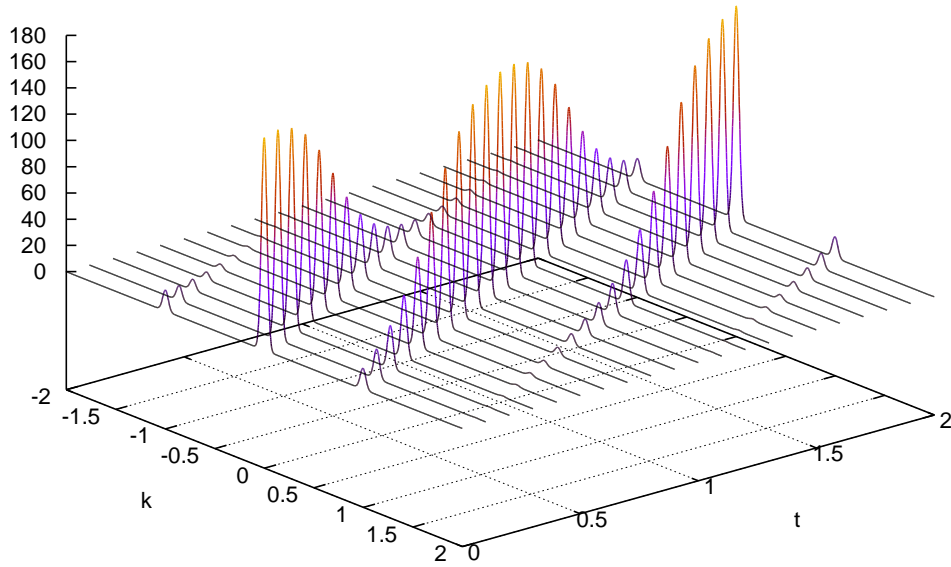


Figure 2.4: Density pattern of the momentum distribution for different values of time of Bloch oscillation, for a non-interacting system. The interference pattern oscillates periodically with period $T = h/Fd$.

2.3. Periodic potentials

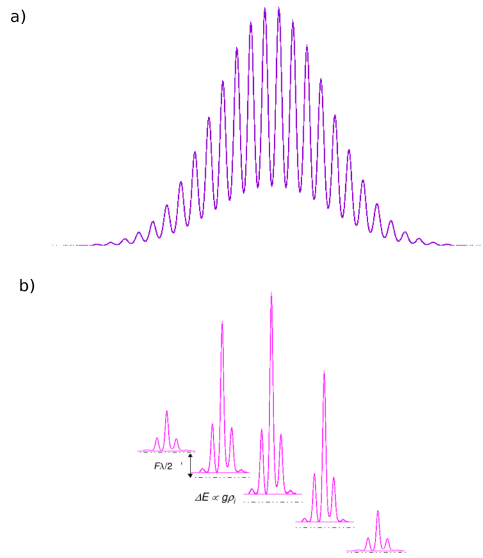


Figure 2.5: (a) Spatial density of the ground state of the condensate in the optical trap combined with the vertical optical lattice. (b) Projection of the ground state on the Wannier-Stark functions (2.32). Considering the inhomogeneous distribution the interaction-induced phase term is not constant over the various states ($\delta\varphi_i \propto g\rho_i$).

proportional to the local interaction energy: $\delta\varphi_i \propto g\rho_i t$, where g is the interaction strength proportional to the scattering length a . Since the population of the various W-S functions is inhomogeneously distributed (Fig. 2.5), this interaction-induced phase term is not constant over the various states. These causes broadening and destruction of the interference pattern (Fig.2.6).

In Section 4.2 we describe how we exploited the interaction induce decoherence of Bloch oscillations in order to precisely locate the magnetic field which gives the smallest interaction possible in our system.

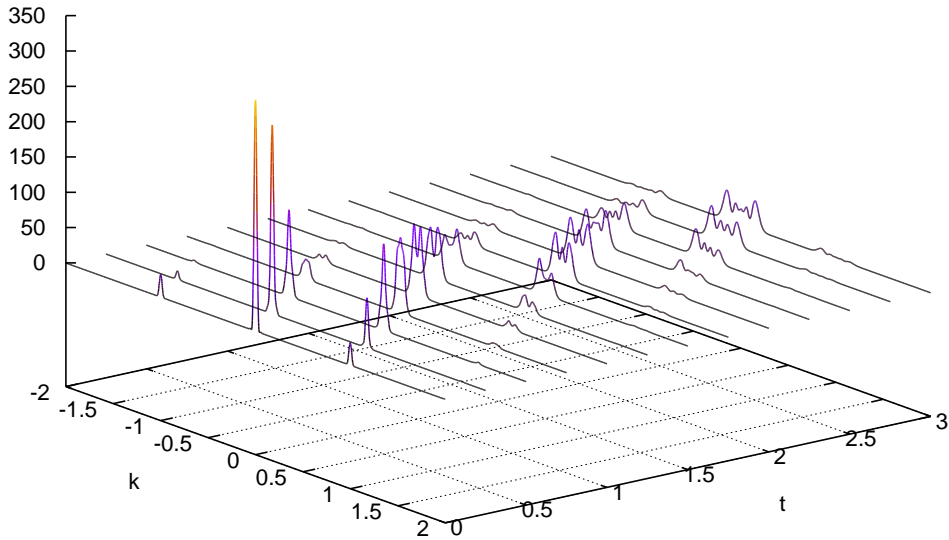


Figure 2.6: Density pattern of the momentum distribution for different values of time of Bloch oscillation, for an interacting system. After three Bloch periods the interference pattern is drastically broadened as an effect of the interaction.

2.4 Disordered optical potentials

So far we analysed the case of a perfect periodic potential, but in order to study Anderson localization we also need to introduce a disorder. We present now two experimental possibilities to realize disordered periodic potentials.

2.4.1 Laser speckles

The first one is the creation of laser speckles, i.e. the random distribution of intensity that derives from the scattering of a coherent laser light on a rough surface (Fig.2.7). This scattering can be done in reflexion or in transmission. In both cases, the basic principle of formation of speckles is the same and consists in a spatial modulation of the phase and of the amplitude of the electric field of the incident light [53, 54, 55], due to the random path that each wave, scattered from a facet of the surface, can follow. The dipole potential generated by a laser beam is proportional to its intensity (eq. 2.13); the disordered spatial intensity produced by optical speckles creates a spatially disordered potential with a random distribution (Fig. 2.8). This kind of

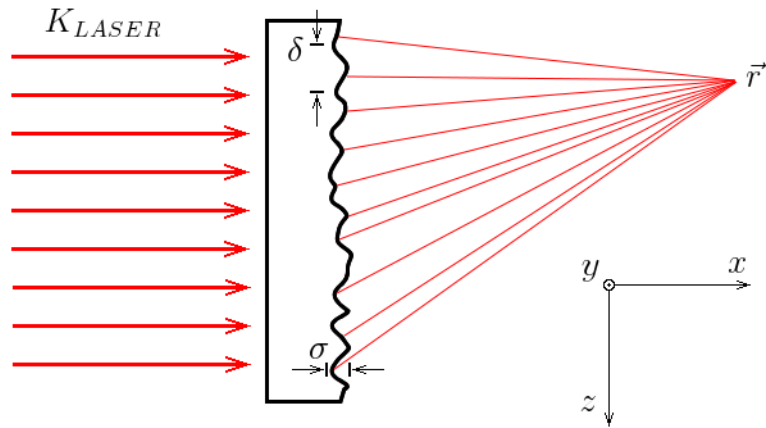


Figure 2.7: Scattering of a coherent plane wave from a rough glass. Each facet of the rough surface generate partial waves that have different random paths in r . This produces the interference of random distributed phases.

disorder is stationary in time, so its characterization is mainly determined

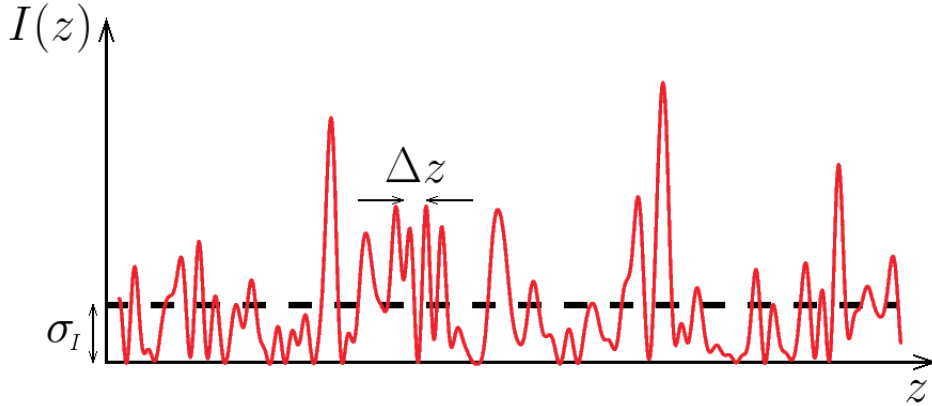


Figure 2.8: Spatial distribution of the intensity in one direction of the space. The standard deviation σ_I characterizes the amplitude of the disorder. The length Δz characterized the spatial scale of the intensity modulation.

from the evaluation of the amplitude and of the typical spatial lengthscale. The standard deviation of the intensity σ_I , characterizes the variations of the intensity of the speckles field. Over the spatial profile of the speckles intensity, σ_I describes the typical amplitude of the intensity peaks. From σ_I it is possible to define the standard deviation of the dipolar potential associated to the intensity distribution:

$$\sigma_V = \frac{2 \hbar \gamma^2 \sigma_I}{3 8 I_{sat} \delta} \quad (2.36)$$

The lengthscale of the disorder is defined as the width of the self correlation function C_I of the intensity distribution

$$C_I(\delta \mathbf{r}) = \langle I(\mathbf{r}) I(\mathbf{r} + \delta \mathbf{r}) \rangle \quad (2.37)$$

where $I(\mathbf{r})$ is the intensity in the point \mathbf{r} and $\langle \rangle$ indicates the statistic mean. This is given by the smallest disorder grain size, whose value is diffraction limited by the numerical aperture of the optical system and by the laser wavelength λ employed to create the speckles pattern:

$$\sigma_z = \frac{\Delta z}{2} \approx 1.22 \lambda \frac{l}{D} \quad (2.38)$$

where D is the beam diameter and l is the distance of the diffusive plate from the atoms. The speckle grain size is inversely proportional to the dimension

of the laser beam on the diffusive plate, which sets the limit on the number of effective scatterers.

In the case of our apparatus, the optical access is limited. The best configuration we could achieve is that of a lens with $D \sim 5$ cm at $l \sim 20$ cm from the atoms, which could give a speckle grain size of $\sigma_z \sim 5 \mu\text{m}$, with the laser beam at $\lambda \approx 1030$ nm of our optical lattice. A distance between the grains of $\sim 10 \mu\text{m}$ however is too big if we consider that we have a BEC with a comparable dimension ($10 \div 20 \mu\text{m}$). This prevented us to use speckles disorder in our apparatus, and forced us to choose a different possibility to create disorder on a smaller scale. One possibility is a quasi-periodic lattice, which introduces a disorder on the energy of each minimum of the lattice, as we will see in the following subsection. In this case the distance between two consecutive "impurities" can be evaluated as the lattice constant $\sigma_z \sim 0.5 \mu\text{m}$.

2.4.2 Quasi periodic one-dimensional optical lattices

The quasi-periodic potential can be created by superposing to the primary optical lattice a weak secondary one with incommensurate wavelength $\lambda_2/\lambda_1 \in \mathbb{R}/\mathbb{Q}$:

$$V(x) = s_1 E_{r1} \sin^2(k_1 x) + s_2 E_{r2} \sin^2(k_2 x) \quad (2.39)$$

This kind of system, commonly called *bichromatic lattice*, is characterized by the fact that the perturbation due to the second lattice induces a quasi-periodic modulation on the energy of the minima of the main lattice (Fig. 2.9), with a distance between two "impurities" ten times smaller than which one we can obtain with speckles.

Generally, if the second lattice has a depth comparable with the first one, it could change the position of the minima of the bichromatic potential $V(x)$. In the case in which, instead, the secondary lattice can be considered as a perturbation to the first one ($V_2 \ll V_1$), the position of the minima of the potential $V(x)$ can be approximated with the position of the minima $x_j = j\pi/k_1 = j\lambda_1/2$ of the main lattice $V_1 \sin^2(k_1 x)$ [56]. The deviation of the actual minima positions can be calculated by expanding in series around the points x_j

$$x_j + \xi \simeq V_2 \sin^2 \pi \beta j + \xi k_2 V_2 \sin 2\pi \beta j + \xi^2 (k_1^2 V_1 + k_2 V_2 \cos 2\pi \beta j) \quad (2.40)$$

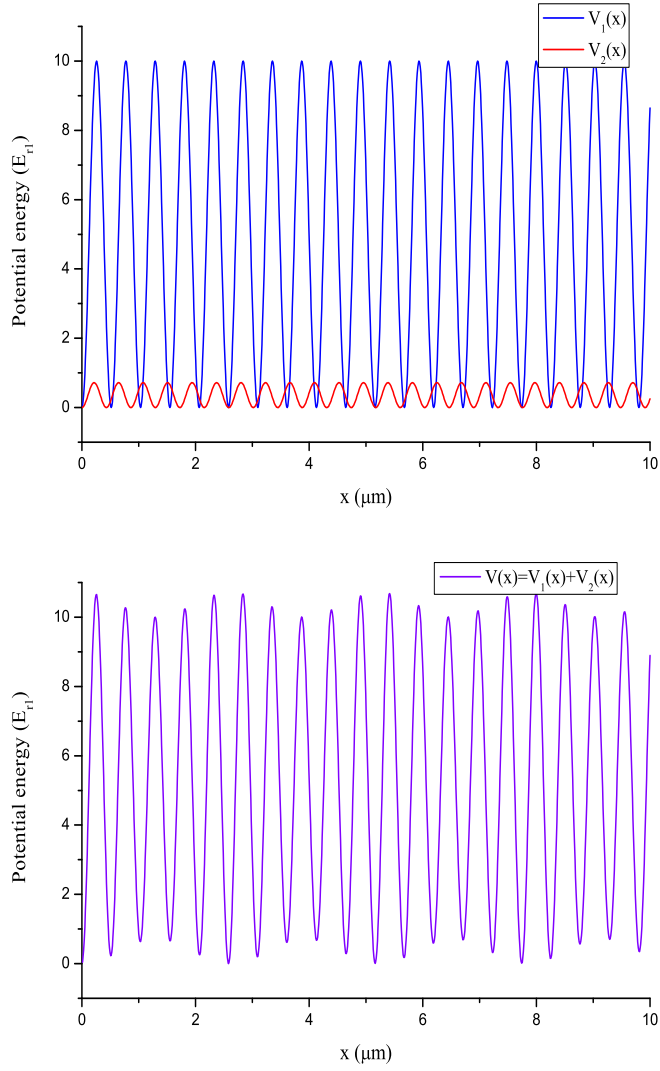


Figure 2.9: A quasi-periodic optical lattice created by superposition of a main lattice with $s_1 = 10$ and $\lambda_1 = 1032$ nm and a secondary one with $s_2 = 0.5$ and $\lambda_2 = 862$ nm. The position is expressed in μm and the potentials are expressed in units of energy recoil $E_{r1} = \hbar^2 k^2 / 2m$.

2.4. Disordered optical potentials

where $\beta = k_2/k_1$. By requiring the stationarity of $V(x_j + \xi)$ is possible to find that the correction to the minima position is

$$\xi_j \propto \frac{k_2 V_2}{k_1 V_1} \sin \pi \beta j \quad (2.41)$$

Usually this correction can be neglected, and the second lattice introduces a compositional disorder over the regular structure defined by the main lattice, differently from the topological one created by optical speckles. The energy in the potential minima can be calculated as

$$E_j = V(x_j + \xi_j) \simeq V_2 \sin^2 \pi \beta j \left(1 - 2 \frac{k_2^2 V_2}{k_1^2 V_1} \cos^2 \pi \beta j \right) \simeq V_2 \sin^2 \pi \beta j \quad (2.42)$$

where the correction due to finite ξ_j can be neglected in the hypothesis that $V_2 \ll V_1$. Two adjacent sites have an energy difference of

$$\delta_j = E_{j+1} - E_j = V_2 \left[\sin^2 \pi \beta (j+1) - \sin^2 \pi \beta j \right] = V_2 \sin \pi \beta \sin \pi \beta (2j+1) \quad (2.43)$$

where the maximum energy difference depends on the ratio $\beta = \lambda_1/\lambda_2$.

We can now analyse the distribution of the on-site potential energy of the bichromatic lattice, comparing it to the random disorder with uniform (speckles) and gaussian (Anderson model [1]) distributions. The qualitative difference of the bichromatic potential, with respect to random ones with uniform and gaussian distribution, is apparent from the plot of the on-site potential energy over a large spatial range ($L = 10^3$ sites) that we report in Fig. 2.10. Contrarily to the random cases, in the case of the bichromatic lattice the pattern that we obtain reveals a deterministic and correlated character of the quasi-periodic potential. In Fig. 2.10 we compare also the different energy distributions, calculated in a range of 10^4 sites. In the central region the distribution of the quasi-periodic lattice is very similar to the uniform and the gaussian one. The important difference are the peaks at the borders ($E = \pm E_{r1}$ in this case). This is due to the fact that the on-site energies follow the sinusoidal shape of the beating between the two lattices, whose derivative is almost constant in the central region and is smaller close to the maxima and the minima (Fig. 2.10).

The most important difference of the quasi-periodic potential is in the cor-

2. ULTRA-COLD GASES IN DISORDERED POTENTIALS

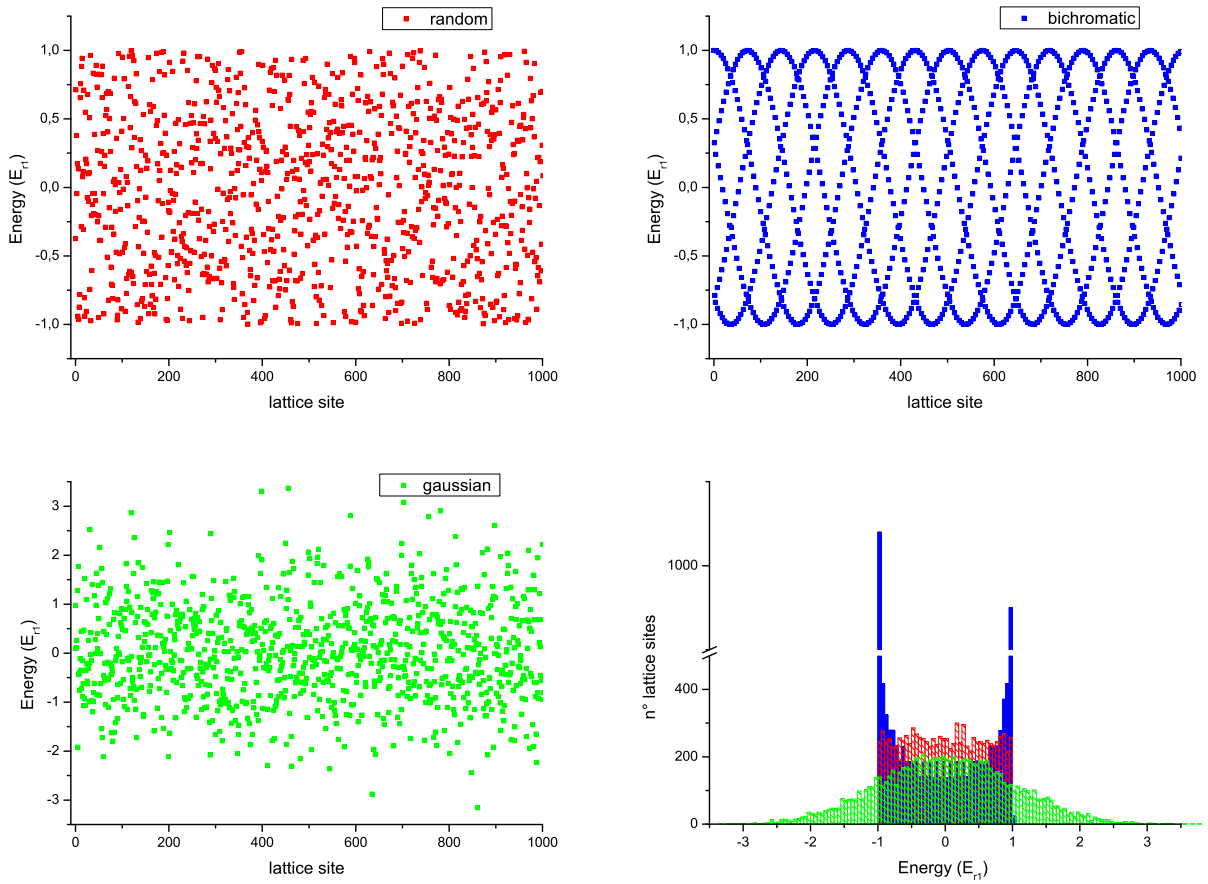


Figure 2.10: Energy distributions for random (red), bichromatic (blue) with and gaussian (green) disorder (estimated over 10000 sites). In the random and bichromatic disorder we chose $E_j \in [-E_{r1}, E_{r1}]$ and in the gaussian one we put the width equal to E_{r1} .

2.4. Disordered optical potentials

relation between the energies E_i , that is defined as:

$$C(j) = \langle E_i E_{i+j} \rangle - \langle E_i \rangle^2 \quad (2.44)$$

In the case of the bichromatic lattice the correlation function has a well defined sinusoidal shape (Fig. 2.11). The quasi-periodic potential is therefore deterministic and correlated.

The main difference between random and quasi-periodic potentials is in the fact that a purely random disorder in a 1D infinite system is able to localize it for any vanishing intensity, whereas in the bichromatic lattice, as we will analyze in details in Chapter 3, the system is localized only if the disorder is strong enough to overcome a certain threshold which separates localized from extended states. Therefore, if the degree of disorder is great enough, also the one-dimensional incommensurate optical lattice reproduces the same localization physics of the pure random system [30, 57].

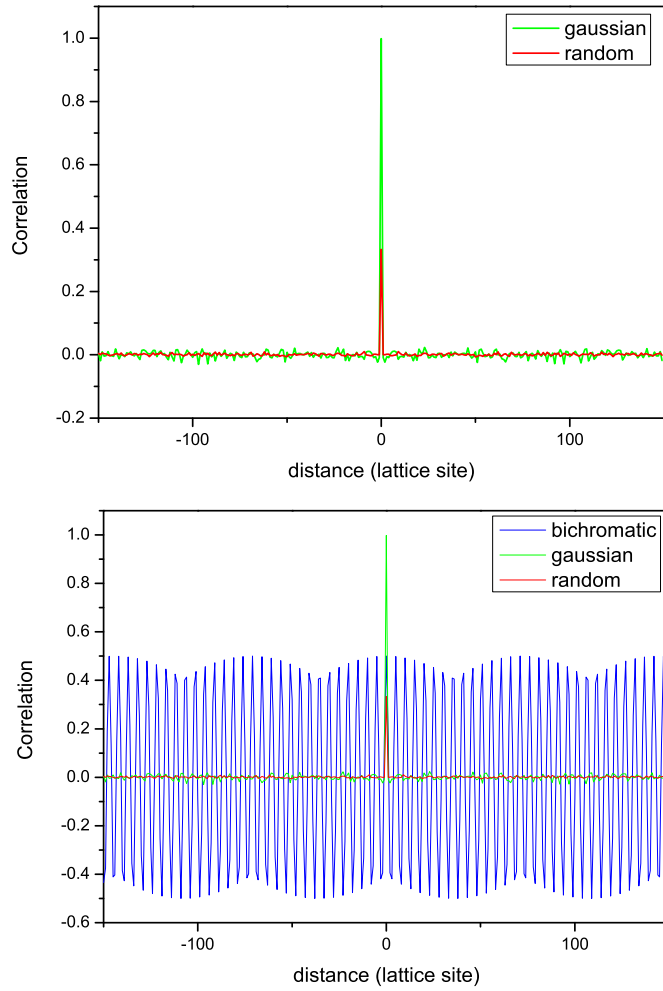


Figure 2.11: Correlation function (eq. 2.44) of the energy in the minima for random (red), gaussian (green) and bichromatic (blue) disorder. The correlation function in the quasi-periodic case presents a deterministic behaviour.

Chapter 3

Anderson localization in incommensurate lattices

It is well known that the Anderson transition from extended to localized states induced by purely random disorder can be observed only in systems with two dimensions or more. In an infinite 1D system, in fact, even an arbitrarily small amounts of disorder is able to localize the system. On the contrary in a quasi-periodic system like a bichromatic incommensurate lattice, localization transition can be observed even in 1D. This possibility has been shown by Aubry-André model, which predicts to have localized wavefunctions only for a degree of disorder larger than a certain threshold [14].

We discuss here the analogy between the transition predicted by the Aubry and André in their model and the Anderson transition in a 1D system. While in the case of a random disorder the threshold of localization changes with the finite dimension of the system L , the Aubry-André model has a unique value of the critical disorder for localization.

In the first part of the Chapter (Section 3.1) we limit our analysis to the non interacting system, which represents the case we mainly studied from the experimental point of view. The situation is instead different if interactions between particles are present in the system. Since we have the possibility to tune interactions in the experiment, we briefly analyse the case of a weakly repulsive interaction, which tend to contrast localization (Section 5.2).

3.1 Theory of localization of non-interacting particles

The Anderson model considers a 3D periodic system in which a disorder has been introduced on the site energy E_j , randomly distributed with probability $P(E_j)$ characterized by a width W . A *tunneling* matrix element $V_{jk}(\mathbf{r}_{jk})$ couples the sites, transferring atoms from one site to the next. The Anderson model is a single particle model and is defined in terms of the probability amplitude a_j that a particle is on the site j , whose dynamics is described by the equation

$$i\hbar\dot{a}_j = E_j a_j + \sum_{k \neq j} V_{jk} a_k \quad (3.1)$$

Since we are considering a periodic lattice, we can expand the particle wavefunction over a set of Wannier states (Subsection 2.3.1) $|w_j\rangle$

$$|\psi\rangle = \sum_j c_j |w_j\rangle \quad (3.2)$$

and the Anderson model's Hamiltonian becomes

$$H = \sum_{j,k \neq j} V_{j,k} |w_j\rangle \langle w_k| + \sum_j E_j |w_j\rangle \langle w_j| \quad (3.3)$$

This is the Hamiltonian in the case of purely random disorder, as considered by Anderson in his model. We can now consider the case of our experiment where we introduce the disorder with the secondary incommensurate lattice, whose theoretical treatment follows the Aubry-André model. In this case the Hamiltonian is the following:

$$\begin{aligned} H &= -\frac{\hbar^2}{2m} \nabla_x^2 + s_1 E_{r1} \cos^2(k_1 x) + s_2 E_{r2} \cos^2(k_2 x + \phi) = \\ &= -\frac{\hbar^2}{2m} \nabla_x^2 + V_1(x) + V_2(x) \end{aligned} \quad (3.4)$$

We can project the wavefunction $|\psi\rangle$ over a set of maximally localized Wannier states $|w_j\rangle$

$$H \longrightarrow \sum_{i,j} |w_i\rangle \langle w_i| H |w_j\rangle \langle w_j| \quad (3.5)$$

3.1. Theory of localization of non-interacting particles

where we can calculate

$$\begin{aligned} \langle w_i | H | w_j \rangle &= \int dx w_i^*(x) H w_j(x) = \int dx w_i^*(x) \left(-\frac{\hbar^2}{2m} \nabla_x^2 + V_1(x) \right) w_j(x) + \\ &+ \int dx w_i^* V_2(x) w_j(x) \quad (3.6) \end{aligned}$$

In tight binding limit and in the case in which we have only coupling towards neighbouring sites, we obtain:

$$\langle w_i | H | w_j \rangle \longrightarrow \epsilon_0 \delta_{i,j} - J E_{r1} \delta_{i,j \pm 1} + \delta_{i,j} \int dx s_2 E_{r2} \cos^2(k_2 x + \phi) |w_i(x)|^2, \quad (3.7)$$

where J is the tunneling matrix element between neighboring lattice sites. The latter depends on the depth of the main lattice as [58]

$$J \simeq 1.43 s_1^{0.98} e^{-2.07 \sqrt{s_1}}, \quad (3.8)$$

in units of the recoil energy E_{r1} of the main lattice. Neglecting the constant terms and using the relation $\cos^2(\alpha) = (\cos(2\alpha) + 1)/2$, with $\alpha = k_2 x + \phi$ we obtain

$$\langle w_i | H | w_j \rangle \longrightarrow -J E_{r1} \delta_{i,j \pm 1} + \delta_{i,j} \frac{s_2 E_{r2}}{2} \int dx \cos(2k_2 x + \phi') |w_i(x)|^2 \quad (3.9)$$

it is possible to demonstrate that

$$\begin{aligned} \int dx \cos(2k_2 x + \phi') |w_i(x)|^2 &= \cos(2k_2 x_i + \phi') \int dx \cos(2k_2 x) |w(x)|^2 = \\ &= \cos(2\pi\beta i + \phi') \int dx \cos(2\beta k_1 x) |w(x)|^2 \quad (3.10) \end{aligned}$$

where $\beta = \lambda_1/\lambda_2$ is the ratio of the two lattice wave numbers. Using a gaussian approximation for the Wannier function:

$$|w(x)|^2 \simeq \frac{k_1}{\sqrt{\pi}} s_1^{1/4} e^{-\sqrt{s_1}(k_1 x)^2} \quad (3.11)$$

we have

$$\int dx \cos(2\beta k_1 x) |w_x|^2 = e^{-\frac{\beta^2}{\sqrt{s_1}}} \quad (3.12)$$

and

$$\langle w_i | H | w_j \rangle \longrightarrow -J E_{r1} \delta_{i,j \pm 1} + \delta_{i,j} \frac{s_2 E_{r2}}{2} \cos(2\pi\beta i + \phi') e^{-\beta^2/\sqrt{s_1}} \quad (3.13)$$

3. ANDERSON LOCALIZATION IN INCOMMENSURATE LATTICES

Defining

$$\Delta = \frac{s_2 E_{r2}}{2E_{r1}} e^{-\beta^2/\sqrt{s_1}} \quad (3.14)$$

we obtain the Hamiltonian of the Aubry-André model [15]

$$H = -J \sum_j (|w_j\rangle\langle w_{j+1}| + |w_{j+1}\rangle\langle w_j|) + \Delta \sum_j \cos(2\pi\beta j + \phi') |w_j\rangle\langle w_j| \quad (3.15)$$

In the limit in which $\sqrt{s_1} \gg \beta^2$, we can approximate the disorder parameter Δ with [59]

$$\Delta = s_2 \frac{E_{r2}}{2E_{r1}} \quad (3.16)$$

that is directly connected to the energy distribution of the minima of the lattice (E_j) induced by the perturbation of the second lattice, in units of recoil energy of the main lattice (E_{r1}) (Subsection 2.4.2):

$$E_j = \frac{s_2 E_{r2}}{E_{r1}} \cos^2(k_2 x_j + \phi) = \Delta (\cos(2\pi\beta j + 2\phi) + 1) \quad (3.17)$$

The Aubry-André Hamiltonian (eq. 3.15) can be written as:

$$H = -J \sum_j (|w_j\rangle\langle w_{j+1}| + |w_{j+1}\rangle\langle w_j|) + \sum_j E_j |w_j\rangle\langle w_j| \quad (3.18)$$

which corresponds to (eq. 3.3). An other representation that we can use for the Aubry-André model consists on using the amplitude coefficients c_j over each Wannier function (eq. 3.2):

$$\begin{aligned} \langle \psi | H | \psi \rangle &= \sum_{l,k} c_l^* \langle w_l | \left[\sum_{i,j} \langle w_i | H | w_j \rangle \langle w_j | \right] c_k | w_k \rangle = \sum_{i,j} c_i^* c_j \langle w_i | H | w_j \rangle = \\ &= -J \sum_j (c_{j+1}^* c_j + c_j^* c_{j+1}) + \Delta \sum_j \cos(2\pi\beta j + \phi') c_j^* c_j \end{aligned} \quad (3.19)$$

This model was originally studied by Harper [13], with $\Delta = 2J$ and variable β . The model by Aubry-André, instead, finds that a transition from extended to localized states occurs by increasing the potential strength $\lambda = \Delta/J$, considering for β a so-called irrational diophantic number, that is kept fixed. Usually it is convenient to choose $\beta = \frac{F_{i-1}}{F_i}$ as the ratio between two successive Fibonacci number F_{i-1} and F_i [60]. In the limit of large systems, β approaches the inverse of the golden mean, $(\sqrt{5} - 1)/2$. In this case the

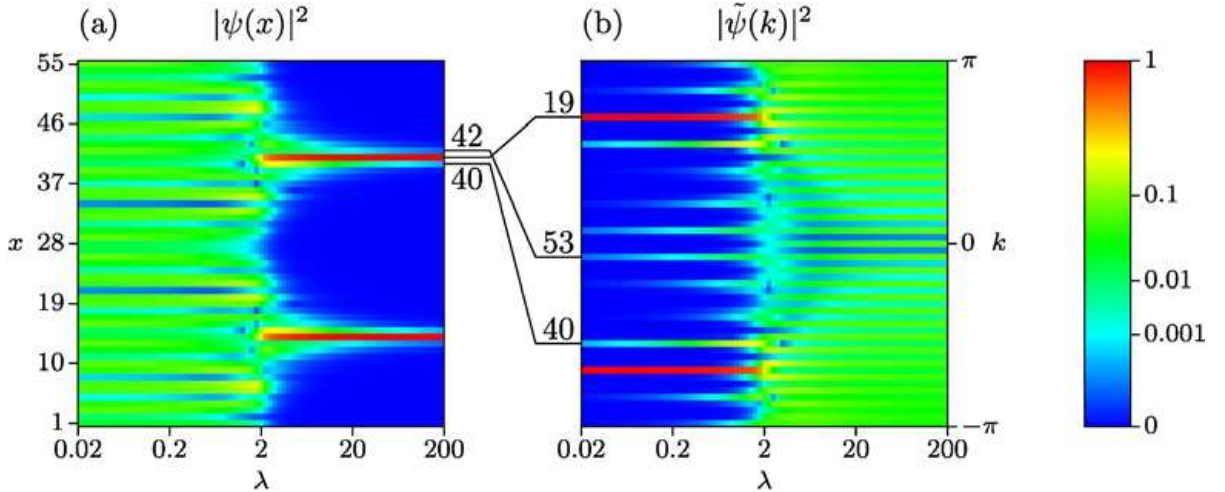


Figure 3.1: Real space (a) and momentum space (b) probability density as a function of the potential strength $\lambda = \Delta/J$. On the real space we can observe the transition between extended states (for $\lambda < 2$) and localized states (for $\lambda > 2$). On the contrary, on the momentum space the transition is between localized states (for $\lambda < 2$) and extended states (for $\lambda > 2$). Taken from [15].

model predicts a sharp "metal-insulator" transition to localized states, for $\lambda > 2$.

This peculiarity of the Aubry-André model to have a unique threshold of the transition, can be shown if we express the problem in the momentum space. We transform the Wannier states into the eigenfunction of the momentum operator

$$|k\rangle = \frac{1}{\sqrt{L}} \sum_j e^{i2\pi k\beta j} |w_j\rangle \quad (3.20)$$

which are eigenstates of the momentum operator to eigenvalues $kF_{i+1} \bmod F_i$. Neighbouring values of k therefore do not imply neighbouring momentum eigenvalues. We obtain for the Hamiltonian

$$H = \frac{\lambda}{2} \left[\sum_k (|k\rangle\langle k+1| + |k+1\rangle\langle k|) + \frac{4}{\lambda} \sum_k \cos(2\pi\beta k) |k\rangle\langle k| \right] \quad (3.21)$$

where $\lambda = \Delta/J$ is the potential strength (App. B).

The Hamiltonian in the phase space (eq. 3.21) is practically identical to the one in the real space (eq. 3.15). The only difference is the parameter which determines the transition point: in the real space it is equal to λ , whereas

3. ANDERSON LOCALIZATION IN INCOMMENSURATE LATTICES

in the momentum space it is $4/\lambda$. On the other hand the point in which the system localizes on the real space, has to be the same respect to the point in which there is a delocalization in the momentum space. Therefore the only possibility is to have the self-dual point

$$\lambda = \frac{4}{\lambda} = 2 \quad (3.22)$$

which separates the regimes of extended and localized states (both in the real and in the momentum space).

The duality of the model can be observed also in (Fig. 3.1), where are reported the densities in the real ($|\psi(x)|^2$) and in the momentum spaces ($|\tilde{\psi}(k)|^2$) as a function of the potential strength λ .

The ideal case $\beta = (\sqrt{5} - 1)/2$ is not easy to be reproduced experimentally; in our experiment, for example, we have a $\beta = 1.197$ and the theory predicts that the transition occurs with a crossover, whose broadening and onset depend on the degree of "irrationality" of β (Fig. 3.2). The system presents extended states for $\Delta/J < 2$, where it starts to localize over increasingly small distances. When $\Delta/J > 7$ the system gets localized over a single lattice constant. In this regime the eigenstates are localized states with a distance each other of ~ 5 lattice sites, corresponding to the beating of the bichromatic lattice.

Others important peculiarities of the Aubry-André Hamiltonian can be found if we write it in the space of quasimomentum vectors:

$$|l\rangle = \frac{1}{\sqrt{L}} \sum_j e^{i2\pi j \frac{l}{L}} |w_j\rangle \quad (3.23)$$

whose eigenvalues are $k_l = 2k_1 l/L$. It is possible to demonstrate (App. B) that, in the case of $\beta > 1$, the term of disorder in the Hamiltonian couples only eigenstates with a difference

$$\begin{aligned} \Delta l &= l' - l = \pm(\beta - 1) \\ \Delta l &= l' - l = \pm(2 - \beta) \end{aligned} \quad (3.24)$$

The quasimomentum $k = 0$ therefore is coupled only with

$$\begin{aligned} k' &= \pm 2(k_2 - k_1) \\ k'' &= \pm(2k_1 - 2(k_2 - k_1)). \end{aligned} \quad (3.25)$$

3.1. Theory of localization of non-interacting particles

We will later see how these can be observed in the experiment. In the Anderson model each quasimomentum vector has a finite coupling with all the others and this causes the peculiarity that a vanishing amount of disorder is enough to localize the system (delocalization in the momentum space). The Aubry-André Hamiltonian, instead, is able to localize the system only if the amplitude of the disorder is able to couple more quasimomentum states.

An often employed quantity, useful to give a more quantitative analysis, is

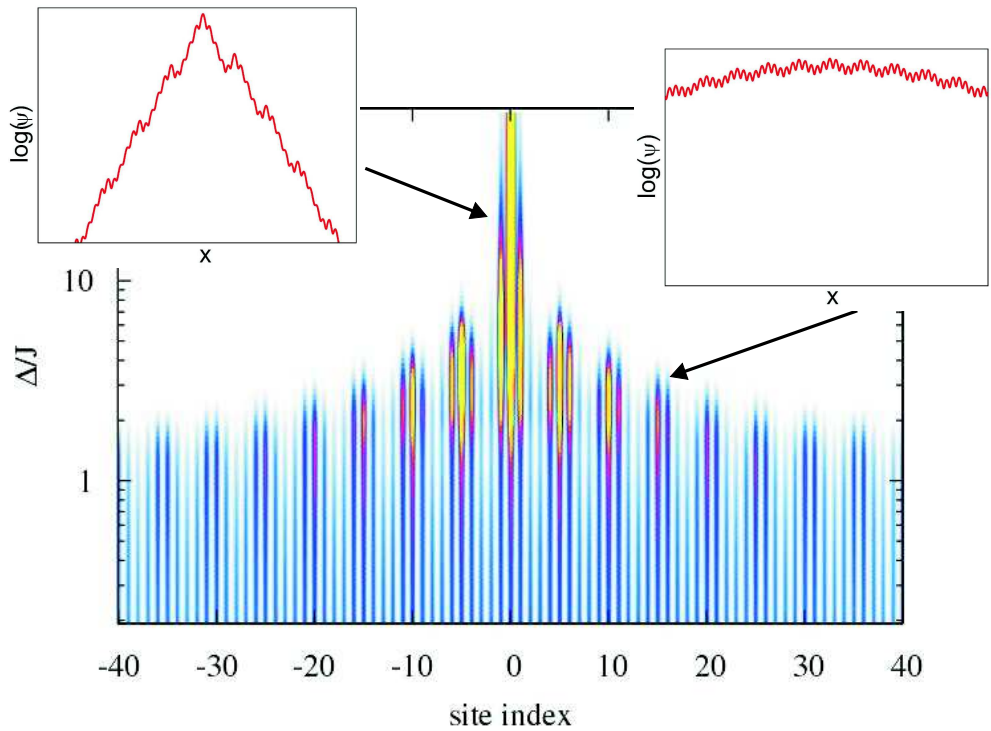


Figure 3.2: Real space probability density as a function of the potential strength Δ/J for $\beta = 1.197$. On the real space we can observe the crossover between extended states (for $\Delta/J < 2$) and states exponentially localized on length smaller than the lattice constant (for $\Delta/J > 7$), with Δ defined as eq. 3.16.

the inverse participation ratio in real space [61, 62]:

$$P_x = \sum_j |c_j|^4 \quad (3.26)$$

where the coefficients $c_j = \langle w_j | \psi \rangle$ of the expansion of the wavefunction on the set of Wannier states (eq. 3.2) are normalized according to $\sum_j |c_j|^2 = 1$.

3. ANDERSON LOCALIZATION IN INCOMMENSURATE LATTICES

The inverse of P_x is the number of lattice sites over which the wave function is distributed. In fact, if the state ψ is localized over a single state w_l , we have that $c_j = \delta_{j,l}$ and $P_x = 1$. If the state is equally distributed over N sites, we instead obtain that $c_j = 1/\sqrt{N}$ and $P_x = 1/N$.

We can define the correspondent quantity in the momentum space:

$$P_k = \sum_j |d_j|^4 \quad (3.27)$$

where

$$d_j = \sqrt{L} \sum_l e^{(i2\pi j \frac{l}{L})} c_l \quad (3.28)$$

The inverse participation ratio is useful if we want to analyse the difference between the Anderson and the Aubry-André model. We can compare this quantity for the two different models as a function of the height of disorder (Fig. 3.3). Both models present a monotonic increase of the spatial inverse participation ratio as the disorder increases, corresponding to the transition towards localized states. Conversely, the inverse participation ratio on the momentum space decreases as the strength of disorder increases. The behavior in both models appears to be the same, with an important difference when the system size is changed. In the Anderson model, in fact, when $L \rightarrow \infty$ the eigenvalues are exponentially localized for any vanishing degree of disorder. Conversely, in the Aubry-André model, for sufficiently large system size, there is a sharp transition fixed at $\lambda = 2$, for any size of the system. In this case, by increasing the size L the transition becomes sharper (Fig. 3.4). We can conclude that the disorder due to the incommensurate secondary lattice induces a localization with a universal scaling behaviour. The position of the transition, in fact, doesn't depend separately from the disorder Δ or from the tunneling rate J of the main lattice, but only from the ratio between these two values $\lambda = \Delta/J$.

It is possible to demonstrate also that [14]:

- for $\lambda > 2$ the eigenfunctions are localized with the same localization length ℓ , which depends only from λ as:

$$\ell = \frac{1}{\log \frac{\lambda}{2}} \quad (3.29)$$

in units of the lattice constant.

3.1. Theory of localization of non-interacting particles

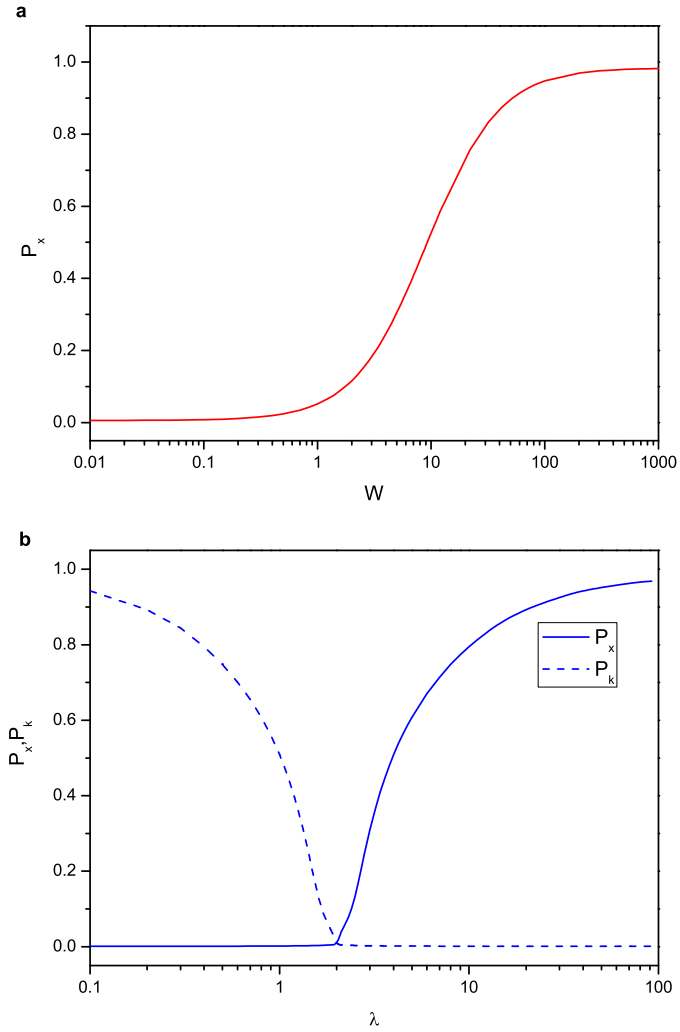


Figure 3.3: Inverse participation ratio in real space (full line) and momentum space (dashed line) as a function of disorder strength for the Anderson model with $L = 1000$ (a) and Aubry-André model with $L = 1600$ (b) calculated for our experimental case ($\beta = 1.197$). The curves represent averages over all the eigenstates of the Hamiltonians eq. 3.3 and eq. 3.15 for the Anderson and Aubry-André model respectively. In the Anderson case the curves represent an average over 50 disorder realizations.

3. ANDERSON LOCALIZATION IN INCOMMENSURATE LATTICES

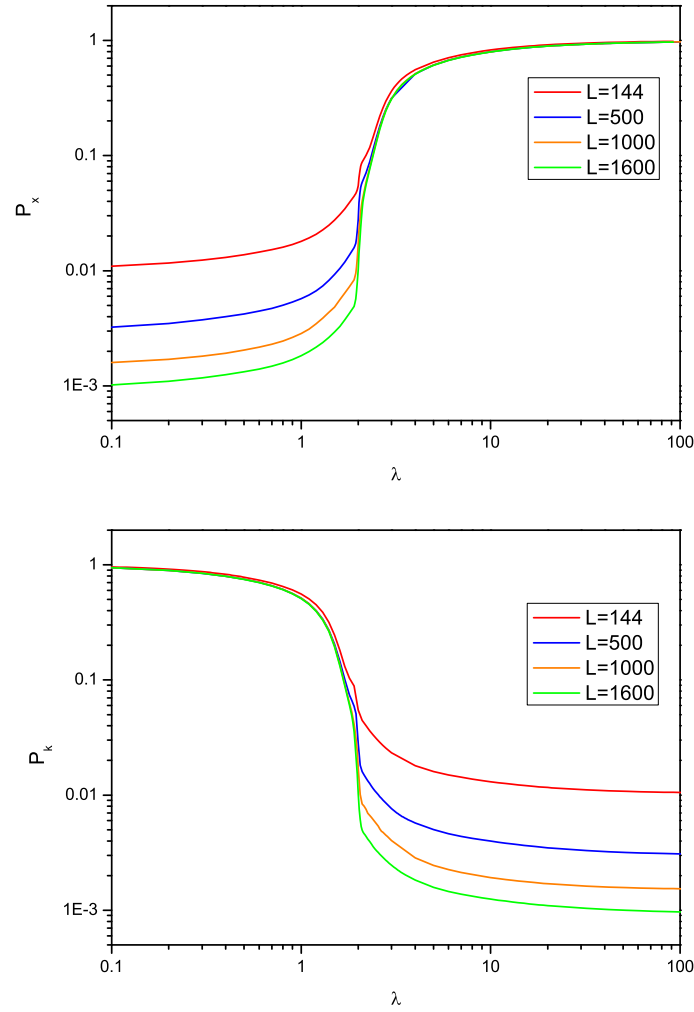


Figure 3.4: Inverse participation ratio in real space (a) and momentum space (b) as a function of disorder strength λ for the Aubry-André model with different values of the system size L ($L = 144, 500, 1000$ and 1600) calculated for our experimental case ($\beta = 1.197$).

3.1. Theory of localization of non-interacting particles

- Conversely, for $\lambda < 2$ the eigenfunctions are extended modulated plane waves.
- The case of $\lambda = 2$ represents a limiting case, in which the eigenfunctions are neither extended plane waves nor exponentially localized functions.

3. ANDERSON LOCALIZATION IN INCOMMENSURATE LATTICES

Chapter 4

Experimental realization of a weakly interacting Bose-Einstein condensate

The starting point of the experiments described in this thesis is a Bose-Einstein condensate of ^{39}K with tunable interactions [12], as we discussed in Chapter 3. In order to experimentally reproduce the Aubry-André model, we want to create a system constituted by non-interacting particles. As we said in Section 5.2, in fact, interactions could mask the physics of Anderson transition. Potassium-39 has a natural negative scattering length [63, 64], corresponding to an attractive interaction, which would induce an instability towards the collapse for the BEC [65, 66, 67]. However, by using a Feshbach resonance, it is possible not only to condense ^{39}K , by tuning the scattering length to positive values, but also to reduce the interaction energy almost to zero. ^{39}K actually is an excellent system for the creation of a weakly interacting BEC, thanks to the presence of a broad resonance combined with a small background scattering length [68]. Indeed, considering the dependence of the scattering length from the magnetic field, on a Feshbach resonance at $B = B_0$ (Section 2.1)

$$a(B) = a_{bg} \left(1 - \frac{W}{B - B_0} \right) \quad (4.1)$$

we can extrapolate the behavior of a around the magnetic field B_{zc} at which a crosses zero:

$$a(B) \sim \frac{a_{bg}}{W} (B - B_{zc}) \quad (4.2)$$

4. EXPERIMENTAL REALIZATION OF A WEAKLY INTERACTING BOSE-EINSTEIN CONDENSATE

The parameter that is important in order to control interaction around $a = 0$ is the ratio a_{bg}/W : the smaller it is, the better is the accuracy in tuning the interaction.

For the resonance in $|1, 1\rangle$ close to 400 G, whose width is $W = 52$ G and $a_{bg} \simeq -29a_0$, the theoretical prediction for the slope is of $da/dB \sim 0.55a_0/\text{G}$ around $B = 350$ G. This degree of control is superior than to most other species, which present narrower resonances and/or larger background scattering lengths. The only species which could be better respect to ^{39}K in order to control the scattering length around the zero crossing is ^7Li [69]. In our experiment the stability of the Feshbach magnetic field is of the order of 0.1 G, which allows a control on the tuning the scattering length to zero to better than $0.1 a_0$. In this regime the magnetic dipole-dipole interaction energy, which is usually negligible in standard alkali condensate, becomes important. The requirement to study Anderson localization, it is to minimize the total interaction energy. We studied the interplay of the two different interactions and we found that they can partially compensate each other. Therefore the best choice is a scattering length value able to compensate for the dipolar interaction.

As we will describe later, one possibility to find the magnetic field value able to minimize the interaction energy it is to study the energy released from the condensate during the expansion from the trapping potential. However, a more sensitive method is to minimize the decoherence induced by interactions during the phenomenon of Bloch oscillation into a vertical lattice.

4.1 Realization of BEC of ^{39}K with tunable interaction

At zero magnetic field the collisional properties of ^{39}K do not favour direct evaporative cooling [70, 71]. However it is possible to use ^{87}Rb in order to sympathetically cool ^{39}K . The sympathetic cooling for ^{39}K has been proven to work [71], with the same efficiency that has been observed for the other potassium isotopes (^{41}K and ^{40}K) [72, 73], in spite of the small heteronuclear scattering length ^{39}K - ^{87}Rb [74, 75].

The apparatus that we used in order to prepare the ^{39}K BEC is accurately

4.1. Realization of BEC of ^{39}K with tunable interaction

described in previous thesis in our group [76, 77, 78, 79, 80]. I will describe now just a brief summary of the experimental techniques that we used, which are similar to the ones already used for the other potassium isotopes [72, 73]:

- Laser cooling and trapping of ^{87}Rb and ^{39}K atoms in a magneto-optical trap [81]
- Transfer of the two species in a magnetic potential in their stretched Zeeman states $|F = 2, m_f = 2\rangle$
- Selective μ -wave evaporation of ^{87}Rb atoms and sympathetic cooling of ^{39}K ones, via ^{87}Rb - ^{39}K collisions. The temperature of the mixture is lowered from about $100\ \mu\text{K}$ to $T = 800\ \text{nK}$. At this point it becomes necessary to use Feshbach resonances in order to further cool K atoms. Therefore we need a different kind of trapping potentials that is compatible with the application of the Feshbach magnetic field.
- Loading of ^{39}K - ^{87}Rb mixture into the optical dipole trap and transfer of the two species in their absolute ground state $|F = 1, m_f = 1\rangle$. The optical trap is produced with two focused laser beams at wavelength $\lambda = 1032\ \text{nm}$ (Fig. 4.1).
- An homogeneous magnetic field is applied in order to tune inter- and intraspecies interactions. Atoms are further cooled by reducing the intensity of the optical trap. The evaporation in the optical trap is performed in two steps. During the first one the magnetic field is on one of the heteronuclear Feshbach resonances that exist in this mixture [75], so that collisions between Rb and K atoms increase. The evaporation is performed in order to evaporate atoms in the vertical direction, that corresponds to evaporate mainly the heavier Rb atoms. K in this first step is sympathetically cooled. When K is close to quantum degeneracy, the magnetic field is tuned on the homonuclear Feshbach resonance [79] in order to have a positive value of a . In this second step of the evaporation Rb is completely evaporated from the trap and cooling of K relies just with intraspecies collisions (Fig. 4.3).

4. EXPERIMENTAL REALIZATION OF A WEAKLY INTERACTING BOSE-EINSTEIN CONDENSATE

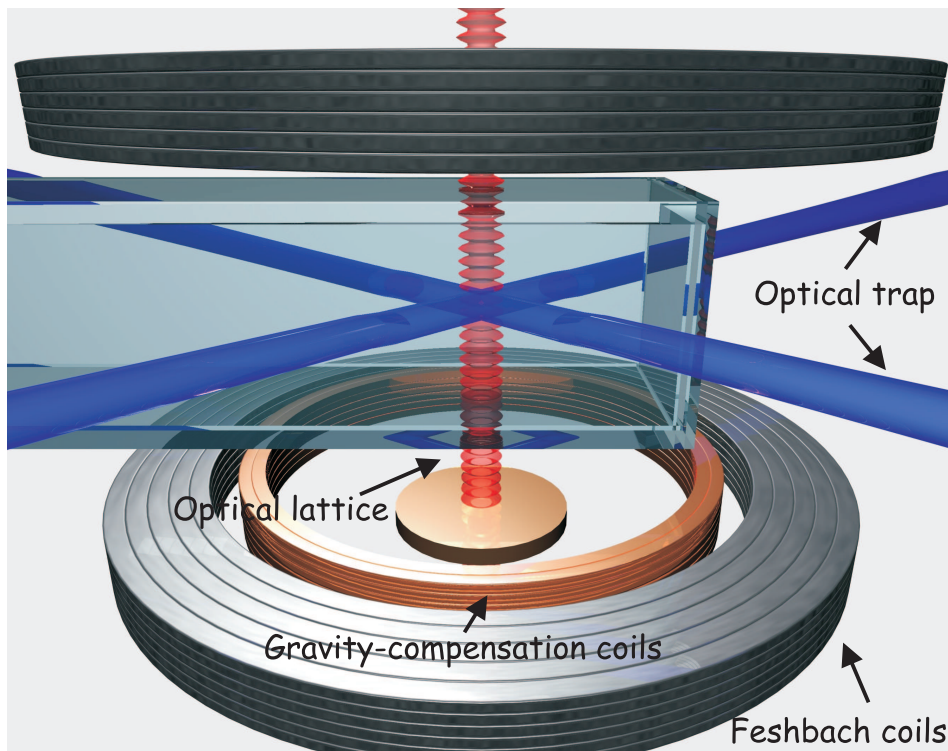


Figure 4.1: Scheme of the experimental apparatus. The optical dipole trap is created by means of two focused laser beam (waist $\simeq 100 \mu\text{m}$) with $\lambda = 1032 \text{ nm}$, crossing on the horizontal plane. The Feshbach magnetic field is generated by means of a couple of coils in Helmholtz configuration, with axis in the vertical direction and centered on the optical trap position. The Feshbach field can be controlled in the range $0 \div 1000 \text{ G}$ with an accuracy better than 100 mG . The lattices that we used for the experiments described in this thesis are aligned in the vertical direction. Another couple of coils is used to compensate the gravity.

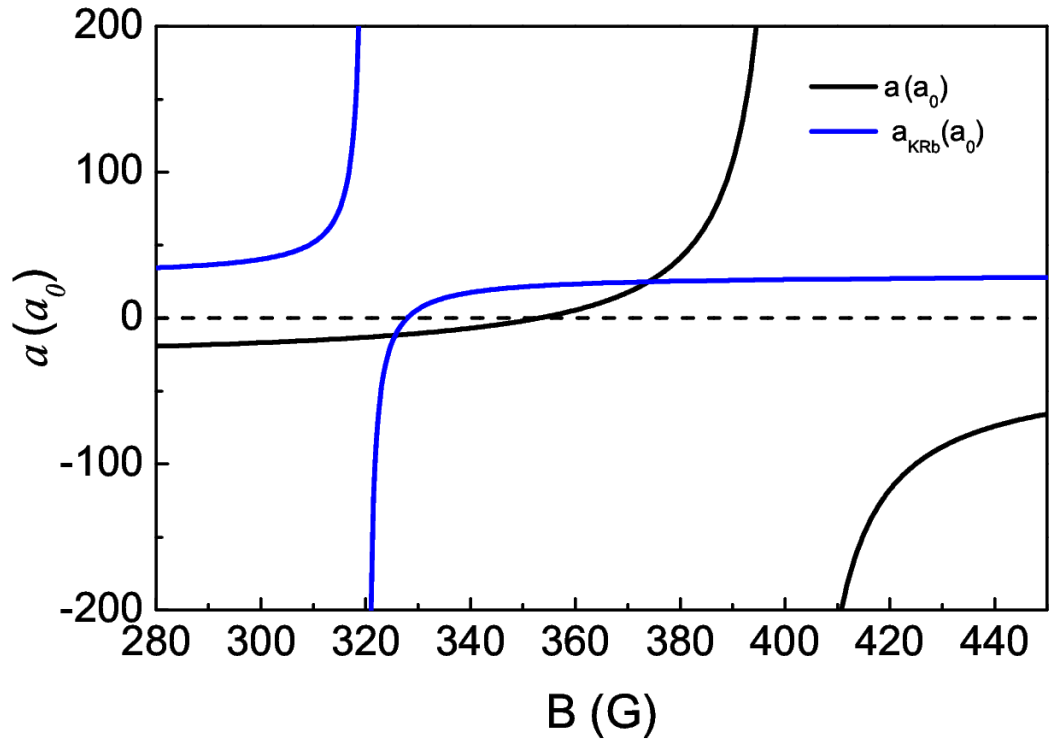


Figure 4.2: Behaviour of a (black line) and of a_{KRb} (blue line) as a function of the magnetic field. The first part of evaporation, on the heteronuclear Feshbach resonance, is performed at $B = 316$ G, where $a = -33a_0$ and $a_{KRb} = 150a_0$. The second part of the evaporation is done on the homonuclear resonance at $B = 395.2$ G, where $a = 180a_0$ and $a_{KRb} = 28a_0$.

4. EXPERIMENTAL REALIZATION OF A WEAKLY INTERACTING BOSE-EINSTEIN CONDENSATE

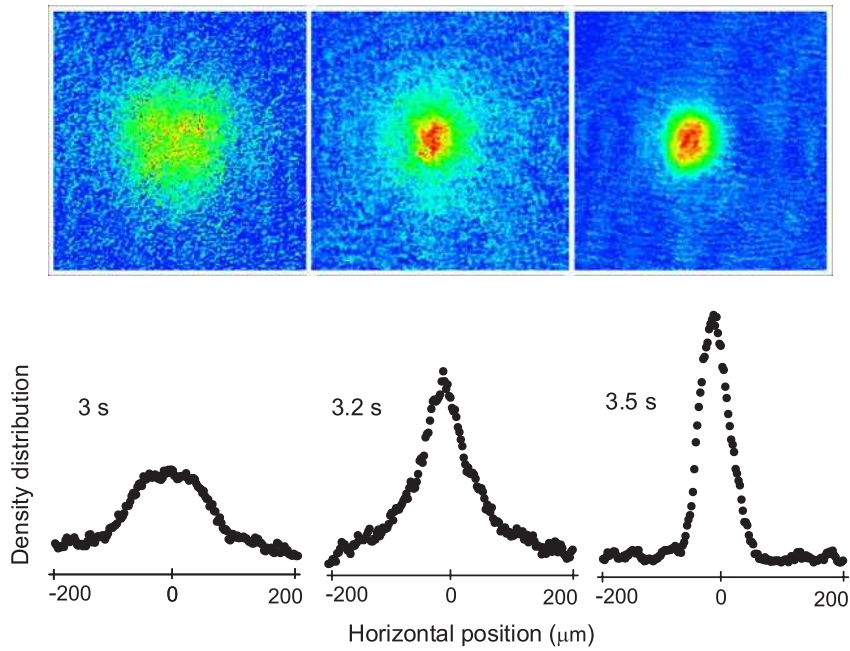


Figure 4.3: Phase transition to a BEC in the final part of the evaporation in the optical trap. The images are taken after 15 ms of ballistic expansion and for three different times of the evaporation. The profiles are obtained by an integration of the density in the vertical direction.

4.1.1 Weakly interacting ^{39}K condensate

Once the condensate is produced, a can be further tuned in order to produce a weakly interacting condensate. By means of Feshbach spectroscopy [68] we have developed a collisional model able to predict the magnetic field dependence of the scattering length a . In particular, we are interested in the magnetic field value for which the scattering length is zero. For the resonance at about 400 G, the theoretical model is able to predict the zero crossing position with an accuracy of $0.4 a_0$. We briefly describe now the first experiment we used in order to check our capability of tuning interactions in the ^{39}K condensate. More details about this experiment are given in [12]. One can get an estimation of the interaction energy by measuring the release energy of the condensate from the trap. This is in general a sum of the kinetic energy and of the interaction energy in the trap. For sufficiently large a the latter dominates over the first.

The experiment started with a pure BEC created at a fixed value of magnetic field on the left side of the resonance (395 G), where $a = 180 a_0$, which was then adiabatically brought to a final field in about 100 ms. We explored the magnetic field region 350 – 402 G where the scattering length is positive and the condensate is stable. The atoms were imaged after a long ballistic expansion of 31 ms, after released from a trap with a mean oscillation frequency of 90 Hz. We extract the release energy of the atoms from the rms size of the cloud after the expansion (Fig. 4.4). For large values of a the release energy is dominated by interaction energy, which we measure to be of the order of 400 Hz. By reducing a the interaction energy decreases, until in the zero-crossing region the energy is purely kinetic, due to the zero point motion in the trap. For sufficiently large negative a the condensate collapses, and the total energy of the system rises abruptly. Comparing the experimental values of the release energy with the theoretical prediction, the collapse happens at a slightly subcritical scattering length. This could be due to a loss of adiabaticity of the magnetic field ramp in the region of negative scattering length. When the scattering length approach zero, in fact, the condensate has a vanishing frequency and could be excited [82], although the ramp duration is much longer than the trap period. However, this experiment confirms

4. EXPERIMENTAL REALIZATION OF A WEAKLY INTERACTING BOSE-EINSTEIN CONDENSATE

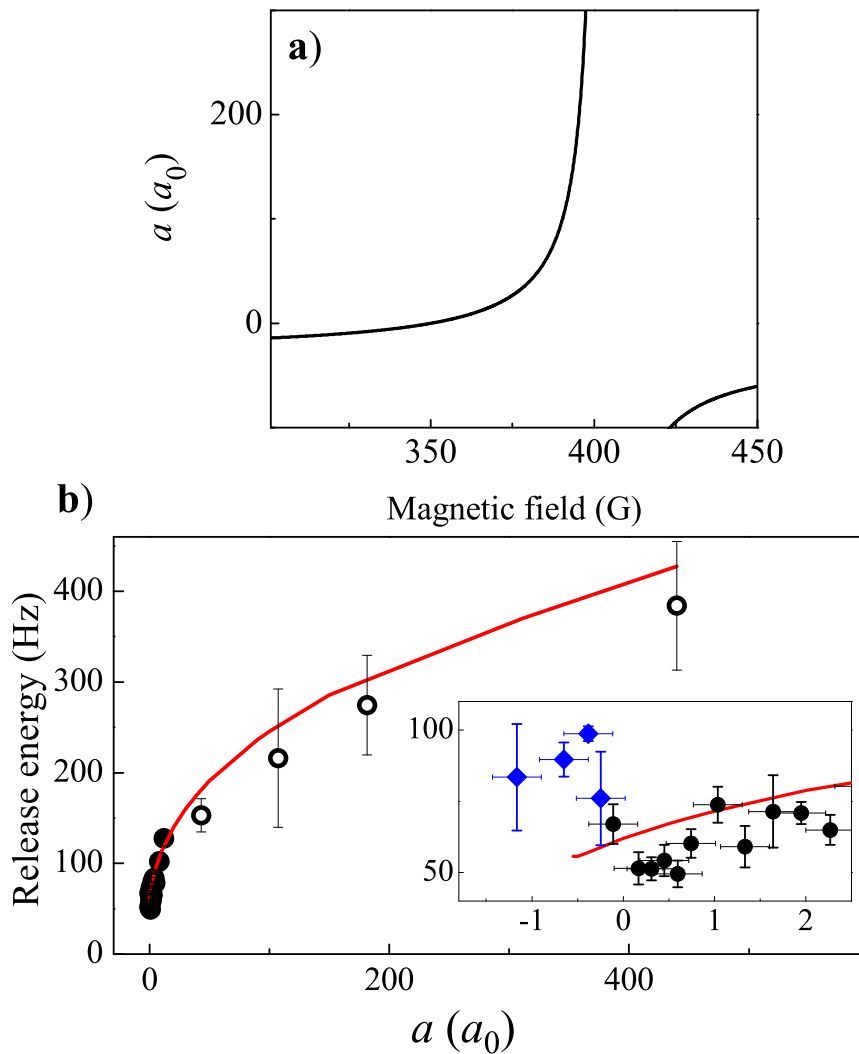


Figure 4.4: Control of the interaction in a ^{39}K condensate. a) The broad Feshbach resonance in the absolute ground state employed in this experiment. b) Release energy per atom in the condensate, as extracted from the rms size of the cloud after a long free expansion. The increase of energy for negative scattering lengths signals a collapse of the condensate. The continuous line is the prediction of the Gross-Pitaevskii theory.

our capability to tune interactions, and in particular to produce a weakly interacting BEC. In order to be more precise in the determination of the zero crossing position, we need to perform another kind of experiment.

4.2 Interferometric determination of the zero crossing position

The most sensitive technique to determine the magnetic field value of the zero-crossing is to perform an interferometric measurement which is strongly affected by the presence of interactions.

One possibility in this direction is to study the phenomenon of Bloch oscillation for a BEC in a periodic potential submitted to an external force (subsection 2.3.3). The interferometer we realized is established by a standing wave with wavelength $\lambda = 1032$ nm along the vertical direction (Fig. 4.5). The BEC prepared in the optical trap is adiabatically loaded in the vertical lattice; then the confinement of the optical trap is switched off, and atoms start to perform Bloch oscillations in the lattice under the effect of gravity, with period $T_B = 2h/F\lambda$. For ^{39}K under gravity the Bloch period is $T_B = 2$ ms. The possibility to tune interactions in the system allow us

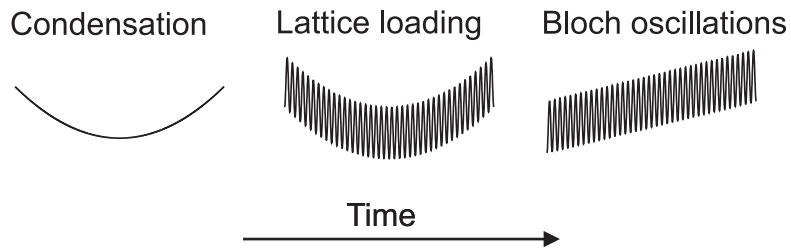


Figure 4.5: Cartoon of the experimental sequence for Bloch oscillation measurements. The atoms, condensed in the optical potential, are loaded in a vertical optical lattices, created by a back-reflected laser beam. When the optical trap is switched off, the atoms evolve in the lattice under the action of gravity and starts to perform Bloch oscillations. After a certain evolution time, the atoms are released from the lattice potential and expand freely, until we take the absorption image.

to control the decoherence induced by interactions; as we saw in subsection 2.3.3, in fact, interactions induce a destruction of the interference pattern.

4. EXPERIMENTAL REALIZATION OF A WEAKLY INTERACTING BOSE-EINSTEIN CONDENSATE

We can qualitatively see the effect of interactions on Bloch oscillations from the first experiment that we report in Fig. 4.6, where we show the absorption images of BECs released from the lattice after different times of Bloch oscillation evolution in strongly interacting ($100a_0$) and weakly interacting ($1a_0$) case. In the $a = 100a_0$ measurement the interference pattern is completely broadened and the two momentum peaks are no more distinguishable. On the contrary, in the weakly interacting case the broadening is not appreciable after only two Bloch oscillations, as an effect of the fact that reducing the scattering length we reduce the interaction-induced decoherence.

A more quantitative analysis of the effect of the interactions on the co-

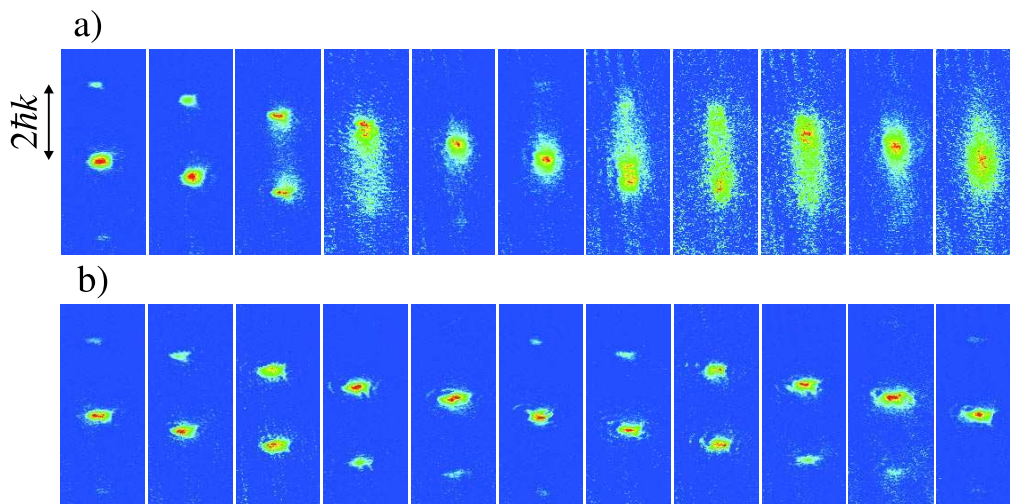


Figure 4.6: Absorption images of the cloud, taken in steps of 0.4ms from 0 to 4ms, after release from the lattice during the first two periods of Bloch Oscillations for a condensate with (a) $100a_0$ and (b) $1a_0$ of scattering length. The expansion time is 12.5 ms and the scattering value during the expansion is changed to $-33a_0$ only 3 ms before image acquisition.

herence of Bloch oscillations is reported in Fig. 4.7. We repeated the same experimental sequence for different a , measuring the width of the central peak at integer times of the Bloch period as a function of oscillation time for different values of the scattering length. The width starts to increase linearly with time, as an effect of the phase terms $\delta\varphi_i \propto g\rho_i t/h$, that evolve linearly in time. When the momentum distribution occupies the whole first Brillouin zone, the widths saturate. We can fit the linear region, and extract the de-

4.2. Interferometric determination of the zero crossing position

coherence rate, that is defined as the the slope at short times of the width of the central interference peak in units of $2\hbar k$. In Fig. 4.7(b) we compare the measured decoherence rate with theory. The theoretical curve is derived from a numerical calculation of ρ_i and the analysis described in [52]. The experimental data feature an almost linear decrease of the decoherence rate with decreasing a . The rate varies from about 500 s^{-1} for $a = 100 a_0$ to about 2 s^{-1} for $a = 1 a_0$. Below $1 a_0$ we find that noise in the lattice laser starts to significantly contribute to the decoherence, preventing a quantitative comparison of the observation with theory.

Since we are interested to precisely determine the zero crossing position, we

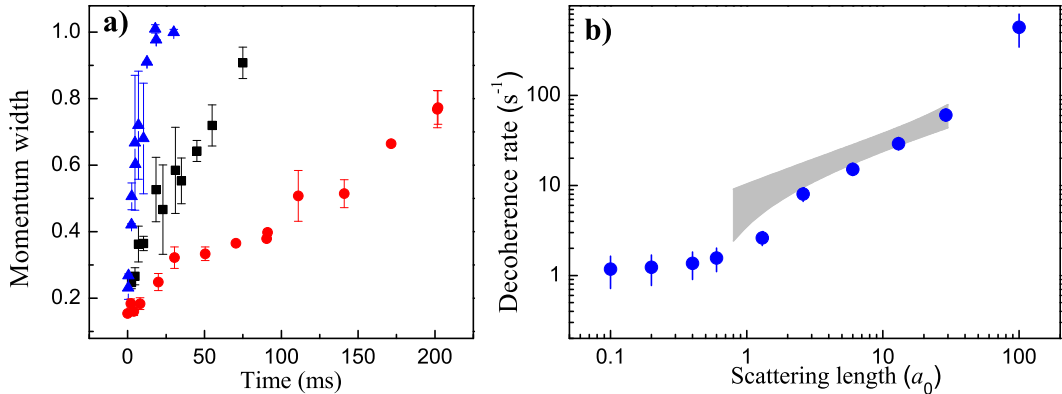


Figure 4.7: Decoherence in the interferometer with tunable interaction. a) Time evolution of the vertical $1/\sqrt{e}$ width (in units of $2\hbar k$) of the central peak of the density profile at integer times of the Bloch period for three different values of a : $29 a_0$ (triangles), $6 a_0$ (squares), $2.5 a_0$ (circles). b) Decoherence rate, defined as the slope of the curves in a), vs the scattering length. The grey region is the theoretical prediction of the model in [52]. Below $1 a_0$ the decoherence rate is dominated by laser noise.

can focus on the weakly interacting regime. If we fix the evolution time and we repeat the measurement of the width of the central peak as a function of the scattering length, we obtain an observable that gives us a quantitative measurement of the decoherence induced by interactions. We use a dense cloud, in order to increase the effect of interaction, but sufficiently diluted in order to neglect three body losses and avoid collapse for negative values of the scattering length. The cloud is loaded in the vertical lattice at a fixed

4. EXPERIMENTAL REALIZATION OF A WEAKLY INTERACTING BOSE-EINSTEIN CONDENSATE

value of scattering length $a_{in} = 3a_0$, in order not to have a dependence from the initial density, and the value of a is tuned to the final one in the first 2 ms of Bloch oscillations. After 180 ms of evolution in the lattice (90 Bloch oscillations), the potential is switched off and the images are taken after 12 ms of expansion. The width presents a minimum of decoherence at (349.9 ± 0.1) G, that corresponds to the magnetic field value for which the interaction is smaller (Fig. 4.8). This value is compatible with the expected position of the zero-crossing (350.4 ± 0.4) G. More details on the experiment can be found in [86].

However, when the s -wave contact interaction energy is tuned to zero, we cannot neglect any more the magnetic dipole-dipole interaction [87]. Usually, in ultra-cold alkali atoms, the dipolar interaction energy $E_d < 0.01E_s$, where E_s is the s -wave contact interaction energy. This interaction is anisotropic and contributes to the interaction energy with a sign related to the geometry of the system. For ^{39}K atoms in the $|F = 1, m_f = 1\rangle$ the magnetic dipole moment $\vec{\mu}$ is parallel to the Feshbach magnetic field \vec{B} that in our case is aligned along the vertical direction. With atoms in a vertical optical lattice, interaction between atoms within the same site of the lattice is mainly repulsive (Fig. 4.8(a)). Weaker but not negligible is the attractive interaction between atoms from distant sites, due to the long range character of the dipolar interaction. A proper attractive contact interaction (a negative value of the scattering length a) reduces the interaction in the system and is able to increase the coherence time of the Bloch oscillations. We repeated the same measurement in a different configuration, with the optical lattice orthogonal to the dipoles (Fig. 4.8(b)), where Bloch oscillations are induced by a spurious magnetic field gradient, generated by the Feshbach coils, with a resulting force on the atoms 6 times smaller than the gravity. In this configuration, the interaction is mainly attractive between atoms in the same site and weakly repulsive between atoms in different sites. The decoherence is reduced with a proper repulsive interaction (a positive value of the scattering length a), in fact, the minimum of decoherence is shifted towards positive values of the scattering length (350.59 ± 0.1) G. In the two cases of vertical and horizontal lattice the minimum of decoherence occurs respectively on the left and on the right of the predicted position of the zero

4.2. Interferometric determination of the zero crossing position

crossing, as we can expect from the qualitative idea presented above.

A perfect cancellation of the interaction energy is not possible, but a partial

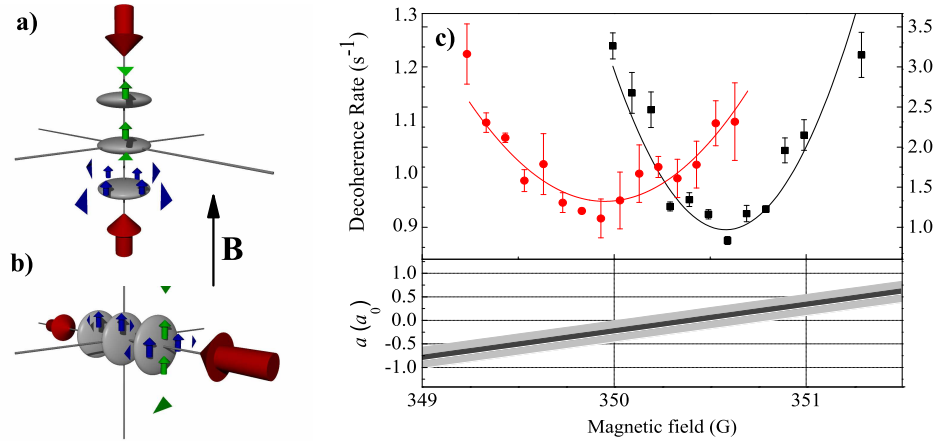


Figure 4.8: Decoherence rate of the interferometer as a function of the external magnetic field applied during Bloch oscillation, in the case of lattice aligned with dipoles (red circles, left vertical scale) and orthogonal to them (black squares, right vertical scale).

compensation of the dipolar interaction allows a reduction of the decoherence rate of our interferometer. In the experiments described in this thesis we used a value of the contact energy which minimizes the decoherence. This corresponds to the minimum of the non homogeneity in the energy. With a theoretical model, described in detail in [87], we can predict a decoherence rate of 1 Hz for $a = 0$ and a residual rate of 0.5 Hz on the minima, as an effect of the uncompensated dipolar interactions.

4. *EXPERIMENTAL REALIZATION OF A WEAKLY INTERACTING
BOSE-EINSTEIN CONDENSATE*

Chapter 5

Experimental observation of Anderson localization with a non-interacting BEC

5.1 Observation of Anderson localization

We have already said that the system we use in order to study Anderson localization is a non-interacting BEC in a periodic lattice, where the disorder is introduced by the perturbation of a weak incommensurate lattice. In this kind of quasi-periodic potential, the Aubry-André model predicts a transition from extended to exponentially localized states, for a fixed value of the disorder (Chapter 3). However, in our system it is impossible to directly observe the transition by measuring the extension of the atom cloud in the potential, because it is typically smaller than the resolution of our imaging system.

A possible experimental direction to observe the localization is the study of the transport properties of the condensate in the lattice. The transition to localized states can indeed be revealed by studying the diffusion of the condensate.

Another possibility it is to investigate the momentum distribution, which can be detected imaging the atoms after a ballistic expansion from the lattice. The localization in the real space, in fact, corresponds to a delocalization in the momentum space, as we said in Chapter 3. So the study of the transition in the momentum distribution is completely analogous to the study in the

real space.

We characterized the transition, finding the scaling behaviour with Δ/J that we described in Chapter 3. We found, in fact, that for strong enough disorder the system is characterized by exponentially localized states, with a localization length increasingly smaller, as expected from the theory (Section 3.1).

5.1.1 Realization of the quasi-periodic lattice

The quasi-periodic potential is obtained by superimposing two optical lattices with incommensurate wavelength along the vertical direction. The main one is created by a single-mode Yb:YAG laser of wavelength $\lambda_1 = 1032$ nm, with a stabilization in frequency and intensity. The second one is created by a single-mode Ti:Sapphire laser of wavelength $\lambda_2 = 862$ nm. The incoming beams are focused on the atoms with a waist of $\sim 150\mu\text{m}$. The optical power of the two lattices can be independently controlled with two acousto-optic modulator, and the lattice depth can be calibrated via Bragg diffraction measurements. We can adjust the potentials in the ranges: $V_1 = 0 \div 10E_1$ for the main lattice, and $V_2 = 0 \div 4E_2$, with $E_i = \hbar^2/2m\lambda_i^2$. We prepare the BEC in the optical trap and then we load it into the bichromatic lattice. In order to prevent excitations of the condensate, the loading is performed with s-shaped ramps for the lattice intensities, on a long timescale of 100 ms. However, the loading is not completely adiabatic and the BEC doesn't remain in the ground state. As an effect of this, in the regime in which the theory predicts that the condensate is localized on a single state, we produce a superposition of various states, with a localization length $\ell \sim d$ and with a distance each other of ~ 5 lattice sites.

5.1.2 Diffusion dynamics

The first experiment that we performed with the non interacting BEC in the quasi periodic potential is the study of transport properties. Anderson localization, indeed, is expected to stop the transport into the lattice, when the strength of the disorder is high enough to localize the system. Let us start by considering the evolution of the atoms into the main lattice potential alone. When the system is in the combined potential of the harmonic trap

5.1. Observation of Anderson localization

with frequency ω and of the optical lattice $V_{latt}(x)$, it is governed by the equation:

$$\left(-\frac{\hbar^2 \nabla^2}{2m} + V_{latt}(x) + \frac{1}{2}m\omega^2 x^2\right) \psi = E\psi \quad (5.1)$$

We have seen in Chapter 2 that the dynamics in a lattice can be described, in the quasi momentum space, with an effective mass m^* . This approach starts from the assumption to consider a wavepacket as a superposition of Bloch waves with a small spread δq respect to the Brillouin zone. This corresponds to have $\delta x \sim 1/\delta q$ very large respect to the spatial scale of the lattice sites. In this approach one loses information on the details of the wavefunction on a lengthscale smaller than the lattice site constant d . This is actually our case, where the resolution of the imaging system is larger than d , and we are just interested in the shape of the envelope of the function. By introducing the effective mass to take into account the effects of the lattice:

$$-\frac{\hbar^2 \nabla^2}{2m} + V_{latt}(x) = -\frac{\hbar^2 \nabla^2}{2m^*} \quad (5.2)$$

and an effective frequency $\omega^* = \sqrt{m/m^*}\omega$; eq. 5.1 becomes

$$\left(-\frac{\hbar^2 \nabla^2}{2m^*} + \frac{1}{2}m^*\omega^{*2}x^2\right) \psi = E\psi \quad (5.3)$$

So the envelope of the ground state of the system into the combined potential of the optical lattice and the harmonic trap has the following shape:

$$\psi_0 \sim e^{-x^2/2a_{ho}^2} \quad (5.4)$$

where $a_{ho}^* = \sqrt{\hbar/\omega^*m^*}$.

Once we obtained the expression for the initial wavefunction, we can study the diffusion in the lattice. After the harmonic confinement is switched off, the temporal evolution of the system is governed by the equation:

$$i\hbar \frac{\partial}{\partial t} \psi = -\frac{\hbar^2 \nabla^2}{2m^*} \psi = -\frac{\hbar^2 \tilde{\nabla}^2}{2m^* a_{ho}^{*2}} \psi = -\frac{\hbar \omega^*}{2} \tilde{\nabla}^2 \psi \quad (5.5)$$

where we substitute $\tilde{x} = x/a_{ho}^*$. From this equation it is possible to demonstrate that the envelope of the ground state evolves during the time maintaining a gaussian shape, whose root-mean-squared evolves during the time

5. EXPERIMENTAL OBSERVATION OF ANDERSON LOCALIZATION
WITH A NON-INTERACTING BEC

with the following relation:

$$\langle \tilde{x}^2 \rangle(t) = \langle \tilde{x}^2 \rangle(0) \sqrt{1 + \omega^{*2} t^2} \quad (5.6)$$

Practically, by releasing the atoms from the harmonic trap, the cloud diffuses into the lattice and expands with a rate which depends from the frequency of the initial harmonic confinement and from the effective mass related with the potential of the optical lattice and in particular with the band curvature. The effective mass, in fact, is defined as (eq. 2.29):

$$m_n^* = \hbar^2 \left[\frac{\partial^2 E_n(q)}{\partial q^2} \right]^{-1}. \quad (5.7)$$

If we consider that the energy of the first band, in the case of a single lattice, can be written as $E(q) = E_0 - 2J \cos(kd)$, we can derive the expression of m^* :

$$m^* = \frac{\hbar^2}{2Jd^2} \left(\frac{1}{1 - \frac{d^2 k^2}{2}} \right) \quad (5.8)$$

These guesses are valuable in the case of the dynamics into a single lattice, but we are interested to study the effect of the disorder introduced by means of the secondary lattice. We can expect to observe a decreasing in the expansion rate of eq. 5.6, as the second lattice depth increases. The addition of the secondary lattice, in fact, modifies the band structure by introducing a series of "mini-gaps" [83, 9, 84] whose width increases with s_2 . The formation of the mini-gaps has the effect to reduce the derivative of the energy; the effective mass increases (eq. 5.8) and the frequency ω^* reduces.

In the experiment the BEC is first loaded in the bichromatic lattice and the optical trap is then switched off abruptly. We use a magnetic gradient to keep atoms against the gravity, such a way that the BEC expands along the lattice. We can observe the diffusion of the envelope of the wavefunction, using absorption images *in situ* (Fig. 5.1). To quantify the diffusion, we plot the root-mean-squared width of the cloud as a function of the evolution time (5.1(b)). We observe that in a single lattice ($\Delta = 0$) the BEC expands ballistically, after the harmonic confinement has been switched off, following eq. 5.6. Adding the perturbation of the second lattice, the ballistic expansion takes place with reduced speed, as expected. When $\Delta/J > 4$, the diffusion is

suppressed as an effect of the large disorder. In this case, in fact, theory predicts that the BEC occupies a localized state. Note that, as we said above, in the experiment the BEC occupies several localized states, as an effect of the non adiabaticity in the loading of the bichromatic lattice. Consequently the width of the spatial distribution is larger than the width estimated for a single state.

To quantitatively analyze the transition from delocalized to localized states, we fix the evolution time and study the problem as a function of the disorder strength. In Chapter 3 we found that in a quasi-periodic potential the transition from extended to localized states depends only from the disorder parameter Δ/J . In our system we have the possibility to change both the depth of the main lattice s_1 and the depth of the secondary one s_2 , related respectively with the tunneling rate J and the disorder strength Δ . We are interested to characterize the position of the transition and to check that the behaviour depends only from Δ/J . We performed the same experiment for three different values of the depth of the main lattice with $s_1 = 5.6, 8.4$ and 10.6 . We measured the width of the BEC in the lattice direction for different values of the depth of the second lattice in the range between $s_2 = 0$ and $s_2 = 4$. We compare the three different measurements on the same plot as a function of s_2 (Fig. 5.2). In all three cases we can see that for large enough s_2 , the system enters in the non diffusing region, where the width remains equal to the initial size of the BEC.

In the single lattice case ($s_2 = 0$), the width decreases by increasing the value of s_1 . This is due to the fact that the effective mass increases as the potential depth s_1 increases. s_1 , indeed, is inversely proportional to the tunneling rate J , which is inversely related to the effective mass (eq. 5.8). Moreover, an increase of m^* corresponds also to a decrease of ω^* , related to the rate of diffusion (eq. 5.6). We can actually estimate what we expect to measure after 750 ms of diffusion for the three different values of s_1 . From eq. 5.8 we can estimate the effective mass m^* in the centre of the band (in the hypothesis of $k = 0$) and we obtain $m^*/m \sim 5, 3, 1.5$ respectively for $s_1 = 10.6, 8.4, 5.6$. From these values we find final widths of $15.4, 20.1, 29.4 \mu\text{m}$, that are smaller than the experimental values. We considered, indeed, the kinetic energy of the ground state, while in the experiment the non adiabaticity produces ex-

5. EXPERIMENTAL OBSERVATION OF ANDERSON LOCALIZATION
WITH A NON-INTERACTING BEC

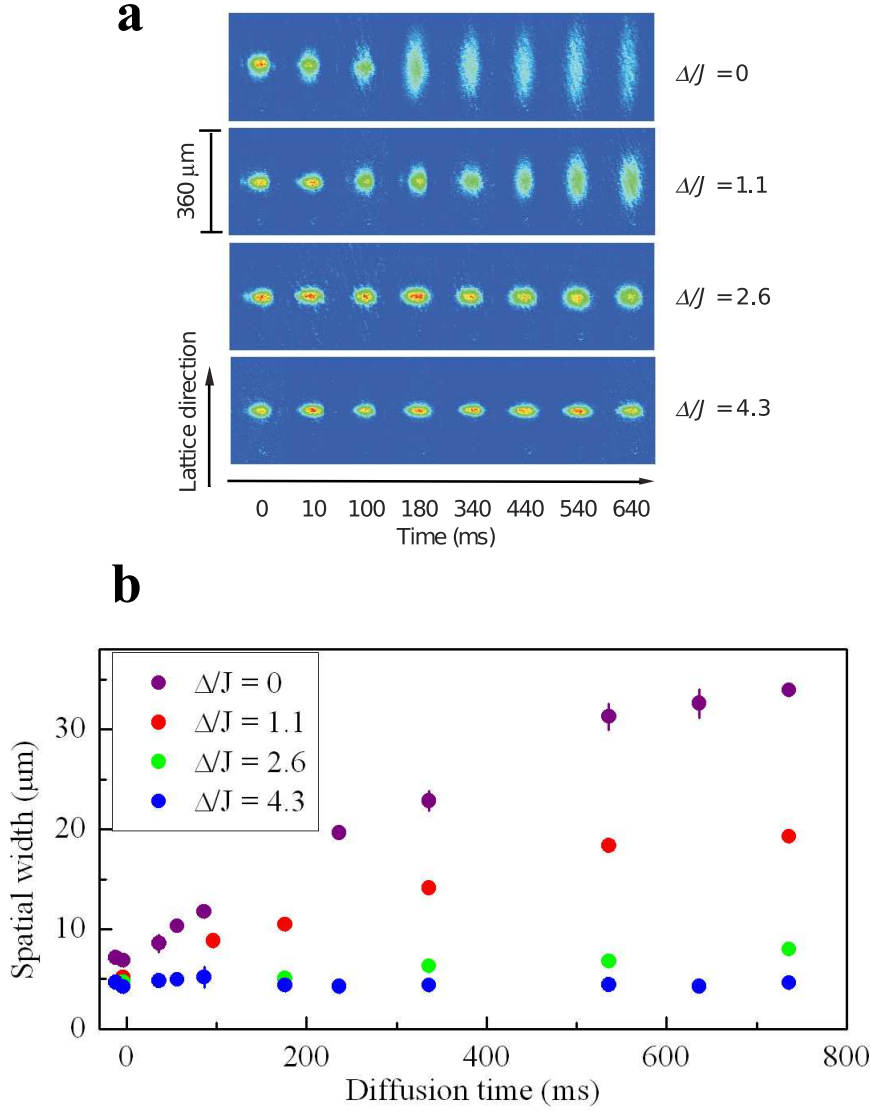


Figure 5.1: Absorption images *in situ* of the BEC diffusing along the quasi periodic lattice for different values of Δ and $J/h = 136$ Hz. Whereas for $\Delta/J = 0$ diffusion time the width of the condensate increases, for $\Delta/J > 4$ the size sties constant over time.

5.1. Observation of Anderson localization

citation in the system. The crossover between diffusing and localized states

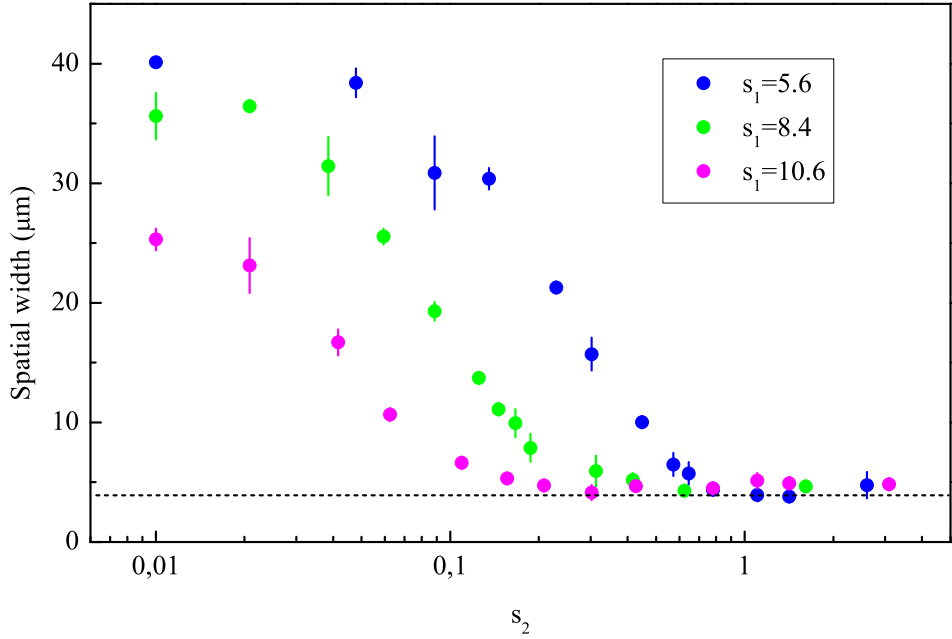


Figure 5.2: Root-mean-squared size of the condensate for three different values of the main lattice, at a fixed value of the evolution time of 750 ms, as a function of the depth of the secondary lattice. The system needs a finite amount of disorder to stop the diffusion in the lattice. A 10% of uncertainty on the horizontal scale must be considered mainly due to the non linearity of the modulators' response that we use to control the depth of the two lattices.

shifts towards smaller strength of disorder, as the value of s_1 increases. If we rescale the data as a function of the disorder parameter Δ/J (Fig. 5.3), for the three different values of J the system needs the same disorder strength in order to enter in the localized regime. This is an evidence of the scaling behavior intrinsic in the Aubry-André Hamiltonian (eq. 3.15). In the regime $\Delta/J > 4$ the value of the width is saturated at $5 \mu\text{m}$ by diffraction limit. Note that Δ/J is estimated by using eq. 3.8 for J and eq. 3.14 for Δ and not the approximated one (eq. 3.16) used in [11].

5. EXPERIMENTAL OBSERVATION OF ANDERSON LOCALIZATION
WITH A NON-INTERACTING BEC

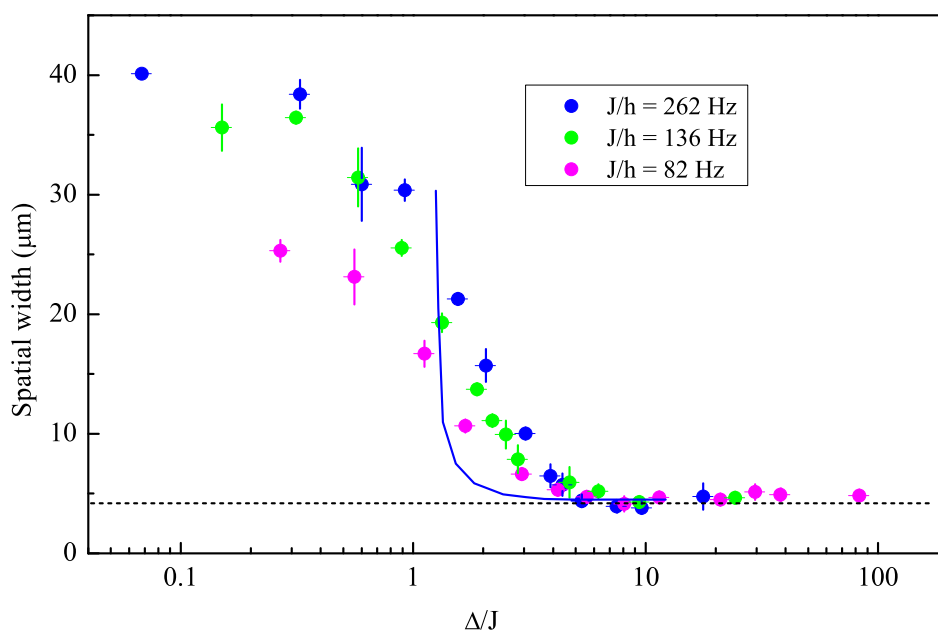


Figure 5.3: Root-mean-squared size of the condensate of the measurements in Fig. 5.2 as a function of the rescaled disorder strength Δ/J . The onset of localization appears in the same range of values Δ/J for the three data sets. We report with the continuous line also the convolution $\sqrt{l^2 + \sigma^2}$ of the width of the localized state l predicted from the theory with the resolution of the imaging system $\sigma \sim 5\mu\text{m}$. This is a lower limit, due to the fact that in the experiment the BEC occupies more than one localized state. This shows also that for $\Delta/J > 4 \div 5$ we are limited by the imaging resolution (dashed line).

5.1.3 Exponential distribution of the localized BEC

As we saw in Chapter 3, in the localization regime we expect to have eigenstates with an exponential distribution [85]. We can study the shape of the wavefunction by analyzing the spatial distribution of the condensate from the *in situ* images. However, as we said above, as an effect of the non adiabaticity in the loading of the bichromatic lattice, in the experiment the BEC occupies various states. Let us discuss what information we can extract from the images in which we have more than one localized state. We can consider, for example, the case in which the condensate is occupying three different states. The resulting profile is the sum of the three functions for the single localized state:

$$f_i(x) = A_i e^{-\frac{|x-x_i|}{\ell}} \quad (5.9)$$

where we chose the localization length $\ell = 1$ and $x_i - x_{i-1} = 5$ in units of lattice constant d . The sum of the three profiles maintains the exponential behaviour only in the region of the space where the three functions are all decreasing or all increasing (Fig. 5.4). Our imaging system is not able to resolve the structure on a scale of the single lattice; in the central part, in fact, we expect to detect a gaussian profile. Consequently, in order to distinguish between the exponential behaviour in the localized regime and the gaussian one in the extended regime, we can analyse only the tails of the spatial distribution along the direction of the lattice (Fig. 5.5). We obtained the optical density profiles by integrating the images on the radial direction and we fitted the axial one with an exponential function of the form

$$f_\alpha(x) = A e^{-\left|\frac{(x-x_0)}{\ell}\right|^\alpha}, \quad (5.10)$$

where α is a fitting parameter. We chose to exclude from the fit the central part of the distributions, within 0.6 times the root-mean-squared width from the centre, in order to drop the effect due to the gaussian resolution. Two examples of this analysis are shown in Fig. 5.5 (a) and (b), respectively for weak ($\Delta/J \sim 0.5$) and strong ($\Delta/J \sim 10$) disorder, where the fits are compared with a gaussian one. In the first case the experimental profile is well fitted with a gaussian function, whereas for strong disorder the gaussian fit is not able to fit the tails of the distribution. We repeated this analysis for

5. EXPERIMENTAL OBSERVATION OF ANDERSON LOCALIZATION
WITH A NON-INTERACTING BEC

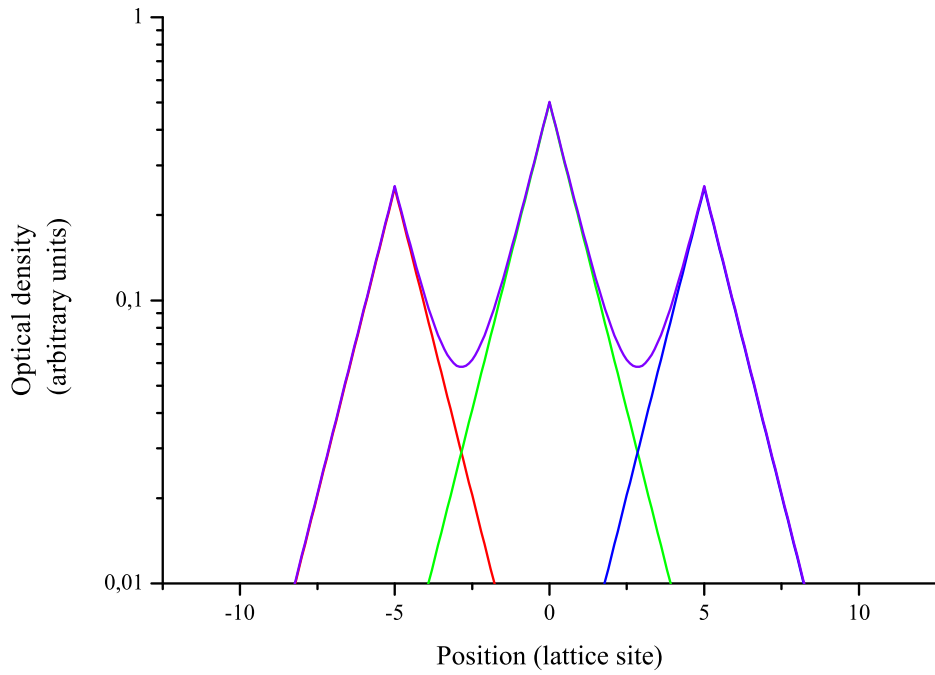


Figure 5.4: Simulated spatial distributions of three states localized with a localization length of 1 site and with a spatial distance of 5 sites each other. The parameters we used are $x_1 = -5$, $a_1 = 0.25$ (red line), $x_2 = 0$, $a_2 = 0.5$ (green line), $x_3 = 5$, $a_3 = 0.25$ (blue line). The resulting distribution (violet line) presents an exponential behaviour only in the regions $x < -5$ and $x > 5$.

5.1. Observation of Anderson localization

the various values of Δ we investigated in the experiment. In Fig. 5.5 (c) we report the fitting parameter α as a function of the disorder Δ/J . We observe a crossover from $\alpha = 2$ (gaussian profiles) to $\alpha = 1$ (exponential profiles) as Δ/J increases. We repeated the same analysis on the radial direction, where there is only the harmonic confinement, and in this case we obtained that the spatial distributions are well fitted by a gaussian function (α) for all disorder strengths.

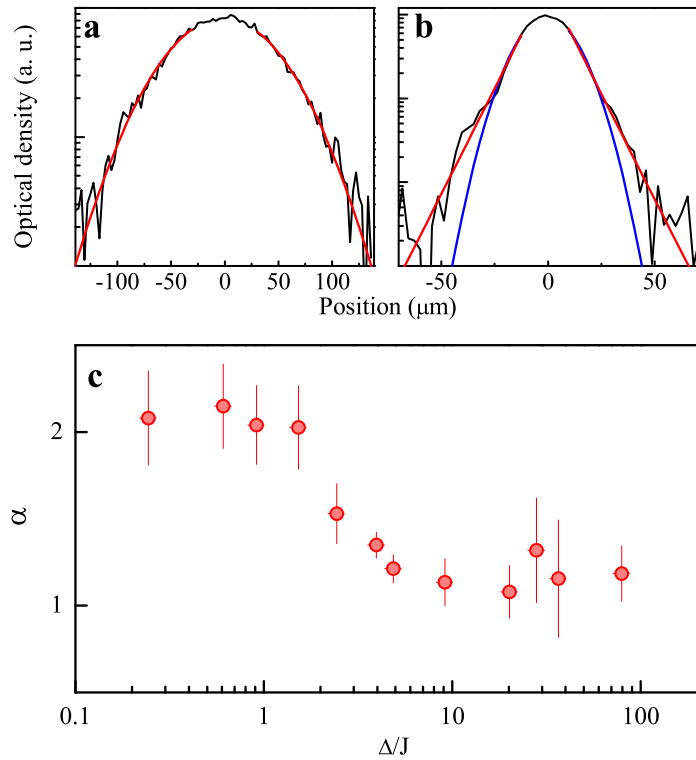


Figure 5.5: (a),(b) Experimental profiles (black) and fitting function $f_\alpha(x)$ (red) for (a) $\Delta/J \approx 0.5$ and (b) $\Delta/J \approx 10$ with a logarithmic scale on the vertical axis. The blue line in (b) represents a gaussian fit ($\alpha = 2$), that is not able to reproduce the tails of the experimental profile. (c) The fitting parameter α as a function of disorder parameter Δ/J . There is a transition from a gaussian ($\alpha = 2$) to an exponential ($\alpha = 1$) distribution. Each data point is obtained by the mean of the fits of 4-5 different images.

5.1.4 Analysis of the momentum distribution

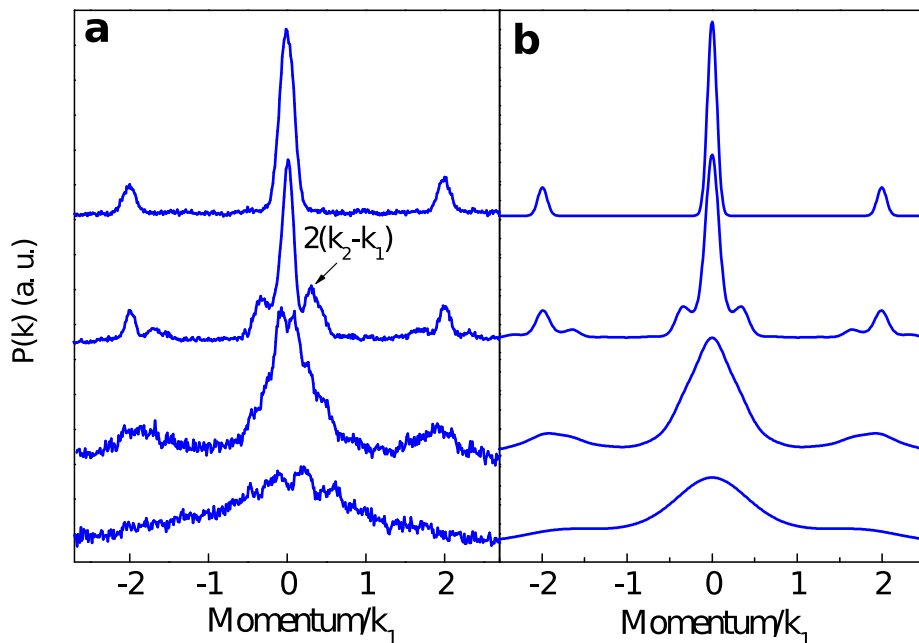


Figure 5.6: (a) Experimental and (b) theoretical momentum distributions $P(k)$, measured along the horizontal axes in units of k_1 , for increasing Δ/J values (0, 0.7, 4.4 and 15.3, from top to bottom). At $\Delta = 0$ the system presents the typical interference pattern of the single lattice, which is first modified by the appearance of peaks at the beating between the two lattices. For stronger disorder the momentum peaks gradually broaden. The experimental momentum distribution profiles are obtained by integration in the radial direction of the two dimensional distributions.

As we described in Chapter 3, to a localization of the spatial wavefunction corresponds a delocalization in the momentum space; the width of the axial momentum distribution, in fact, is inversely proportional to the spatial extent in the lattice. We can measure it by realising the atoms from the lattice and imaging them after a ballistic expansion. When the cloud expands to many times his original size, in fact, the time-of-flight images represent the velocity distribution of the sample.

In Fig. 5.6, we report some examples of the experimental momentum distribution that can be compared with the theory. From the model, in fact, it is possible to predict the momentum distribution as the Fourier transform of the spatial wavefunction. We can see an excellent agreement between

experiment and theory. Without disorder, the system is characterized by the typical momentum distribution of the single lattice, with three peaks at $k = 0, \pm 2k_1$ which reflect the periodicity of the main lattice. The wavefunction extends over many lattice sites, and the width of the peak at $k = 0$ is very small, due to the extended nature of $\psi(x)$.

In the case of weak disorder, not strong enough to localize the BEC, the eigenstates of the Aubry-André Hamiltonian are still extended and additional momentum peaks start to appear at a distance of $\pm 2(k_1 - k_2)$ from the main peaks, corresponding to the beating of the two lattices. By further increasing Δ/J , the momentum distribution broadens, as an effect of the localization of the spatial wave, and eventually its width becomes comparable with the width of the Brillouin zone k_1 . This corresponds to the fact that the extension of the localized states becomes of the order of the lattice spacing. This behaviour for different values of the disorder is more evident in the spatial wavefunction, that we obtain with the Fourier transform of the momentum distribution (Fig. 5.7). It is important to remind that while the theoretical model estimates the ground state of the system, in the experiment we occupy several ($5 \div 10$) localized states. This means that the experimental momentum distribution results from the interference pattern of the different states. The envelope of the interference pattern of the experimental profiles is the Fourier transform of all the localized states. The small modulation on top of the experimental profiles is actually the effect of the interference between the several states that the condensate is occupying.

Important informations on the spatial distribution can be obtained by analysing the Fourier transform of the momentum distribution (Fig. 5.7). The system presents the typical extended wavefunction of the single lattice at $\Delta = 0$. By introducing the disorder the spatial profile is first modified by the appearance of a secondary state shifted of 5 lattice sites and becomes localized on states with an extension of 1 lattice constant for stronger disorder. We fitted the spatial profiles obtained by the Fourier transform of the measured momentum distributions with an exponential function of the form

$$g_{\ell,\alpha}(x) = \sum_{i=1}^3 A e^{-|\frac{x-x_i}{\ell}|^\alpha} (A_i \cos(2k_1 x + \varphi_i) + B_i) \quad (5.11)$$

where we take into account the contribution of three states centered at $x_1 =$

5. EXPERIMENTAL OBSERVATION OF ANDERSON LOCALIZATION
WITH A NON-INTERACTING BEC

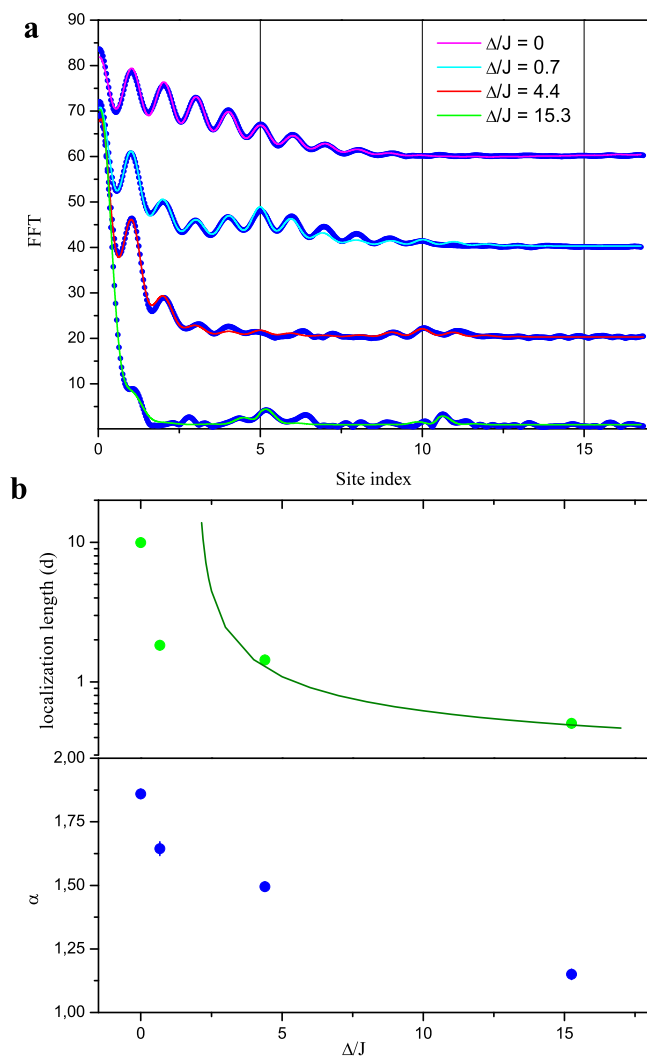


Figure 5.7: (a) FFT of the experimental momentum distributions in Fig. 5.6(a). The fitting function is the $g_{\ell,\alpha}(x)$ described in the text. measured along the horizontal axes in units of lattice constant, for increasing Δ/J values. At $\Delta = 0$ the system presents the typical extended wavefunction of the single lattice, which is first modified by the appearance of a secondary state shifted of 5 lattice sites. For stronger disorder the wavefunction is localized on states with an extension of 1 lattice constant. (b) The fitting parameters ℓ and α as a function of Δ/J . The parameter ℓ is compared with the localization length predicted from the Aubry-André model (eq. 3.29).

5.1. Observation of Anderson localization

0, $x_2 = 5d$ and $x_3 = 10d$. From the fit we can extract the parameters ℓ and α . The parameter α , as we obtained from the analysis of the *in situ* images (Fig. 5.5), shows the transition from a gaussian ($\alpha = 2$) to an exponential ($\alpha = 1$) distribution. The parameter ℓ decreases by increasing the disorder Δ/J , showing the localization of the system. In the regime with $\Delta/J > 2$ we can compare the measured ℓ with the localization length predicted from the Aubry-André model (eq. 3.29). The good agreement that we obtained confirms the dependence of the localization length from the disorder parameter Δ/J predicted from the theory.

The spatial extension of the wavefunction is inversely proportional to the width of the central momentum peak $P(k)$. A gaussian fit is not able to take into account the secondary peaks at $2(k_2 - k_1)$, so that we extracted the root-mean squared width as

$$rms = \sqrt{\left| \sum_i I(i)i^2 - \left(\sum_i I(i)i \right)^2 \right|} \quad (5.12)$$

where the index i runs over the pixels of the experimental images. We measured it as a function of the depth of the second lattice s_2 , for three different values of the depth of the main one s_1 (Fig. 5.8). The three data sets show a transition from spatial extended states to localized ones, with a crossover that moves towards larger values of the disorder s_2 as we decrease the main potential s_1 . If we rescale the measurement as a function of the disorder parameter Δ/J , the three data sets move to the same line, confirming the scaling behaviour observed with the diffusion measurements (Fig. 5.9).

From the same data we analyzed the visibility defined as:

$$V = \frac{P(2k_1) - P(k_1)}{P(2k_1) + P(k_1)}. \quad (5.13)$$

The visibility V quantifies the occupation of the momentum states $\pm k_1$, which signals the spatial localization with an extension comparable with the lattice spacing. The experimental data in Fig. 5.9 are in good agreement with the visibility predicted from the theoretical model, and in the three cases the visibility starts to decrease for $\Delta/J \approx 2 \div 3$. This value is in excellent agreement with the theoretical prediction (Fig. 3.2).

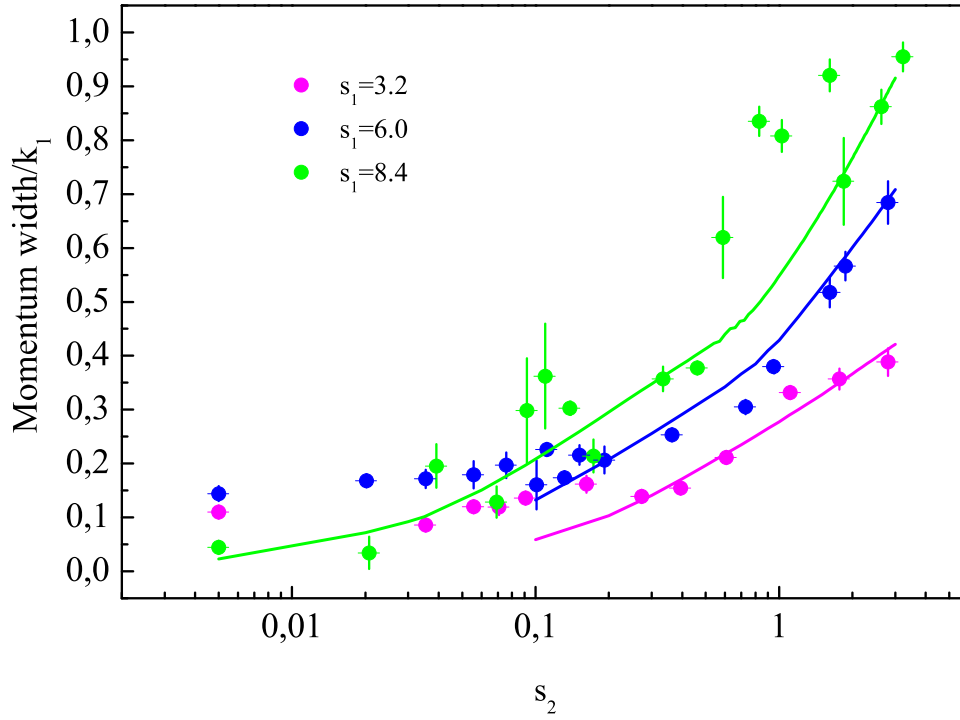


Figure 5.8: Root-mean squared size of the central peak $P(k)$ as a function of s_2 , for three different values of s_1 . The data show a transition from extended states to localized ones, with a crossover that moves towards larger values of the disorder s_2 as we decrease the main potential s_1 . For each value of s_1 the experimental behaviour is in excellent agreement with predictions from the theory (continuous lines). For the analysis of the momentum width, we directly measured the root-mean-squared size of the central peak, when this could be distinguished from the side peaks. Otherwise, if the three peaks were superimposed we fitted them with three gaussian profiles and we extracted the width of the central one. We followed this method for both theoretical and experimental data.

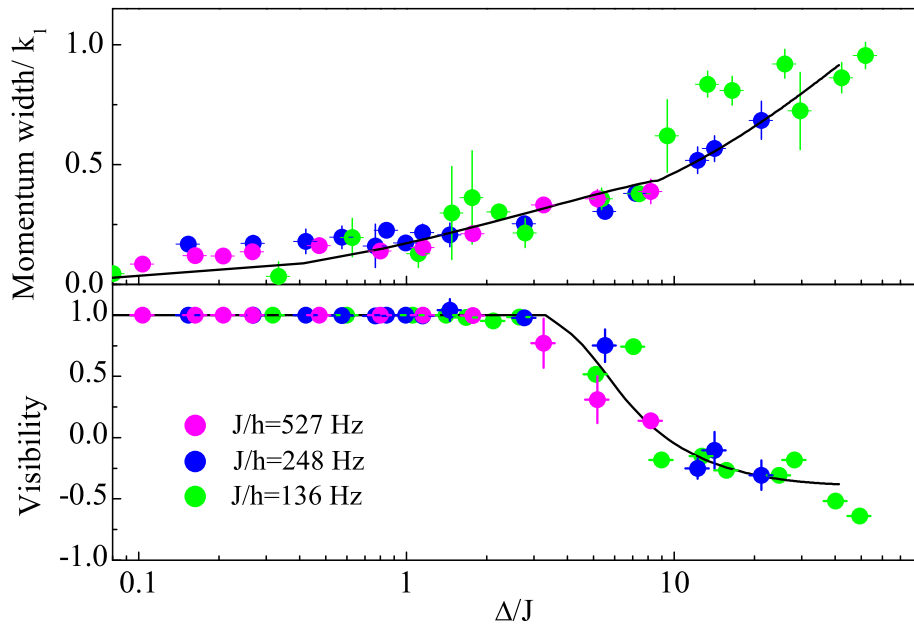


Figure 5.9: Root-mean squared size of the central peak $P(k)$ of the measurements of Fig. 5.8 as a function of Δ/J , for three different values of J . For each value of J the experimental behaviour is the same and is in excellent agreement with predictions from the theory (continuous line). We plot also the visibility of the interference pattern, defined by eq. 5.13, versus Δ/J . In both experiment and theory (continuous line) the visibility decreases abruptly for $\Delta/J \sim 2 \div 3$, when the system localizes with a localization length of the order of lattice constant.

5.1.5 Interference of multiple localized states

In the experiments we described above, the system was occupying several localized states. In this case the momentum distribution results in the momentum distribution of the single localized states, where the random phases of the different states practically erases the interference between them. However, if we decrease the number of states occupied by the system, it becomes possible to study their interference and to obtain more information on the localized states. We have, in fact, the possibility to change with the harmonic confinement, the number of localized states overlapped with the cloud. In Fig. 5.10 we report some example of possible harmonic confinement compatible with the occupation of different numbers of localized states. The momentum distribution is given by the multiple-slit interference pattern.

The interference pattern of two states can be analyzed using the following function for the fit:

$$f(x) = \left[a_1 e^{-\frac{(x-x_0)^2}{2\sigma^2}} + a_2 \left(e^{-\frac{(x-x_0-\delta)^2}{2\sigma^2}} + e^{-\frac{(x-x_0+\delta)^2}{2\sigma^2}} \right) \right] (1 + a_3 \cos(2\pi k(x - x_0) + \varphi)) \quad (5.14)$$

where the first part describes the envelope due to the three momentum peaks of the single localized state as three gaussian functions centered at ($k = 0, \pm k_1$) with σ as width. The second part, instead, describes the modulation due to the interference between different localized states, with amplitude a_3 and phase φ . The spacing between the fringes is related to the spatial separation between the two different localized states of about five lattice sites. An important information can be obtained from the phase φ of the interference pattern. For a non interacting sample, the wavefunction of different localized states are orthogonal, since they are eigenstates of the system, and due to the large separation between them (5 lattice sites) with respect to the spatial extension of the single state (< 1 lattice constant), they are independent. Since the minimum of the harmonic confinement varies from shot to shot, the phase φ varies randomly in the range $[-\pi, \pi]$ (Fig. 5.11).

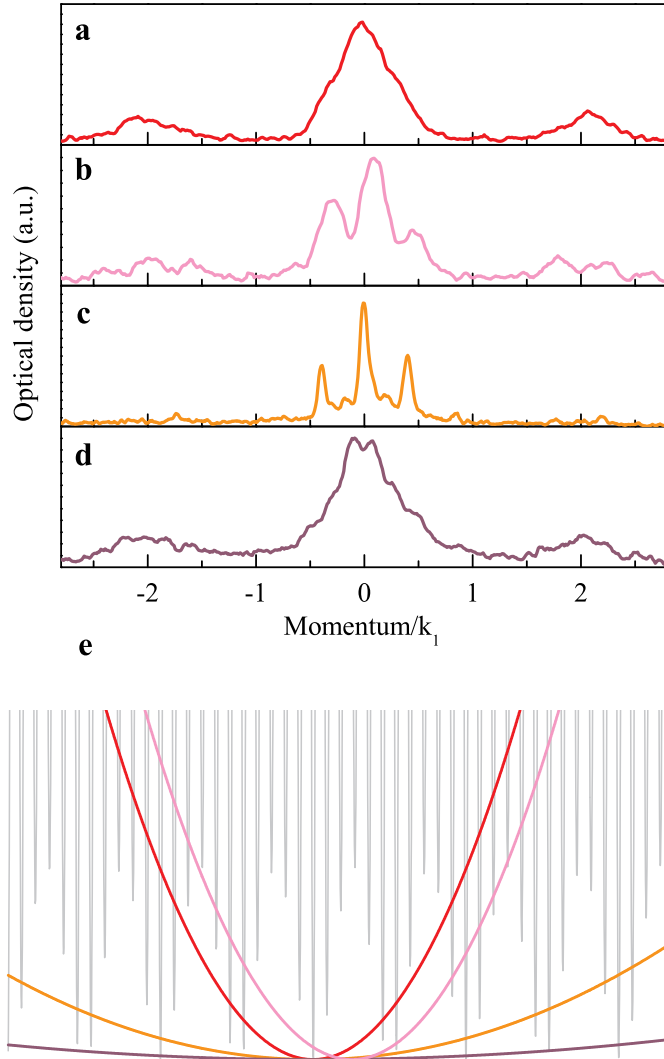


Figure 5.10: Momentum distribution of the condensate prepared in a disordered lattice with $\Delta/J \approx 6$, for different values of the harmonic confinement. (a) Profile of a single localized state (initial spatial size of the condensate, $\sigma = 1.2\mu\text{m}$ and $\nu_{ht} = 100$ Hz); (b) interference of two localized states ($\sigma = 1.2\mu\text{m}$ and $\nu_{ht} = 100$ Hz); (c) interference of three localized states ($\sigma = 2.1\mu\text{m}$ and $\nu_{ht} = 30$ Hz); (d) interference of about ten localized states ($\sigma = 5\mu\text{m}$ and $\nu_{ht} = 10$ Hz). (e) Cartoon of the bichromatic potential and the harmonic one for the different frequencies of $\nu_{ht} = 100$ Hz (red-pink), $\nu_{ht} = 30$ Hz (orange), $\nu_{ht} = 5$ Hz (violet), from which we can intuitively understand how the number of occupied states depends from the confinement.

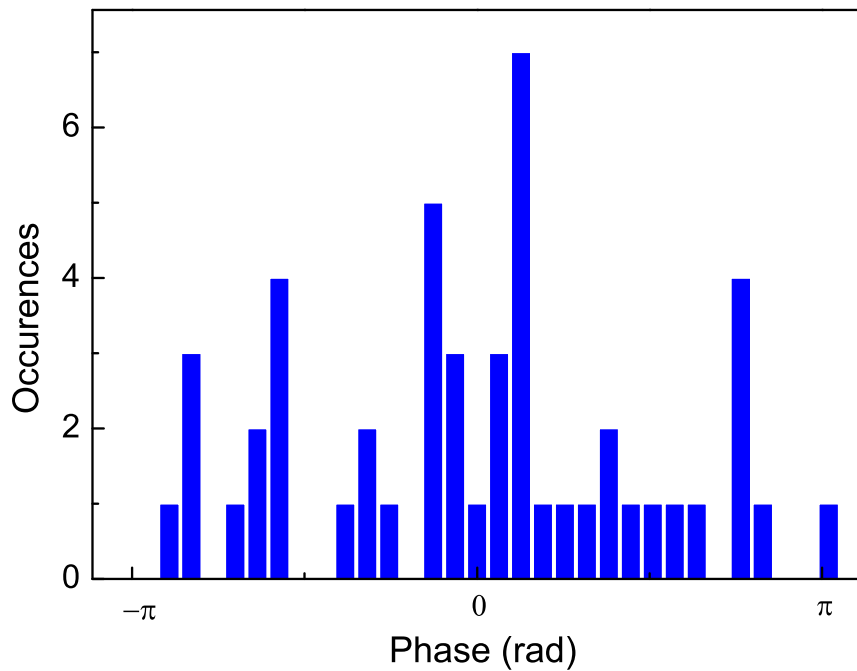


Figure 5.11: Distribution of the interference phase in an harmonic confinement with $\nu = 100$ Hz. The phase is randomly distributed in the range $[-\pi, \pi]$, as an effect of the fact that different localized states are spatially not overlapped and the interference phases are independent.

5.2 Interacting one dimensional disordered system

In Chapter 3 we have resumed the theory of Anderson localization for non-interacting particles in a one-dimensional lattice and noted that disorder induces localization of the particles in few lattice sites. Also in the experiment we described in this thesis we used a non-interacting system. However, our system offers also the opportunity to tune the interaction between atoms and to study the interplay of disorder and interaction.

What happens to the Anderson transition if we add a small repulsive interactions between particles? Intuitively repulsion would induce a delocalization, by inducing atoms not to occupy the same lattice site to minimize the energy. In the Aubry-André model for non interacting particles we found the Hamiltonian (eq. 3.19):

$$\langle \psi | H | \psi \rangle = -J \sum_j (c_{j+1}^* c_j + c_j^* c_{j+1}) + \Delta \sum_j \cos(2\pi\beta j + \phi') c_j^* c_j \quad (5.15)$$

where the c_j are the amplitude coefficients over each Wannier function. If we consider the interacting system we have to add a non linear term, analogous to the GPE interaction term, which takes into account the interaction energy that each particle feels as a combined effect from all the other particles in the system. We obtain the following Hamiltonian:

$$\langle \psi | H | \psi \rangle = -J \sum_j (c_{j+1}^* c_j + c_j^* c_{j+1}) + \Delta \sum_j \cos(2\pi\beta j + \phi') c_j^* c_j + \frac{1}{2} g \sum_j |c_j|^4 \quad (5.16)$$

with $g = 4\pi\hbar^2 a/m$ (Appendix A). The interaction energy U_{int} for a system with N particles can be written as:

$$U_{int} = \frac{4\pi\hbar^2 a}{m} N \int d^3x |\psi(\mathbf{x})|^4 \quad (5.17)$$

We estimate U_{int} using a gaussian approximation for the wavefunction in the separable axial ($\varphi(x)$) and radial ($\wp(r)$) directions

$$\psi(\mathbf{x}) = \wp(r)\varphi(x) \quad (5.18)$$

For the radial part we have:

$$\wp(r) = \frac{1}{\sqrt{\pi\sigma}} e^{-\frac{r^2}{2\sigma^2}} \quad (5.19)$$

5. EXPERIMENTAL OBSERVATION OF ANDERSON LOCALIZATION WITH A NON-INTERACTING BEC

where σ is the sigma of the gaussian distribution in the radial direction, related to the frequency of the harmonic confinement ($\sigma = \frac{\hbar}{m\omega}$). For the axial part we consider a strongly localized wavefunction:

$$\varphi(x) = \frac{1}{\sqrt{\pi}\ell^{1/2}} e^{-\frac{x^2}{2\ell^2}} \quad (5.20)$$

where ℓ is the localization length.

In this approximation the contribution to the integral in (eq. 5.17) for the radial and the axial direction are respectively

$$\int d^2r |\varphi(r)|^4 = \frac{1}{2\pi\sigma^2} \quad \text{and} \quad \int dx |\varphi(r)|^4 = \frac{1}{\sqrt{2\pi}\ell} \quad (5.21)$$

For the interaction energy U_{int} we obtain:

$$U_{int} = \sqrt{\frac{2}{\pi}} \hbar\omega N a \frac{1}{\ell}. \quad (5.22)$$

This expression is useful to quantify the amount of the interaction in the system, whose physics now depends on the competition between disorder Δ which tends to localize particles and interaction energy U_{int} which tends to delocalize. We can try to understand the effects of interaction in an intuitive picture. In a localized regime the N particles of a non interacting system occupy the some localized state with the smaller energy. If we add a weak interaction to this system, U_{int} increases only the energy of the state with an occupation different from zero. When U_{int} becomes comparable with the energy difference between the non-interacting ground state and the first excited one, the occupation of one state alone is no more favourable and some atoms can move to the other state. The eigenstate of the interacting system therefore becomes a superposition of an increasing number of non-interacting eigenstates. These new eigenstates are no more orthogonal and the effective coupling between them increases as an effect of the increased overlap.

5.2.1 Experimental observation of effects of weak interaction

We have already seen that our experimental case is different from the picture we presented above, because also in the non interacting case our BEC

5.2. Interacting one dimensional disordered system

occupies more than one state. However, we observed the independence of the different non interacting states, as a random distribution of the interference phase (5.1.5). In the interacting regime we should expect that the

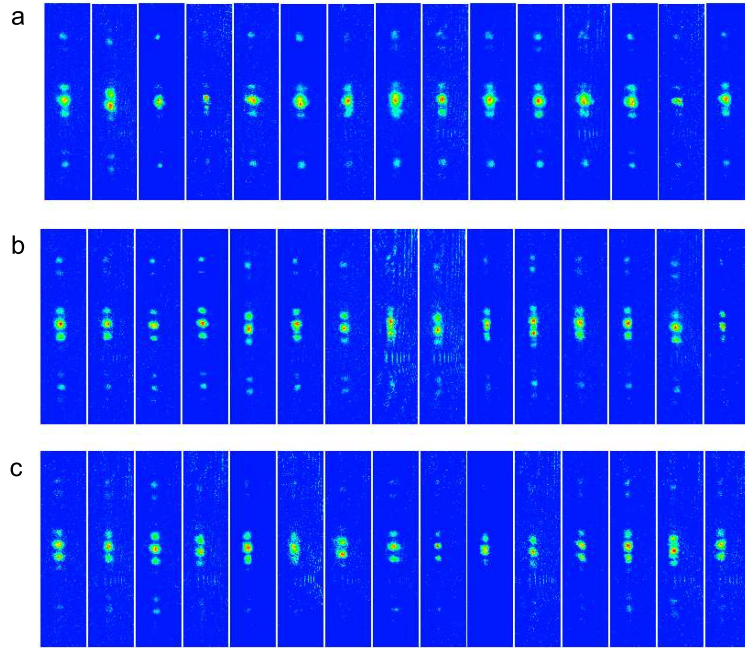


Figure 5.12: Interference pattern between different localized states for different values of the scattering length (a) $a = 1.7a_0$, (b) $a = 9.4a_0$, (c) $a = 23.4a_0$. The BEC is loaded in the bichromatic lattice with a parameter $\Delta/J \sim 16$ and with an harmonic confinement with $\nu \sim 100$ Hz.

different localized states are no more independent. The interference phase should therefore be no more randomly distributed between $[-\pi, \pi]$ but should gradually lock when the interaction increases. We actually found that when repeating the experiment in presence of the interaction the phase is no more randomly distributed. The measurements in (Fig. 5.13) show a locking of the phase at $\varphi = 0$ for increasing values of the scattering length. The phase is significantly locked for $a = 23.4 a_0$.

A comparison of the measured phase with the theory is not easy to do, because the experimental situation is much more complicated than the simulated one. In the experimental case, in fact, the phase appears because the BEC is occupying more than one state, while the theoretical model finds the ground state of the system. To study the dependence of the localization

5. EXPERIMENTAL OBSERVATION OF ANDERSON LOCALIZATION
WITH A NON-INTERACTING BEC

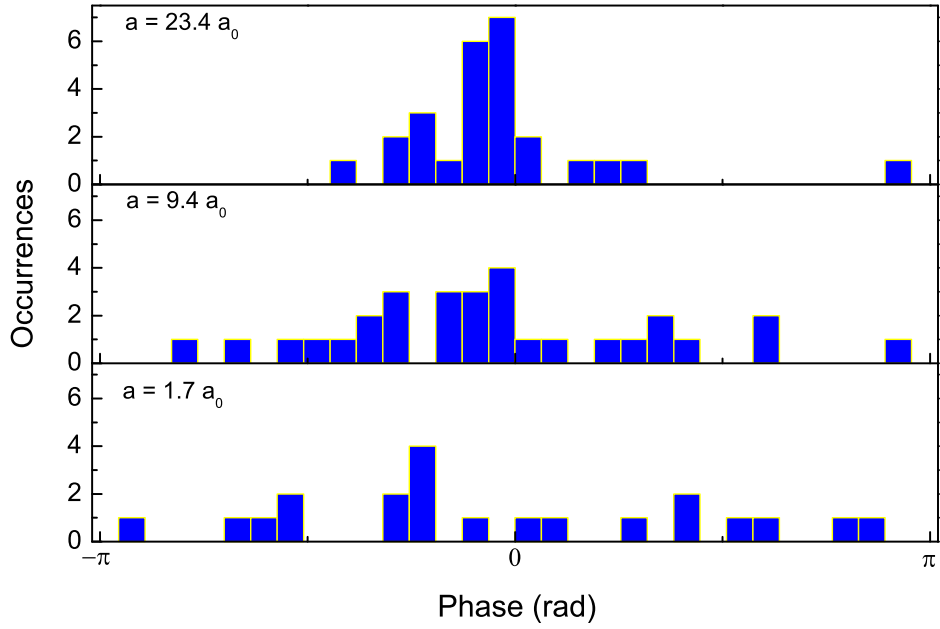


Figure 5.13: Distribution of the interference phase in an harmonic confinement with $\nu = 100$ Hz, with different values of interactions ($1.7a_0$, $9.4a_0$ and $23.4a_0$). The phase is randomly distributed in the range $[-\pi, \pi]$.

5.2. Interacting one dimensional disordered system

from the interactions, a quantitative analysis that we can do on the data reported in Fig. 5.13, it is the measurement of the width of the envelope of the interference pattern that corresponds to the width of the momentum peak of a single localized state. This value can be estimated from the theory for different values of the interactions and it is in good agreement with the experimental one (Fig. 5.14). We observe a decrease of the momentum width as the scattering length increases. This is the direct consequence of the spatial delocalization induced by the interaction energy, which brings back the condensate to a superfluid phase. These preliminary measurements with interacting BEC have been done in presence of an harmonic confinement with a frequency of 100 Hz, which allow to localize the condensate over few states and to have a good visibility of the interference pattern. However, the tight confinement increases the energy difference between two neighbouring localized states and affects the interaction energy necessary to delocalize the system. To quantitatively study the competition between disorder and interaction we will have to decompress the harmonic confinement in such a way that the energy difference between localized states is dominated by disorder. The study of the competition between disorder and interaction enters in a general scenario. If we consider the homogeneous case in which all the sites are at the same energy ($E_i = 0$), the physics of the system is determined by the competition between the tunneling J and the one site interaction energy U . If $U \ll J$ the Hamiltonian is dominated by the tunneling term, the ground state is delocalized over all the lattice sites and the system is in a superfluid state (SF). On the other side, when $U \gg J$, the physics is dominated by repulsion energy, so atoms prefer not to share their site with other particles and tend to remain in the site they are occupying in order to minimize the energy. The system is in a localized Mott insulating (MI) state. Transition between SF and MI state has been experimentally observed in a 3D system [88] and in an array of 1D gas [89]. In the inhomogeneous configuration, with a disorder $E_i \in [-\Delta/2, \Delta/2]$, an other energy scale has to be considered in the Hamiltonian. In the intermediate regime of weak disorder ($\Delta < U$), the MI regions start to shrink and a new phase called *Bose Glass* (BG) appears. Increasing the disorder Δ , the MI region arrive to vanish for $\Delta > U$ (Fig. 5.15). In the regime of strong interaction and strong

5. EXPERIMENTAL OBSERVATION OF ANDERSON LOCALIZATION
WITH A NON-INTERACTING BEC

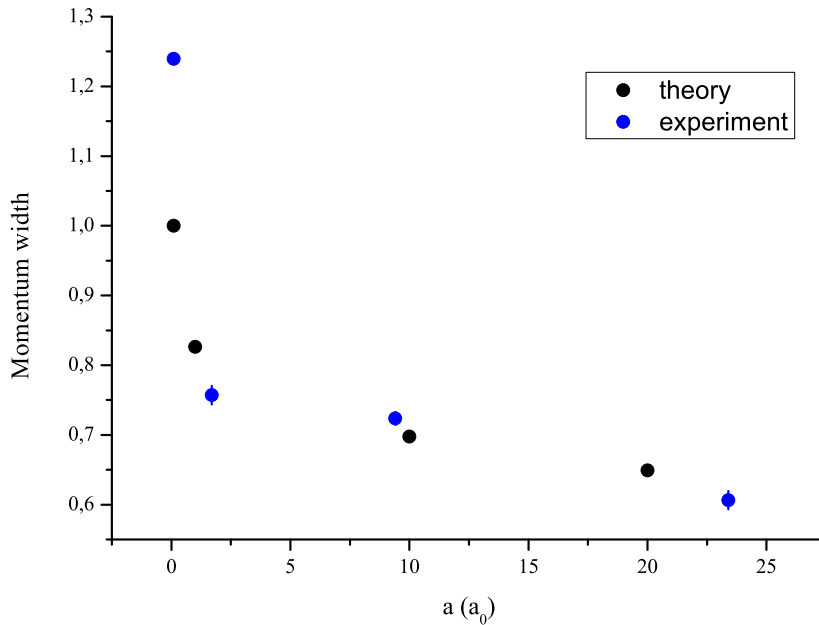


Figure 5.14: Comparison between theory and experiment for the width of the momentum peak, for different values of the scattering length for measurements in Fig. 5.12. For the same degree of disorder $\Delta/J \sim 16$.

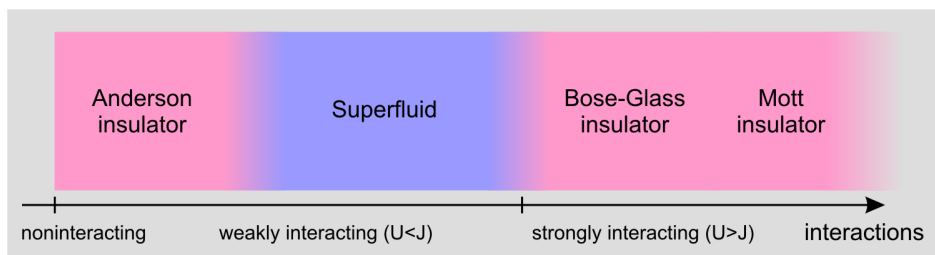


Figure 5.15: The ratio between tunneling J , interaction energy U and disorder Δ , the system is in an Anderson insulating, in a superfluid, in a Mott insulating, or in a Bose Glass state.

5.2. Interacting one dimensional disordered system

disorder, the Bose gas is in the Bose glass phase. This disorder induced phase could be easily described like a phase where there are insulate condensates (superfluid and compressible) which are not in contact each other. The Bose Glass phase, in fact, is a compressible insulating phase, differently from the Mott insulating one that is not compressible.

The interplay between disorder and interaction is still an interesting open question in the modern condensed matter physics and our system could be a good candidate to investigate this field in future experiments.

*5. EXPERIMENTAL OBSERVATION OF ANDERSON LOCALIZATION
WITH A NON-INTERACTING BEC*

Conclusions

In this thesis we reported about the first observation of Anderson localization in matter waves. Localization of waves in disordered media, originally predicted by Anderson in the context of transport of electrons in crystals, has been observed in a large variety of systems, but it has never been observed directly for matter waves, owing to the presence of interaction. By exploiting the possibility to tune atom-atom interaction, thanks to the presence of magnetic Feshbach resonances, we employ for the first time a non-interacting Bose-Einstein condensate to study Anderson localization. We use an optical lattice, where we introduce disorder by means of a weak incommensurate secondary lattice. This corresponds to the realization of a quasi-periodic potential, which is characterized by the presence of a transition from extended to exponentially localized states analogous to the Anderson transition. Localization is clearly demonstrated by investigating transport properties, spatial and momentum distributions. In the first case we studied the diffusion of the BEC in the bichromatic lattice. We prepared the condensate in a combined potential of the harmonic trap and of the bichromatic lattice. Without the perturbation of the secondary lattice, the condensate released from the trapping potential usually diffuses in the single lattice with a rate which depends from the frequency of the initial potential. We studied the diffusion as a function of the disorder strength induced with the secondary lattice. As we expected, Anderson localization is able to stop the transport into the lattice, when the strength of the disorder is high enough to localize the system. The disorder value at the transition is in good agreement with the expected value from the theory. We studied also the spatial distribution and we found that while the condensate after the diffusion in the single lattice has a gaussian profile, when the disorder is strong enough to localize the system the ex-

5. EXPERIMENTAL OBSERVATION OF ANDERSON LOCALIZATION WITH A NON-INTERACTING BEC

perimental profiles are well fitted with exponential distributions, emblematic characteristic of Anderson localization.

The other possibility we exploited to study Anderson transition is the investigation of the momentum distribution, whose width is inversely proportional to the width of the spatial wavefunction. We clearly observed a transition from extended to localized states as the disorder strength increased. In particular, also with this experiment, we found an excellent agreement with theory predictions for the position of the transition.

The possibility to tune interaction via Feshbach resonances is an interesting tool to study the effect of the interaction in the disordered system. A repulsive interaction between particles, in fact, produces a delocalization in the system, by inducing the atoms not to occupy the same lattice site. We are interested to study the interplay between disorder and interaction, that is a still open field of investigation in the modern physics.

Other possible directions for future experiments could be the study of Anderson localization in 2D and 3D disordered systems and the investigation of this phenomenon with the presence of a purely random disorder.

Appendix A

Scattering theory

We can consider the Hamiltonian for two colliding distinguishable atoms of masses m_1 and m_2 :

$$H = \frac{p_1^2}{2m_1} + \frac{p_2^2}{2m_2} + V(\mathbf{r}_1 - \mathbf{r}_2) \quad (\text{A.1})$$

The problem can be decomposed in the study of the center of mass motion and of the relative one. The center of mass moves as a free particle of mass M ; so the interesting part of the problem is to solve the Schrödinger equation for the relative motion

$$\left(\frac{p^2}{2\mu} + V(\mathbf{r}) - \mathbf{E} \right) \psi_{\mathbf{k}}(\mathbf{r}) = 0 \quad (\text{A.2})$$

which corresponds to the scattering of a particle with reduced mass μ by the potential $V(\mathbf{r})$. We look for a solution of (eq. A.2) of the following shape for $r \rightarrow \infty$:

$$\psi_{\mathbf{k}}(\mathbf{r}) \sim e^{i\mathbf{k}\cdot\mathbf{r}} + f(k, \mathbf{n}, \mathbf{n}') \frac{e^{ikr}}{r} \quad (\text{A.3})$$

with $\mathbf{n} = \mathbf{k}/k$ and $\mathbf{n} = \mathbf{r}/r$. $\psi_{\mathbf{k}}(\mathbf{r})$ is a superposition of an incident plane wave with momentum \mathbf{k} and of a diffuse wave function. $f(k, \mathbf{n}, \mathbf{n}')$ is the *scattering amplitude* and it is function of the energy of the particle, the incident and observation direction \mathbf{n} and \mathbf{n}' [90, 91]. The value of the scattering amplitude is related to the differential and the total scattering cross-sections:

$$\frac{d\sigma}{d\Omega} = |f(k, \mathbf{n}, \mathbf{n}')|^2 \quad \sigma(k, \mathbf{n}) = \int |f(k, \mathbf{n}, \mathbf{n}')|^2 d^2n'. \quad (\text{A.4})$$

The solution of the three dimensional Schrödinger equation is generally not trivial. We can consider a simplified case of a spherically symmetric potential $V(\mathbf{r}) = V(r)$. In this case the scattering amplitude depends only on the angle θ between \mathbf{n} and \mathbf{n}' . Due to the symmetry of the problem we can expand the wavefunction in a generic radial and angular part:

$$\psi_{\mathbf{k}}(\mathbf{r}) = \sum_{l=0}^{\infty} \sum_{m=-l}^{m=l} Y_{l,m}(\theta, \phi) \frac{u_{k,l,m}(r)}{r} \quad (\text{A.5})$$

where ϕ is the azimuthal angle around the z axis and the $Y_l^m(\theta, \phi)$ are the spherical harmonic functions. The incident wave function e^{ikz} expansion is independent of the azimuthal angle ($m = 0$):

$$e^{ikz} \simeq \frac{1}{2ikr} \sum_{l=0}^{\infty} (2l+1) P_l(\cos \theta) ((-1)^{l+1} e^{-ikr} + e^{ikr}) \quad \text{for } kr \gg 1 \quad (\text{A.6})$$

where the $P_l(\cos \theta)$ are the Legendre polynomials. The scattering state $\psi_{\mathbf{k}}(\mathbf{r})$ for $r \rightarrow \infty$ is the sum of the incident wave function and the outgoing wave $f(k, \theta) e^{ikr}/r$ (eq. A.3) and can be written:

$$\psi_{\mathbf{k}}(\mathbf{r}) \simeq \frac{1}{2ikr} \sum_{l=0}^{\infty} (2l+1) P_l(\cos \theta) ((-1)^{l+1} e^{-ikr} + e^{i2\delta_l} e^{ikr}) \quad (\text{A.7})$$

where the phase shifts δ_l are real.

The solution of the scattering problem corresponds to solve the 1D Schrödinger equation for every radial wave function $u_{k,l}(r)$:

$$u_{k,l,m}''(r) + \left(k^2 - \frac{l(l+1)}{r^2} - \frac{2\mu V(r)}{\hbar^2} \right) u_{k,l,m}(r) = 0 \quad (\text{A.8})$$

According with (eq. A.7) we obtain:

- the asymptotic behavior of the radial wavefunction

$$u_{k,l,m}(r) \propto (-1)^{l+1} e^{-ikr} + e^{2i\delta_l} e^{ikr} \quad (\text{A.9})$$

- the scattering amplitude

$$f(k, \theta) = \frac{1}{2ik} \sum_l (2l+1) (e^{2i\delta_l} - 1) P_l(\cos \theta) \quad (\text{A.10})$$

-
- the scattering cross-section

$$\sigma(k) = \sum_{l=0}^{\infty} \sigma_l(k) \quad \text{with} \quad \sigma_l(k) = \frac{4\pi}{k^2} (2l+1) \sin^2 \delta_l(k) \quad (\text{A.11})$$

Until now we have considered distinguishable particles. In the case of identical particles we have to take into account the symmetry (antisymmetry) properties for polarized bosons (fermions). Considering the parity $(-1)^l$ of spherical harmonic functions, we can deduce that the expression for identical bosons (fermions) will contain only even (odd) waves. We obtain:

bosons:

$$\sigma(k) = \frac{8\pi}{k^2} \sum_{\text{even}} (2l+1) \sin^2 \delta_l \quad (\text{A.12})$$

fermions:

$$\sigma(k) = \frac{8\pi}{k^2} \sum_{\text{odd}} (2l+1) \sin^2 \delta_l \quad (\text{A.13})$$

It is possible to demonstrate that, in the limit of vanishing k , the phase shifts δ_l are proportional to k^{2l+1} [90], so the scattering cross section is mainly determined by the lower partial waves and in the limit of *zero energy* only *s-wave* scattering ($l=0$) contributes. In the case of identical fermions the scattering processes are completely suppressed; so at low temperature, a gas of polarize fermions, has the same behavior of an ideal gas without interactions. In the case of bosons, instead, the scattering cross section is:

$$\sigma_{l=0}(k) = (2 \times) 4\pi a^2 \quad \text{for } k \rightarrow 0 \quad (\text{A.14})$$

where we defined the *s-wave scattering length* as:

$$a = - \lim_{k \rightarrow 0} \frac{\tan \delta_0(k)}{k} \quad (\text{A.15})$$

In a bosonic gas at low temperature, in the dilute regime (i.e. $n|a|^3 \ll 1$, where n is the spatial density of the gas), interactions between atoms can be described by a single parameter a , *s-wave scattering length*. The many body description of the system depends only on the scattering length and not on the details of the interaction potential. In the many body Hamiltonian, it

is possible to substitute the inter-atomic potentials with a mean field term given by:

$$V(r) = g\delta(r) \tag{A.16}$$

where $g = 4\pi\hbar^2 a/\mu$. We can observe that the sign of a determines the type of interactions: positive values of the scattering length correspond to repulsive interactions and negative values to attractive ones. We can now try to understand how it is possible to tune the scattering length.

Appendix B

Aubry-André Hamiltonian in momentum space

The Hamiltonian of the Aubry-André model (eq. 3.15) is the following:

$$H = \sum_j (|w_j\rangle\langle w_{j+1}| + |w_{j+1}\rangle\langle w_j|) + \lambda \sum_j \cos(2\pi\beta j + \phi') |w_j\rangle\langle w_j| \quad (\text{B.1})$$

We can use the base in the momentum space:

$$|k\rangle = \frac{1}{\sqrt{L}} \sum_j e^{i2\pi k\beta j} |w_j\rangle \quad (\text{B.2})$$

If we consider $\beta = \frac{F_i}{F_{i+1}} = \frac{F_i}{L}$ we can find:

$$\begin{aligned} \sum_k e^{-i2\pi k\beta j'} |k\rangle &= \frac{1}{\sqrt{L}} \sum_j \sum_k e^{i2\pi k\beta(j-j')} |w_j\rangle = \\ &= \frac{1}{\sqrt{L}} \sum_j \sum_{k=1}^L e^{i2\pi F_i \frac{k}{L}(j-j')} |w_j\rangle = \frac{1}{\sqrt{L}} L \delta_{j,j'} |w_j\rangle = \sqrt{L} |w_{j'}\rangle \end{aligned} \quad (\text{B.3})$$

So that

$$|w_j\rangle = \frac{1}{\sqrt{L}} \sum_k e^{-i2\pi k\beta j} |k\rangle \quad (\text{B.4})$$

This expression is useful to find the Hamiltonian eq. B.1. We can estimate:

$$\sum_j |w_j\rangle\langle w_{j+1}| = \frac{1}{L} \sum_j \sum_{k,k'} e^{-i2\pi\beta j(k-k') + i2\pi\beta k'} |k\rangle\langle k'| = \sum_k e^{i2\pi\beta k} |k\rangle\langle k| \quad (\text{B.5})$$

The first term of the eq. B.1 becomes

$$\begin{aligned} \sum_j (|w_j\rangle\langle w_{j+1}| + |w_{j+1}\rangle\langle w_j|) &= \sum_k (e^{i2\pi\beta k} + e^{-i2\pi\beta k}) |k\rangle\langle k| = \\ &= 2 \sum_k \cos(2\pi\beta k) |k\rangle\langle k| \end{aligned} \quad (\text{B.6})$$

The second term of the eq. B.1 is:

$$\sum_j \epsilon_j |w_j\rangle \langle w_j| = \sum_j \frac{\epsilon_j}{L} \sum_{k,k'} e^{-i2\pi\beta j(k-k')} |k\rangle \langle k'| = \sum_{k,k'} \tilde{\epsilon}_{k,k'} |k\rangle \langle k'| \quad (\text{B.7})$$

where

$$\epsilon_j = \cos(2\pi\beta j) = \frac{1}{2} (e^{i2\pi\beta j} + e^{-i2\pi\beta j}) \quad (\text{B.8})$$

We can calculate

$$\begin{aligned} \tilde{\epsilon}_{k,k'} &= \frac{1}{2L} \sum_j (e^{i2\pi\beta j} + e^{-i2\pi\beta j}) e^{-i2\pi\beta j(k-k')} = \\ &= \frac{1}{2L} \sum_j (e^{-i2\pi\beta j(k-k'-1)} + e^{-i2\pi\beta j(k-k'+1)}) = \frac{1}{2} (\delta_{k,k'+1} + \delta_{k,k'-1}) \end{aligned} \quad (\text{B.9})$$

So that

$$\sum_j \epsilon_j |w_j\rangle \langle w_j| = \sum_k \frac{1}{2} (|k\rangle \langle k+1| + |k\rangle \langle k-1|) \quad (\text{B.10})$$

The Hamiltonian in the base of $|k\rangle$ can be written as

$$H_k = \frac{\lambda}{2} \left(\sum_k (|k\rangle \langle k+1| + |k\rangle \langle k-1|) + \frac{4}{\lambda} \sum_k \cos(2\pi\beta k) |k\rangle \langle k| \right) \quad (\text{B.11})$$

Momentum space:

$$|l\rangle = \frac{1}{\sqrt{L}} \sum_j e^{i2\pi j \frac{l}{L}} |w_j\rangle \quad (\text{B.12})$$

$$\begin{aligned} \sum_l e^{-i2\pi j' \frac{l}{L}} |l\rangle &= \frac{1}{\sqrt{L}} \sum_l \sum_j e^{i2\pi \frac{l}{L}(j-j')} |w_j\rangle = \\ &= \frac{1}{\sqrt{L}} \sum_j \sum_l e^{i2\pi \frac{l}{L}(j-j')} |w_j\rangle = \frac{1}{\sqrt{L}} L \delta_{j,j'} |w_j\rangle = \sqrt{L} |w_{j'}\rangle \end{aligned} \quad (\text{B.13})$$

So that

$$|w_j\rangle = \frac{1}{\sqrt{L}} \sum_l e^{-i2\pi j \frac{l}{L}} |l\rangle \quad (\text{B.14})$$

We can estimate:

$$\sum_j |w_j\rangle \langle w_{j+1}| = \frac{1}{L} \sum_j \sum_{l,l'} e^{-i2\pi j \frac{(l-l')}{L} + i2\pi \frac{l'}{L}} |l\rangle \langle l'| = \sum_l e^{i2\pi \frac{l}{L}} |l\rangle \langle l| \quad (\text{B.15})$$

The first term of the eq. B.1 becomes

$$\begin{aligned} \sum_j (|w_j\rangle\langle w_{j+1}| + |w_{j+1}\rangle\langle w_j|) &= \sum_l \left(e^{i2\pi\frac{l}{L}} + e^{-i2\pi\frac{l}{L}} \right) |l\rangle\langle l| = \\ &= 2 \sum_l \cos\left(2\pi\frac{l}{L}\right) |l\rangle\langle l| \end{aligned} \quad (\text{B.16})$$

The second term of the eq. B.1 is:

$$\sum_j \epsilon_j |w_j\rangle\langle w_j| = \sum_j \frac{\epsilon_j}{L} \sum_{l,l'} e^{-i2\pi j \frac{(l-l')}{L}} |l\rangle\langle l'| = \sum_{l,l'} \tilde{\epsilon}_{l,l'} |l\rangle\langle l'| \quad (\text{B.17})$$

We can calculate

$$\tilde{\epsilon}_{l,l'} = \frac{1}{2L} \sum_j \left(e^{-i2\pi j \left(\frac{l-l'}{L} - \beta\right)} + e^{-i2\pi j \left(\frac{l-l'}{L} + \beta\right)} \right) = \quad (\text{B.18})$$

and the sum is different from zero if

$$\left(\frac{\Delta l}{L} \pm \beta \right) = m \in Z \quad (\text{B.19})$$

In our experimental case of $\beta > 1$ the solutions are:

$$\frac{\Delta l}{L} = \pm |\beta - 1| \quad (\text{B.20})$$

and

$$\frac{\Delta l}{L} = \pm |\beta - 2| \quad (\text{B.21})$$

So that the Hamiltonian

$$H_l = 2 \sum_l \cos\left(2\pi\frac{l}{L}\right) |l\rangle\langle l| + \lambda \sum_{l,l'} \tilde{\epsilon}_{l,l'} |l\rangle\langle l'| \quad (\text{B.22})$$

is able to couple the momentum $k = 0$ with $k' = 2 * k_1 * \frac{l'}{L}$

$$k' = \pm 2(k_2 - k_1) \quad (\text{B.23})$$

and

$$k'' = \pm(2k_1 - 2(k_2 - k_1)) \quad (\text{B.24})$$

B. AUBRY-ANDRÉ HAMILTONIAN IN MOMENTUM SPACE

Bibliography

- [1] P. W. Anderson, *Absence of Diffusion in Certain Random Lattices*, Phys. Rev. **109**, 1492 (1958).
- [2] T. Schwartz, G. Bartal, S. Fishman, and M. Segev, *Transport and Anderson localization in disordered two-dimensional photonic lattices*, Nature **446**, 52 (2006).
- [3] Y. Lahini, A. Avidan, F. Pozzi, M. Sorel, R. Morandotti, D. N. Christodoulides, and Y. Silberberg, *Anderson Localization and Non-linearity in One-Dimensional Disordered Photonic Lattices*, Phys. Rev. Lett. **100**, 013906 (2008).
- [4] J. E. Lye, L. Fallani, M. Modugno, D. S. Wiersma, C. Fort, and M. Inguscio, *Bose-Einstein Condensate in a Random Potential*, Phys. Rev. Lett. **95**, 070401 (2005).
- [5] L. Fallani, J. E. Lye, V. Guarrera, C. Fort, and M. Inguscio, *Ultracold Atoms in a Disordered Crystal of Light: Towards a Bose Glass*, Phys. Rev. Lett. **98**, 130404 (2007).
- [6] D. Clément, A. F. Varn, M. Hugbart, J. A. Retter, P. Bouyer, L. Sanchez-Palencia, D. M. Gangardt, G. V. Shlyapnikov, and A. Aspect, *Suppression of Transport of an Interacting Elongated Bose-Einstein Condensate in a Random Potential*, Phys. Rev. Lett. **95**, 170409 (2005).
- [7] C. Fort, L. Fallani, V. Guarrera, J. E. Lye, M. Modugno, D. S. Wiersma, and M. Inguscio, *Effect of Optical Disorder and Single Defects on the Expansion of a Bose-Einstein Condensate in a One-Dimensional Waveguide*, Phys. Rev. Lett. **95**, 170410 (2005).

-
- [8] T. Schulte, S. Drenkelforth, J. Kruse, W. Ertmer, J. Arlt, K. Sacha, J. Zakrzewski, and M. Lewenstein, *Routes Towards Anderson-Like Localization of Bose-Einstein Condensates in Disordered Optical Lattices*, Phys. Rev. Lett. **95**, 170411 (2005).
- [9] J. E. Lye, L. Fallani, C. Fort, V. Guarrera, M. Modugno, D. S. Wiersma, and M. Inguscio, *Effect of interactions on the localization of a Bose-Einstein condensate in a quasiperiodic lattice*, Phys. Rev. A **75**, 061603 (R) (2007).
- [10] J. Billy, V. Josse, Z. Zuo, A. Bernard, B. Hambrecht, P. Lugan, D. Clément, L. Sanchez-Palencia, P. Bouyer, A. Aspect, *Direct observation of Anderson localization of matter waves in a controlled disorder*, Nature **453**, 891 (2008).
- [11] G. Roati, C. D'Errico, L. Fallani, M. Fattori, C. Fort, M. Zaccanti, G. Modugno, M. Modugno, M. Inguscio, *Anderson localization of a non-interacting Bose-Einstein condensate*, Nature **453**, 895 (2008).
- [12] G. Roati, M. Zaccanti, C. D'Errico, J. Catani, M. Modugno, A. Simoni, M. Inguscio, and G. Modugno, *^{39}K Bose-Einstein Condensate with Tunable Interactions*, Phys. Rev. Lett. **99**, 010403 (2007).
- [13] P. G. Harper, Proc. Phys. Soc. London Sect. A **68**, 874 (1955).
- [14] S. Aubry and G. André, *Analyticity breaking and Anderson localization in incommensurate lattices*, Ann. Israel. Phys. Soc. **3**, 33 (1980).
- [15] C. Aulbach, A. Wobst, G-L. Ingold, P. Hänggi and I. Varga, *Phase-space visualization of a metal-insulator transition*, New J. Phys. **6**, 70 (2004).
- [16] E. Abrahams, P. W. Anderson, D. C. Licciardello, and T. V. Ramakrishnan, *Scaling Theory of Localization: Absence of Quantum Diffusion in Two Dimensions*, Phys. Rev. Lett. **42**, 673 (1979).
- [17] S. John, *Electromagnetic absorption a disordered medium near a photon mobility edge*, Phys. Rev. Lett. **53**, 2169 (1984).

BIBLIOGRAPHY

- [18] P. W. Anderson, *The question of classical localization: a theory of white paint?*, Phil. Mag. B **52**, 505 (1985).
- [19] E. Akkermans, and R. Maynard, *Weak localization of waves*, J. Phys. Lett. **46**, 1045 (1985).
- [20] M. P. Van Albada, and A. Legendijk *Observation of weak localization of light in a random medium*, Phys. Rev. Lett. **55**, 2692 (1985).
- [21] P. E. Wolf, and G. Maret, *Weak localization and coherent backscattering of photons in disordered media*, Phys. Rev. Lett. **55**, 2696 (1985).
- [22] D. S. Wiersma, P. Bartolini, A. Legendijk, and R. Righini, *Localization of light in a disordered medium*, Nature **390**, 671 (1997).
- [23] F. Scheffold, R. Lenke, R. Tweert, G. Maret, *Localization or classical diffusion of light?*, Nature **398**, 206 (1999).
- [24] M. V. Berry, and S. Klein, *Transparent mirrors: rays, waves and localization*, Eur. J. Phys. **18**, 222 (1997).
- [25] R. Dalichaouch, J. P. Armstrong, S. Schultz, P. M. Platzman, and S. L. McCall, *Microwave localization by two-dimensional random scattering*, Nature **354**, 53 (1991).
- [26] A. A. Chabanov, M. Stoytchev, and A. Z. Genack, *Statistical signatures of photon localization*, Nature **404**, 850 (2000).
- [27] M. Storzer, P. Gross, C. M. Aegerter, and G. Maret, *Observation of the critical regime near Anderson localization of light*, Phys. Rev. Lett. **96**, 063904 (2006).
- [28] Michael Marder, *Condensed Matter Physics*, (Wiley, New York 1999).
- [29] I. M. Lifshitz, *The energy spectrum in disordered systems*, Adv. Phys. **13**, 483 (1964).
- [30] R. B. Diener, G. A. Georgakis, J. Zhong, M. Raizen, and Q. Niu, *Transition between extended and localized states in a one-dimensional incommensurate lattice*, Phys. Rev. A **64**, 033416 (2001).

- [31] N. F. Mott, W. D. Twose, *Theory of Impurity Conduction*, Adv. Phys. **10**, 107 (1961).
- [32] Jacopo Giacomelli, *Localizzazione di un condensato di Bose-Einstein in potenziali ottici disordinati unidimensionali*, Master Thesis, University of Florence (2007).
- [33] A. A. Gogolin, V. I. Melnikov, and E. I. Rashiba, *Conductivity in a disordered one-dimensional system induced by electron-photon interaction*, Sov. Phys. JETP **69**, 327 (1976).
- [34] A. A. Gogolin, *Electron density distribution for localized states in one-dimensional disordered system*, Sov. Phys. JETP **71**, 1912 (1976).
- [35] J. Fröhlich and T. Spencer, *Absence of Diffusion in the Anderson Tight Binding Model for Large Disorder and Low Energy*, Math. Phys. **88**, 151 (1983).
- [36] M. H. Anderson, J. R. Ensher, M. R. Matthews, C. E. Weiman, and E. A. Cornell, *Observation of Bose-Einstein condensation in a dilute atomic vapor*, Science **269**, 198 (1995).
- [37] K. B. Davis, M. -O. Mewes, M. R. Andrews, N. J. van Druten, D. S. Durfee, D. M. Kurn, and W. Ketterle, *Bose-Einstein Condensation in a Gas of Sodium Atoms*, Phys. Rev. Lett. **75**, 3969 (1995).
- [38] C. C. Bradley, C. A. Sackett, J. J. Tollet, and R. G. Hulet, *Evidence of Bose-Einstein Condensation in an Atomic Gas with Attractive Interactions*, Phys. Rev. Lett. **75**, 1687 (1995).
- [39] H. Feshbach, *A Unified Theory of Nuclear Reactions*, Ann. Phys. **5**, 357 (1958).
- [40] H. Feshbach, *A Unified Theory of Nuclear Reactions. II*, Ann. Phys. **19**, 287 (1962).
- [41] U. Fano, *Sullo spettro di assorbimento dei gas nobili presso il limite dello spettro d'arco*, Nuovo Cimento **12**, 156 (1935).

BIBLIOGRAPHY

- [42] S. Inouye, M. R. Andrews, J. Stenger, H.-J. Miesner, D. M. Stamper-Kurn, and W. Ketterle, *Observation of Feshbach resonances in a Bose-Einstein condensate*, Science **392**, 151 (1998).
- [43] S. L. Cornish, N. R. Claussen, J. L. Roberts, E. A. Cornell, and C. E. Wieman, *Stable ^{85}Rb Bose-Einstein Condensates with Widely Tunable Interactions*, Phys. Rev. Lett. **85**, 1795 (2000).
- [44] C. Chin, V. Vuletić, A. J. Kerman, and S. Chu, *High Resolution Feshbach Spectroscopy of Cesium*, Phys. Rev. Lett. **85**, 2717 (2000).
- [45] C. Cohen-Tannoudji, Nobel lecture, Rev. Mod. Phys. **70**,707 (1998).
- [46] R. Grimm, M. Weidemüller, and Y. B. Ovchinnikov, *Optical dipole traps for neutral atoms*, Advances in Atomic, Molecular and Optical Physics **42**, 95 (2000).
- [47] N. W. Ashcroft and N. D. Mermin, *Solid State Physics*, Saunders College Publishing (1976).
- [48] D. Jaksch, *Bose-Einstein Condensation and Applications*, PhD thesis, Leopold- Franzens-Universität Innsbruck, Austria, (1999).
- [49] C. Kittel, *Quantum Theory of Solids*, John Wiley and Sons, New York, (1963).
- [50] M. L. Chiofalo and M. P. Tosi, Phys. Rev. A **268**, 406 (2000).
- [51] M. Glucka, A. R. Kolovsky, H. J. Korsch, *Wannier-Stark resonances in optical and semiconductor superlattices*, Phys. Rep. **366**, 103 (2002).
- [52] D. Witthaut, M. Werder, S. Mossmann, and H. J. Korsch, *Bloch oscillations of Bose-Einstein condensate: Breakdown and revival*, Phys. Rev. E **71**, 036625 (2005).
- [53] J. W. Goodman, *Speckle Phenomena in Optics: Theory and Applications*, Roberts and Company Publishers, (2007).
- [54] J. W. Goodman, *Laser speckle and related phenomena*, J. C. Dainty, Springer-Verlag, Berlin, (1975).

-
- [55] M. Francon, *La Granularité Laser (speckle) et ses applications en optique*, Masson, Paris, (1978).
- [56] V. Guarrera, L. Fallani, J. E. Lye, C. Fort and M. Inguscio, *Inhomogeneous broadening of a Mott insulator spectrum*, New J. Phys. **9**, 107 (2007).
- [57] R. Roth, and K. Burnett, *Phase diagram of bosonic atoms in two-color superlattices*, Phys. Rev. A **68**, 023604 (2003)
- [58] F. Gerbier, A. Widera, S. Fölling, O. Mandel, T. Gericke, and I. Bloch, *Interference pattern and visibility of a Mott insulator*, Phys. Rev. A **72**, 053606 (2005).
- [59] G. Roux, T. Barthel, I. P. McCulloch, C. Kollath, U. Schollwoeck, and T. Giamarchi, *The quasi-periodic Bose-Hubbard model and localization in one-dimensional cold atomic gases*, cond-mat arXiv:0802.3774 (2008).
- [60] M. Kohmoto, *Metal-Insulator Transition and Scaling for Incommensurate Systems*, Phys. Rev. Lett. **51**, 1198 (1983).
- [61] G-L. Ingold, A. Wobst, C. Aulbach and P. Hänggi, *Delocalization and Heisenbergs uncertainty relation*, Eur. Phys. J. B **30**, 175 (2002).
- [62] A. Wobst, G.-L. Ingold, P. Hänggi, D. Weinmann, *From ballistic motion to localization: a phase space analysis*, Eur. Phys. J. B, **27**, 11 (2002).
- [63] H. Wang, A. N. Nikolov, J. R. Ensher, P. L. Gould, E. E. Eyler, and W. C. Stwalley, *Ground-state scattering lengths for potassium isotopes determined by double-resonance photoassociative spectroscopy of ultracold ^{39}K* , Phys. Rev. A **62**, 052704 (2000).
- [64] T. Loftus, C. A. Regal, C. Ticknor, J. L. Bohn, and D. S. Jin, *Resonant Control of Elastic Collisions in an Optically Trapped Fermi Gas of Atoms*, Phys. Rev. Lett. **88** 173201 (2002).
- [65] Y. Kagan, E. L. Surkov, and G. V. Shlyapnikov, *Evolution and Global Collapse of Trapped Bose Condensates under Variations of the Scattering Length*, Phys. Rev. Lett. **79**, 2604 (1997).

BIBLIOGRAPHY

- [66] C. A. Sackett, H. T. C. Stoof, and R. G. Hulet, *Growth and Collapse of a Bose-Einstein Condensate with Attractive Interactions*, Phys. Rev. Lett. **80**, 2031 (1998).
- [67] M. Ueda and A. J. Leggett, *Macroscopic Quantum Tunneling of a Bose-Einstein Condensate with Attractive Interaction*, Phys. Rev. Lett. **80**, 1576 (1998).
- [68] C. D'Errico, M. Zaccanti, M. Fattori, G. Roati, M. Inguscio, G. Modugno and A. Simoni, *Feshbach resonances in ultracold ^{39}K* , New J. Phys. **9**, 223 (2007).
- [69] L. Khaykovich, F. Schreck, G. Ferrari, T. Bourdel, J. Cubizolles, L. D. Carr, Y. Castin, and C. Salomon, *Formation of a Matter-Wave Bright Soliton*, Science **296**, 1290 (2002).
- [70] M. Prevedelli, F. S. Cataliotti, E. A. Cornell, J. R. Ensher, C. Fort, L. Ricci, G. M. Tino, and M. Inguscio, *Trapping and cooling of potassium isotopes in a double-magneto-optical-trap apparatus*, Phys. Rev. A **59**, 886 (1999).
- [71] L. De Sarlo, P. Maioli, G. Barontini, J. Catani, F. Minardi, and M. Inguscio, *Collisional properties of sympathetically cooled ^{39}K* , Phys. Rev. A **75**, 022715 (2007).
- [72] G. Modugno, G. Ferrari, G. Roati, R. J. Brecha, A. Simoni, and M. Inguscio, *Bose-Einstein Condensation of Potassium Atoms by Sympathetic Cooling*, Science **294**, 1320 (2001).
- [73] G. Roati, F. Riboli, G. Modugno, and M. Inguscio, *Fermi-Bose Quantum Degenerate ^{40}K - ^{87}Rb Mixture with Attractive Interaction*, Phys. Rev. Lett. **89**, 150403 (2002).
- [74] F. Ferlaino, C. D'Errico, G. Roati, M. Zaccanti, M. Inguscio, and G. Modugno, *Feshbach spectroscopy of a K-Rb atomic mixture*, Phys. Rev. A **73**, 040702(R) (2006).

- [75] A. Simoni, M. Zaccanti, C. D’Errico, M. Fattori, G. Roati, M. Inguscio, and G. Modugno *Near-threshold model for ultracold KRb dimers from interisotope Feshbach spectroscopy*, Phys. Rev. A **77**, 052705 (2008).
- [76] G. Roati, *Quantum degenerate Potassium-Rubidium mixtures*, PhD Thesis, University of Trento (2003).
- [77] F. Ferlaino, *Atomic Fermi gases in an optical lattice*, PhD Thesis, University of Florence (2004).
- [78] E. de Mirandes, *Bloch oscillations of ultracold atoms*, PhD thesis, University of Florence (2005).
- [79] C. D’Errico, *Osservazione di Risonanze di Fano-Feshbach in miscele atomiche K-Rb*, Master Thesis, University of Florence (2005).
- [80] M. Zaccanti, *Tuning of the interactions in ultracold K-Rb quantum gases*, PhD thesis, University of Florence (2007).
- [81] E. L. Raab, M. Prentiss, Alex Cable, Steven Chu, and D. E. Pritchard, *Trapping of Neutral Sodium Atoms with Radiation Pressure*, Phys. Rev. Lett. **59**, 2631 (1987).
- [82] S. Stringari, *Collective Excitations of a Trapped Bose-Condensed Gas*, Phys. Rev. Lett. **77**, 2360 (1996).
- [83] D. R. Hofstadter, *Energy levels and wave functions of Bloch electrons in rational and irrational magnetic fields*, Phys. Rev. B **14**, 2239 (1976).
- [84] R. B. Diener, G. A. Georgakis, J. Zhong, M. Raizen, and Q. Niu, *Transition between extended and localized states in a one-dimensional incommensurate optical lattice*, Phys. Rev. A **64**, 033416 (2001).
- [85] J. Zhong, R. B. Diener, D. A. Steck, W. H. Oskay, M. G. Raizen, E. W. Plummer, Z. Zhang and Q. Niu, *Shape of the Quantum Diffusion Front*, Phys. Rev. Lett. **86**, 2485 (2001).
- [86] M. Fattori, C. D’Errico, G. Roati, M. Zaccanti, M. Jona-Lasinio, M. Modugno, M. Inguscio, and G. Modugno, *Atom Interferometry with a*

BIBLIOGRAPHY

- Weakly Interacting Bose-Einstein Condensate*, Phys. Rev. Lett. **100**, 080405 (2008).
- [87] M. Fattori, G. Roati, B. Deissler, C. DErrico, M. Zaccanti, M. Jona-Lasinio, L. Santos, M. Inguscio, and G. Modugno, *Magnetic Dipolar Interaction in a Bose-Einstein Condensate Atomic Interferometer*, Phys. Rev. Lett. **101**, 190405 (2008).
- [88] M. Greiner, O. Mandel, T. Esslinger, T. W. Hänsch, *Immanuel Bloch Quantum phase transition from a superfluid to a Mott insulator in a gas of ultracold atoms*, Nature **415**, 39 (2002).
- [89] T. Stöferle, H. Moritz, C. Schori, M. Köhl, and T. Esslinger, *Transition from a Strongly Interacting 1D Superfluid to a Mott Insulator*, Phys. Rev. Lett. **92**, 130403 (2004).
- [90] L. D. Landau, E. M. Lifshitz, *Quantum Mecanics*, Pergamon Press, Oxford (1977).
- [91] C. J. Joachanin, *Quantum collision theory*, p. 78-105, North-Holland, Amsterdam (1983)